Flash Boiling Atomization of Suspension for Application of Suspension Plasma Spraying

Saeid Amrollahybiouki

A Thesis

in

The Department

of

Mechanical, Industrial, and Aerospace Engineering

Presented in Partial Fulfillment of the Requirements

for the Degree of

Doctor of Philosophy (Mechanical Engineering) at

Concordia University

Montreal, Quebec, Canada

April 2024

Concordia University

School of Graduate Studies

This is to certify that the thesis prepared,

By: **Saeid Amrollahybiouki**

Entitled: **Flash Boiling Atomization of Suspension for Application of Suspension Plasma Spraying**

And submitted in partial fulfillment of the requirement of the degree of

Doctor of Philosophy (Mechanical Engineering)

Complies with regulations of this University and meets the accepted standards with respect to originality and quality.

Signed by the Final Examining Committee:

	Chair
Dr. Andrea Schiffauerova	External Examiner
Dr. Fardad Azarmi	External to the Program
Dr. Alex De Visscher	Examiner
Dr. Lyes Kadem	Examiner
Dr. Charles Basenga Kiyanda	Thesis Supervisor (s)
Dr. Christian Moreau	
Dr. Ali Dolatabadi	

Approved by

	Dr. Martin D. Pugh, Chair Department of Mechanical, Industrial and Aerospace Engineering
April 9th 2024	
Date of Defense	Dr. Mourad Debbabi, Dean Gina Cody School of Engineering and Computer Science

Abstract

Flash Boiling Atomization of Suspension for Application of Suspension Plasma Spraying

Saeid Amrollahybiouki, Ph.D.

Concordia University, 2024

Suspension Plasma Spraying (SPS) is a thermal spray technique used to deposit sub-micron and nano-sized particles. The liquid is evaporated by exposing the suspension to the plasma jet. Then, the particles are melted and directed in the plasma jet to impact the substrate and form a coating. SPS has lower solid feed rates and deposition efficiency compared to other thermal spray techniques. Increasing particle concentration in the suspension can enhance the feedstock deposition rate, but high viscosity and nozzle clogging are issues.

To address these issues, this study explores flash boiling atomization (FBA) as a novel injection method in SPS for high solids concentrations, up to 70 wt.%. FBA uses thermodynamic instability to break up a liquid jet. When superheated suspension is accelerated through a nozzle and its pressure drops below the saturation pressure, rapid boiling occurs. Vapor bubbles expand within the liquid jet, causing it to fragment into smaller parts. FBA has applications in various industries such as fuel injection, desalination, and pharmaceuticals. The main objective is to use FBA to inject high-solids suspensions into the plasma flow to create SPS coatings.

Suspension injection in SPS can be axial or radial. In axial injection, fragmentation occurs inside the torch, while in radial injection, the suspension is injected from outside the torch into the plasma flow. Conventional radial injection methods include spray atomization, which creates disintegrated droplets, and mechanical injection, which produces a continuous jet. This study compared coatings made with FBA to those made with mechanical injection,

assessing microstructure, deposition weight per pass, deposition efficiency, and coating thickness. Results indicated improvements across these parameters.

Water and ethanol are common suspension solvents. Water-based suspensions face challenges with atomization and evaporation resistance, impacting coating properties. FBA can improve fragmentation and prevent clogging by reducing viscosity and surface tension in the superheated state. The effect of high solids concentration and plasma power on coating microstructure, thickness per pass, deposition weight per pass, and deposition efficiency was investigated, showing that a dense coating microstructure with high solids deposition can be achieved using 70 wt.% suspension and a high power torch.

Acknowledgments

I want to express my sincere gratitude to my supervisors, Prof. Ali Dolatabadi and Prof. Christian Moreau, for their continuous support of my Ph.D. study. Without their motivation, knowledge, insightful comments, encouragement, and challenging questions that triggered several innovative solutions during researching and writing the thesis, this accomplishment would not have occurred.

Some particular words of gratitude go to my friends who have been a significant source of support in this project: Dr. Fadhel Ben Ettouli, Dr. Andre Liberati and Dr. Mehdi Jadidi.

I am also grateful to my fellow lab-mates for the stimulating discussions and the laughter moments, which decreased the pressure of hard work. I want to thank my friends for expecting nothing less than triumph during my Ph.D. program.

We gratefully acknowledge funding support from the Natural Sciences and Engineering Research Council of Canada (NSERC), and the Canada Research Chair program.

Contribution of Authors

This thesis is written in a manuscript-based format. Chapters 1, 2, 3 and 6 are the introduction, experimental methodology, Preliminary results and observation, and conclusion of the thesis, respectively. The thesis includes coauthored works in Chapters 4 and 5 that were reprinted from papers published to scientific journals. The contribution of each coauthor is described below:

Chapter 4:

S. Amrollahy Biouki, F. Ben Ettouli, A. C.Liberati, C. Moreau, A. Dolatabadi*, "Flash Boiling Atomization of High-concentration Suspensions in Suspension Plasma Spraying", Published in journal of the thermal spray technology, volume 33 (1) , pages 122-133, 2024.

*Corresponding author

S. Amrollahy Biouki worked on the literature review, designing, and methodology, doing all SPS coating experiments, post-treatment, and collected the data. He performed all characterization tests, analyses, and discussion about the results and wrote the original draft, and review & editing the manuscript. A. C.Liberati helped writing the manuscript. F. Ben Ettouli assisted with the doing SPS experiments. C. Moreau and A. Dolatabadi supervised the research and revised the manuscript.

Chapter 5:

S. Amrollahy Biouki, F. Ben Ettouli, A. C. Liberati, A. Dolatabadi, C. Moreau*, "Microstructure of Deposits Sprayed by a High Power Torch with Flash Boiling Atomization of High-concentration Suspensions", published in journal of Materials, volume 17 (7), 1493, 2024.

*Corresponding author

S. Amrollahy Biouki worked on the literature review, designing, and methodology, doing all SPS coating experiments, post-treatment, and collected the data. He performed all characterization tests, analyses, and discussion about the results and wrote the original draft, and review & editing the manuscript. A. C.Liberati helped writing the manuscript. F. Ben Ettouli assisted with the doing SPS experiments. C. Moreau and A. Dolatabadi supervised the research and revised the manuscript.

All authors reviewed the final manuscript and approved of the contents.

Dedication

To my wonderful family, for their measureless support and unconditional love.

Contents

Table of figures

List of Table

List of Abbreviation

SPS	Suspension plasma spraying
FBA	Flash boiling atomization
APS	Atmospheric plasma spray
TBC	Thermal barrier coating
SEM	Scanning electron microscope
YSZ	Yttria stabilized zirconia
HVOF	High velocity oxy-fuel

Nomenclature

P_{inj}	Injection pressure (Pa)
P_{∞}	Ambient pressure (Pa)
T_{sat}	Saturation temperature (℃)
P_{sat}	Saturation pressure (Pa)
P_v	Vapor pressure (Pa)
R_{cr}	Critical radius (m)
d_l	Liquid jet diameter (m)
Ja	Jakob number
h_{fg}	Latent heat (kJ/kg)
$\emptyset$	Correction factor
R_p	Superheated degree
C_p	Specific heat ($J/kg.K$)
x	Vapor mass fraction
K	Thermal conductivity ($W/m.K$)
$\Delta\theta$	Superheated degree
ρ_g	Gas density (kg/m^3)
ρ_l	Liquid density (kg/m^3)
u_r	Relative velocity (m/s)
S_t	Stokes number
ρ_p	Particle density (kg/m^3)
d_p	Particle diameter (m)

μ_g	Gas viscosity ($kg/m.s$)
v_p	Particle velocity (m/s)
v_l	Liquid velocity (m/s)
L	Thickness of flow boundary (m)
λ	Mean free path (m)
We	Weber number
σ	Surface tension (N/m)
A	Surface area (m^2)

1 Chapter 1: Introduction

Thermal spray coatings refer to a group of industrial processes used to apply coatings or layers of materials onto the surface of various substrates. These coatings are typically applied in a molten or semi-molten state and then solidify to form a protective or functional layer against erosive, corrosive, and/or hot working conditions. Figure 1-1 outlines a basic and general classification of thermal spray processes, dividing them into four main types: flame spraying [1], kinetic processes [2], plasma spraying [3], and wire arc [4]. In flame spraying, the combustion of fuel gases such as Acetylene, Methane, Propane, or Hydrogen with Oxygen generates heat sources that melt particles and direct them toward the substrate. The kinetic method employs a high-velocity gas flow to accelerate particles up to 1000 m/s, impacting them against the substrate to form a coating in the absence of heat sources. Each main category has subdivisions detailing specific methods and techniques, with further information available in the literature [5]. Our research focuses on plasma spraying under atmospheric conditions.

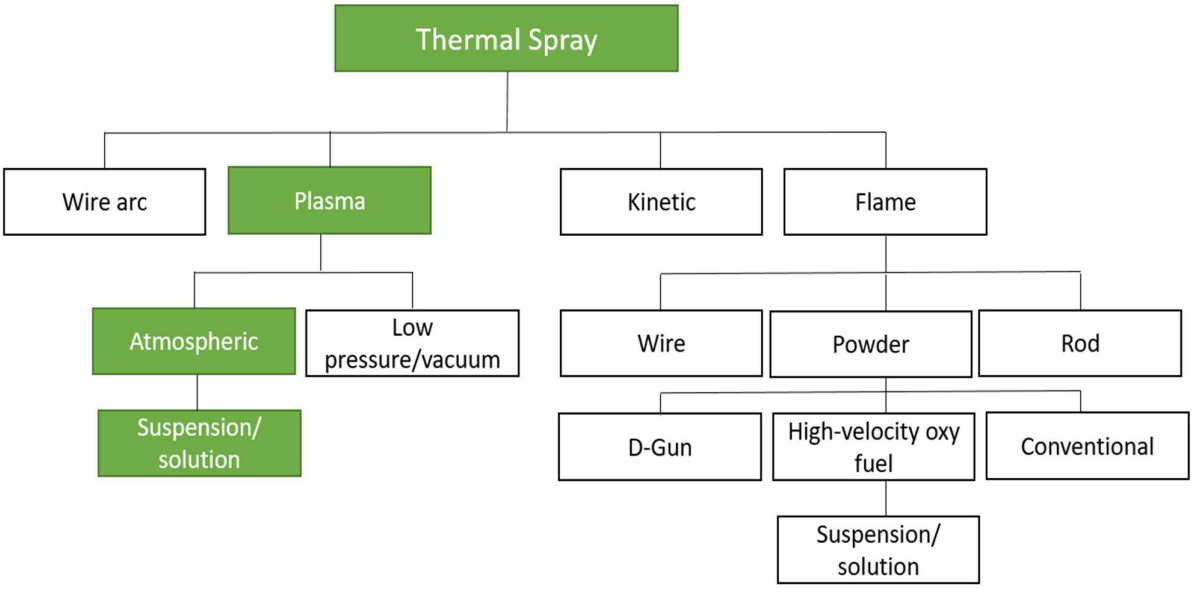

Figure 1-1. Classification of the thermal spray [5].

Plasma spraying is a thermal spray process that uses a plasma torch to heat and melt a feedstock material, typically in powder form. The molten or semi-molten material is then

accelerated and propelled onto a substrate, where it solidifies to form a coating. This process is widely used for applying protective coatings with various properties, such as wear resistance, thermal insulation, and corrosion protection. Atmospheric plasma spraying (APS) and suspension plasma spraying (SPS) are two well-known examples of plasma spraying methods. In APS, a high-powered electric arc is established between an anode and cathode in a mixture of argon, helium, or other gases, forming a high-temperature plasma jet. This jet provides momentum and heat to the coating particles, and the method is widely employed for producing thermal barrier coatings (TBC). The SPS technique will be explained in detail in the next section, covering all important phenomena related to this method as well as some limitations. Following that, flash boiling atomization will be described in detail in the following section, explaining how this suspension injection technique has the potential to address certain limitations.

1.1 Suspension plasma spraying (SPS)

Suspension plasma spraying is a deposition process that enables to spraying of sub-micron and nano-sized particles (usually in the range 500 nm to less than 5 μm) under atmospheric conditions [6]. Despite of conventional plasma spraying that uses carrier gas to inject micrometer size particles (ranging from 10 μm to 100 μm), small particles in SPS can be suspended in a liquid (which usually is water and ethanol) to provide enough momentum for penetration into the plasma jet [6], [7]. Suspension plasma spraying is shown in Figure 1-2, where liquid is evaporated by exposing a suspension to the plasma jet, then particles are melted and accelerated in the plasma jet to impact the substrate and form a coating.

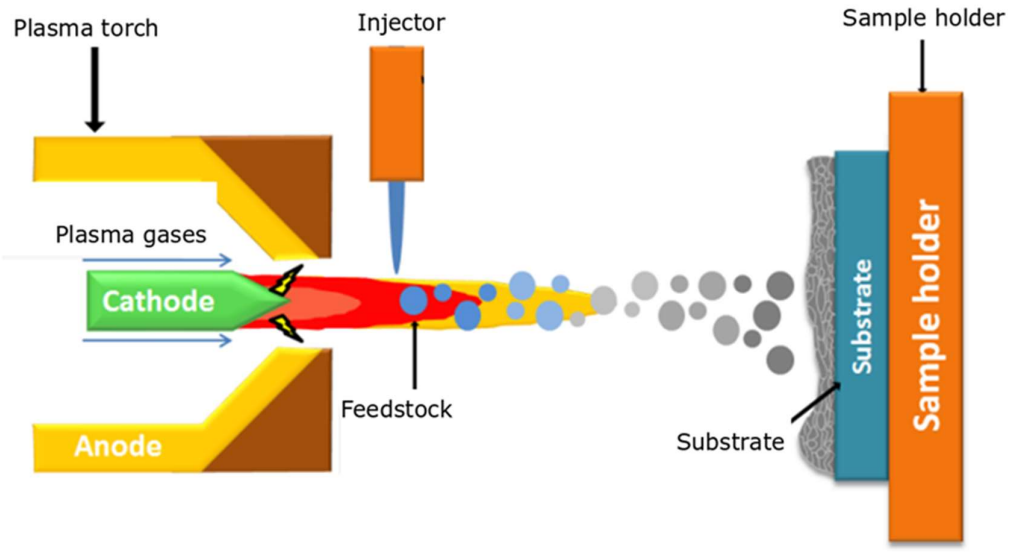

Figure 1-2. Schematic of suspension plasma spray process [8].

When the suspension is injected into the plasma jet, the first phenomenon that occurs is suspension fragmentation. Through this process, the suspension is fragmented into small drops ranging from 2-100 μm [7]. The second phenomenon which takes place is the solvent evaporation. The characterization time for evaporation is two orders of magnitude higher than the characteristic time for fragmentation in the plasma flow [7]. Then, small particles are accelerated by the high speed flow to reach the surface of the substrate.

The Stokes number (S_t), a non-dimensional parameter, evaluates the particles' ability to track the gas flow near the substrate. The Stokes number is defined by [9]:

$$S_t = \frac{\rho_p d_p^2 v_p}{\mu_g L} \quad (1-1)$$

where ρ_p, d_p and v_p are the particle density, particle diameter, and particle velocity, respectively. μ_g is the gas viscosity and L is the thickness of the flow boundary layer created in front of the substrate.

Stokes number close to 1 ($S_t \approx 1$) allows particles to effectively follow the gas streamlines while maintaining enough momentum for substrate impact. In such a case, several particles

impinge on the substrate with a shallow angle leading to the formation of a columnar coating structure due to de shadow effect [9] A significantly higher Stokes number ($S_t \gg 1$) suggests inadequate particle trajectory adjustment, risking erratic substrate impact and coating quality [8], [9]. Conversely, a much lower Stokes number ($S_t \ll 1$) most particles may not impact the substrate at all reducing considerably the deposition efficiency. Thus, precise control of the Stokes number through parameter optimization is essential in SPS for achieving high-quality coatings.

It is known that the momentum of the liquid has to be higher than the momentum of the plasma jet in order to have an appropriate suspension penetration to the hot region of plasma flow. That means:

$$\rho_{liquid} V_{liquid}^2 > \rho_{plasma} V_{plasma}^2 \quad (1-2)$$

ρ is density and V represents the velocity [9]. Droplets with higher momentum that can reach the hot zone of the plasma jet would be fully evaporated and the resultant particle will be melted. Droplets with lower momentum remain at plasma fringes and they cannot be evaporated or the resultant particles cannot be melted completely creating undesirable zones on the coating microstructure. However, some small particles (less than 1 μm) in the hot region may escape rapidly (Figure 1-3) and be cooled due to plasma arc fluctuations and thermophoresis effect [10]. Thermophoresis is a phenomenon that takes place due to a temperature gradient and the movement of gas molecules in the hot region displaces the nanoparticles to the cold zone. In addition, the momentum and heat transfer between plasma flow and small particles at the hot core region may be affected adversely due to Knudsen effect because it decreases their drag coefficient and also Nusselt number [11]. The Knudsen effect happens when the mean free path, λ, for gas molecules would be less than of the particle diameter in suspension.

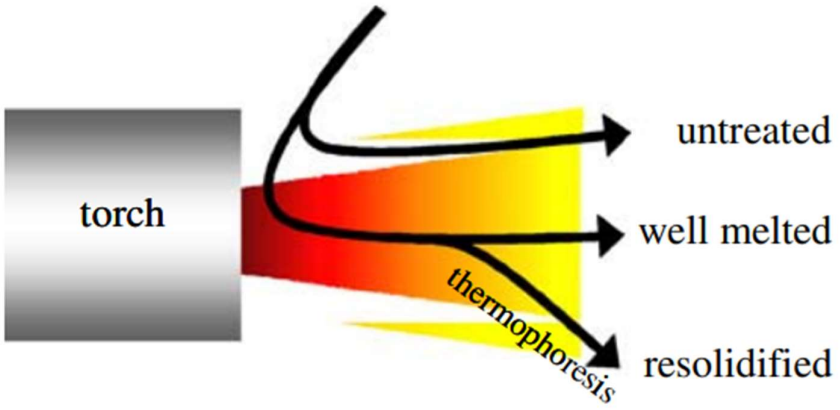

Figure 1-3. Schematic of particle penetration to the plasma jet [12].

In addition, the suspension properties such as surface tension and viscosity play an important role for jet fragmentation inside a plasma jet. More inertial force required to break up high surface tension suspensions. The non-dimensional Weber number represents the ratio of inertia force to surface tension force and it should be higher than 12-14 [9]. It defined by:

$$We = \frac{\rho_{liquid} . V_{liquid}^2 . d_{liquid}}{\sigma_{liquid}} \quad (1-3)$$

ρ_{liquid} is the specific mass, d_{liquid} represents the average diameter of jet, σ_{liquid} is the surface tension and V_{liquid} is the liquid jet velocity.

Based on the We number and momentum flux ratio, different breakup regimes can be observed inside the plasma jet. The better breakup and suspension decomposition happens in high Weber number specifically more than 350. The surface tension is on the denominator of equation and has an adverse effect on suspension breakup. In addition as can be observed on the equation, the Weber number depends on the square of the velocity and the velocity itself is directly proportional to the injection pressure. It means that by increasing the injection pressure (i.e. higher momentum flux ratio) better penetration can be achieved and also suspension breakup inside the plasma would be improved due to having higher Weber number. Fauchais et al. [13] injected an ethanol-based suspension of zirconia into the Ar-He

dc plasma jet with two different injection pressures 0.4 MPa (Figure 1-4.a) and 0.7 MPa (Figure 1-4.b). By increasing the injection pressure, the liquid can penetrate deeper and more liquid can pass the jet axis and fragmentation would be improved as well.

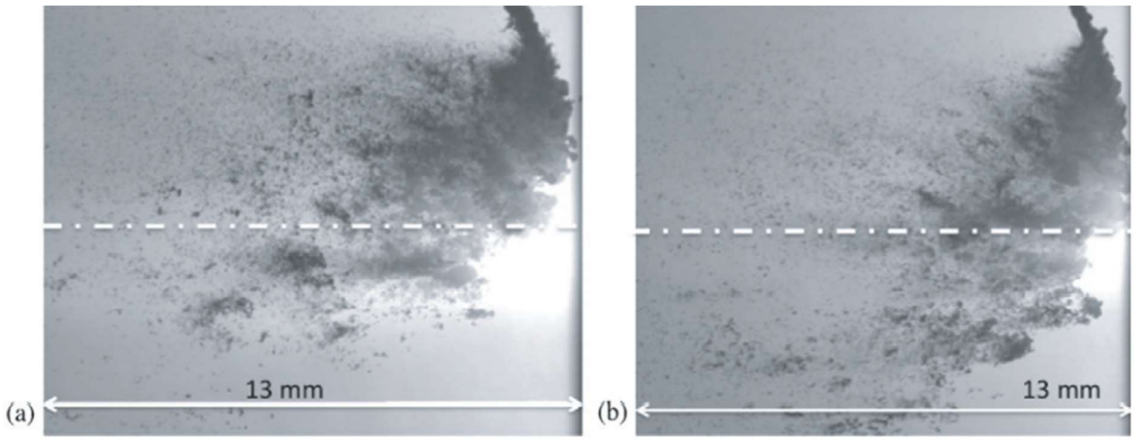

Figure 1-4. Penetration of ethanol-based suspension of zirconia into the plasma flow with two injection pressure (a) 0.4 MPa (b) 0.7 MPa [13].

Fazilleau et al. [14] injected suspension with three different injection pressure (Figure 1-5) and observed that suspension penetration increases by increasing injection pressure. It was discussed that the suspension jet disintegrated into big drops before reaching the fringes of the plasma, then the jet of drops (with size of 220 μm) start to be atomized to smaller droplets in the plasma flow.

Meillot et al. [15] investigated the effect of injection parameters such as injection pressure and injection location in order to find the prefer injection type. They showed that reaching to the core zone of plasma required optimum injection pressure and also up-to-down injection configuration. They discussed that a very high pressure leads to decrease in the deposition efficiency.

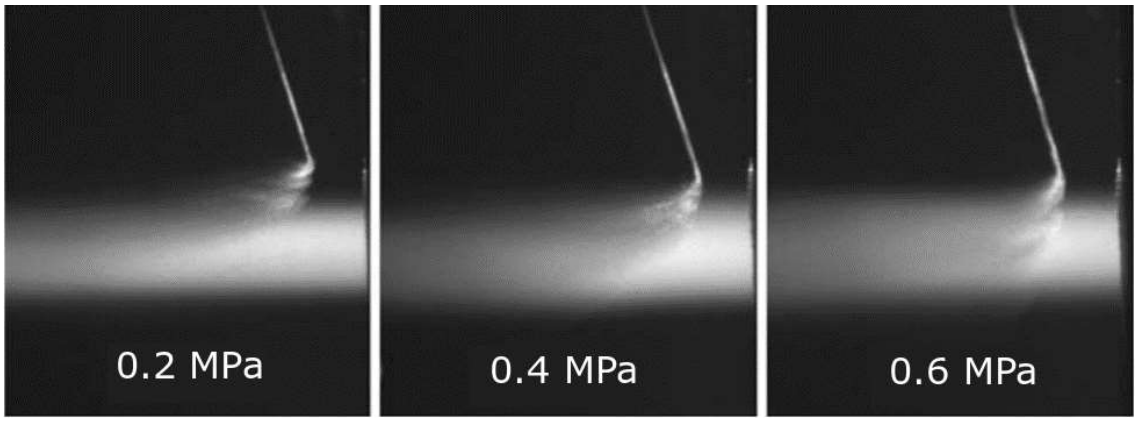

Figure 1-5. The suspension injection for three injection pressures (Ar-H_2 plasma) [14].

The viscosity becomes more significant in jet breakup and decomposition for suspension with higher viscosity [13]. The effect of viscosity can be investigated with Ohnesorge number Oh that is viscose force to surface tension force. The Ohnesorge number defined by:

$$Oh = \frac{\mu_{liquid}}{\sqrt{\rho_{liquid}\sigma_{liquid}d_{liquid}}} \quad (1-4)$$

The μ is the liquid viscosity. The viscosity can be ignored for the value between a few tenths to a few tens of mPa.s, but suspension injection would be difficult for suspension with viscosity more than 0.8 mPa.s [16].

In suspension plasma spraying, the melted and some unmelted particles impact with substrate, spread and solidified to form splats on the substrate. Then, these splats are added on top of each other to generate coatings. The properties of coatings such as porosity, strength, coating microstructure, etc. strongly depend on the shape of these splats and how to bond with each other and with the substrate. In addition, the shape of these splats is affected by particle properties, substrate conditions, particle velocity and temperature and etc. [17]. For instance, Li et al. [18] investigated the effect of substrate temperatures on YSZ splats and concluded that more uniform splat formation with higher particle density can be achieved when substrate temperature increases from room temperature to 900 ℃ (Figure 1-6).

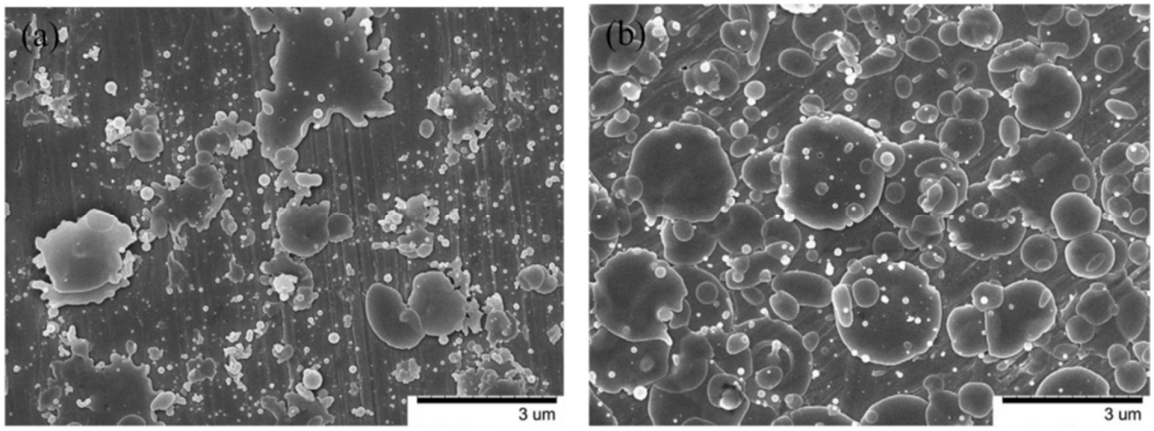

Figure 1-6. Images of splats deposited on stainless steel substrate in two different temperatures (a) room temperature (b) 500 ℃ [18].

Different coating microstructures in SPS can be generated and observed based on their applications. Coating microstructures are influenced by torch operation conditions, suspension properties (density, surface tension and viscosity), spray characteristics like droplet size and fragmentation process by the plasma jet [14]. The more common structures are columnar, dense, porous and vertically cracked coatings.

Coatings with columnar microstructures (Figurer 1-7) can generally have a reduced thermal conductivity due to their porosity. Voids or pores reduce the thermal conductivity by acting as thermal insulators [19]. In addition, columnar microstructures can provide better thermal cyclic fatigue resistance and thermal shock resistance due to the reduction of thermal stress in the coatings [20].

The smaller droplet size distribution is a vital parameter to fabricate coatings with columnar structure. The ethanol-based suspension can be atomized into much lower droplets size compared with water-based suspension due to low surface tension and viscosity. Therefore, the columnar-structured coatings are usually formed by using ethanol-based suspension. The dense coating microstructure (Figure 1-8) is helpful to enhance the mechanical properties by increasing the hardness [21], the elastic moduli [21], and wear resistance [22]. High in-flight

particle velocities with high momentum is required to generate coatings with high dense structure.

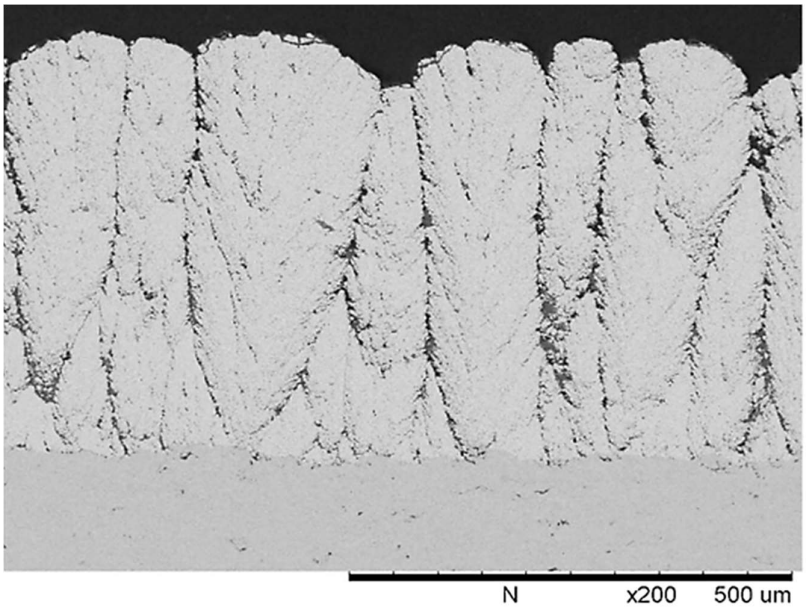

Figure 1-7. The cross-section image of coating with columnar microstructure [23].

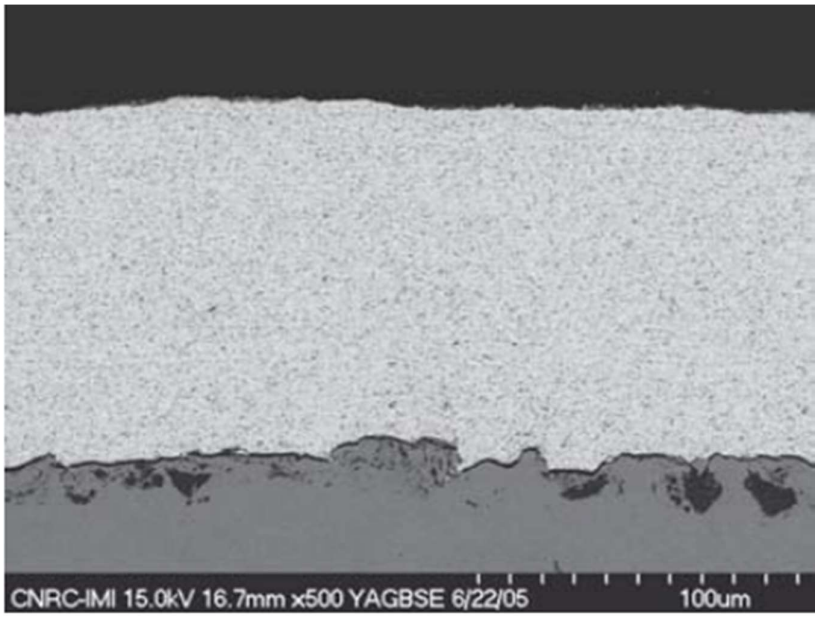

Figure 1-8. The cross-section micrograph for dens coating [3].

Highly porous coatings (Figure 1-9) can be generated by applying large standoff distance and also the high presence of unmelted particles leading to porous coatings. This type of coating can be applicable in membrane fabrication [24] and it can enhance the performance of

photocatalytic materials [25]. The dense vertically cracked (DVC) microstructures (Figure 1-10) could be fabricated with SPS process. In this type of coating, some vertical cracks propagated through the coating that can enhance strain tolerance and improve the thermal cycling life [26].

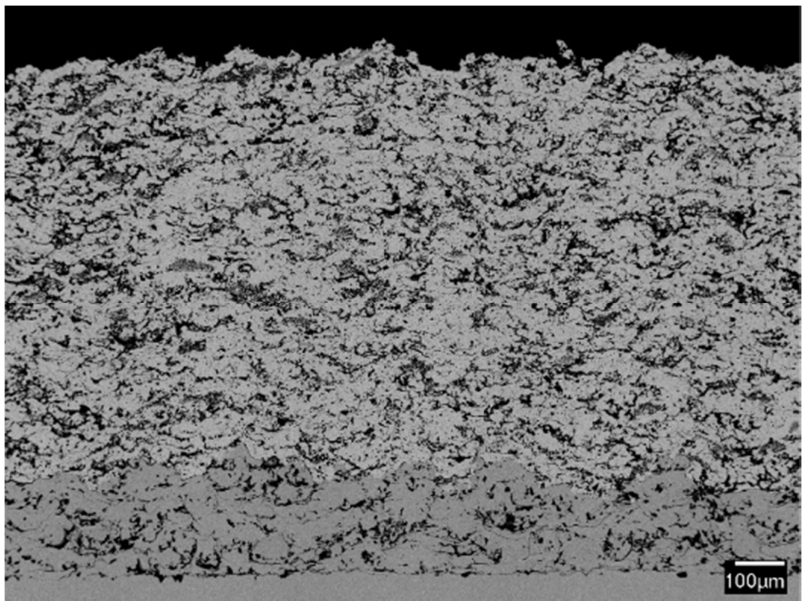

Figure 1-9. The cross-section image of high porous coating [27].

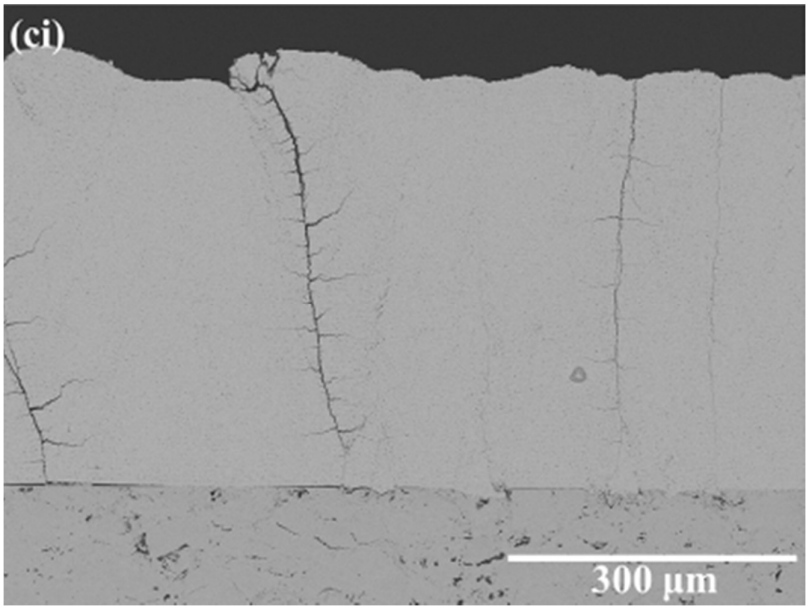

Figure 1-10. The cross section of vertically cracked coating [28].

1.1.1 Suspension injection technique in the SPS

As depicted in Figure 1-11, suspension injection in SPS can either be axial or radial, depending on the torch design. In axial injection, suspension fragmentation occurs inside the torch through interaction with an atomization gas, while in radial injection, suspension is injected from outside the torch into the plasma jet that fragments the injected suspension [29].

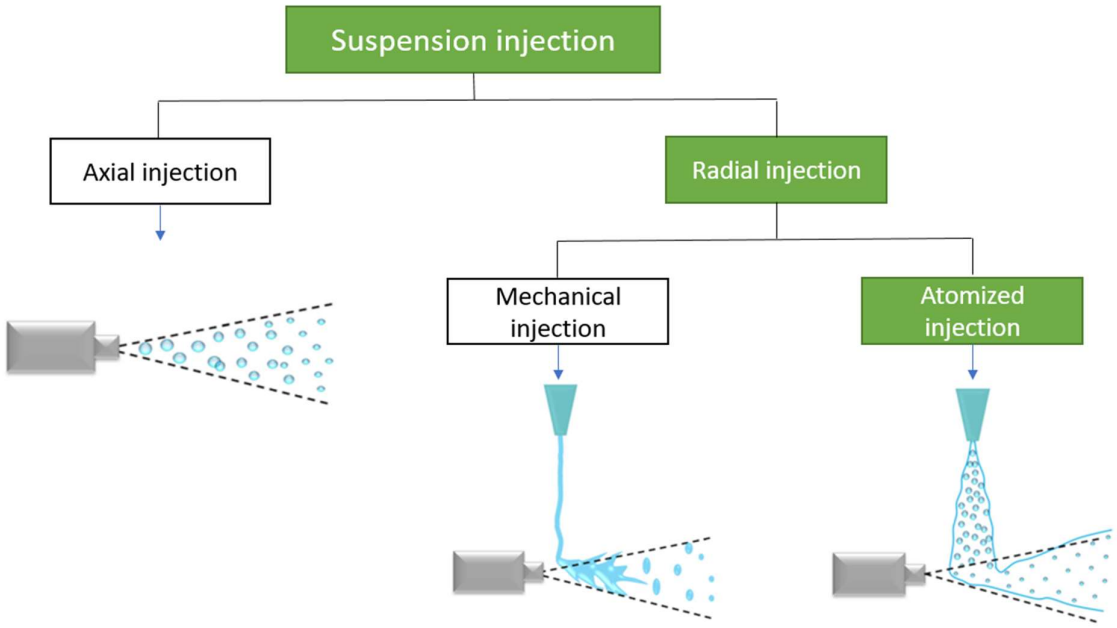

Figure 1-11. Schematic representation of the different suspension injection techniques in SPS [29].

Spray atomization and mechanical injection are two methods usually used to inject suspension radially into the plasma jet. First method is an ensemble of disintegrated droplets resulting from atomization (Figure 1-12a) and later one is a continuous jet comes from mechanical injection (Figure 1-12b). Flash boiling atomization can be considered a subset of the spray atomization technique but without the addition of an atomizing gas. There are some specific features for each methods.

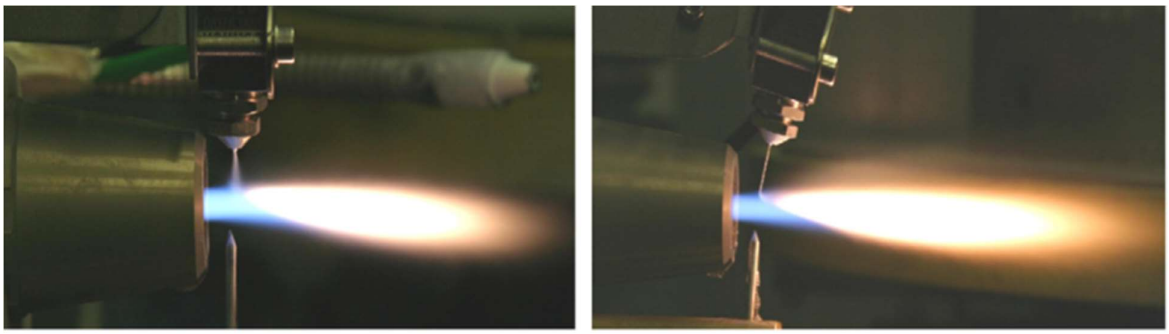

(a) (b)

Figure 1-12. The radial injection of suspension (a) spray atomization (b) mechanical injection (i.e. liquid jet) [30].

- **Mechanical injection**

In most cases in SPS, this method is used for suspension injection. In this method, the suspension is pressurized by compressed gas in the reservoir and is forced to inject through the nozzle. One reservoir is usually considered to store pure liquid in order to clean nozzle and pipe and avoid clogging after injection suspension. The only changeable parameters are injection pressure and the nozzle size. Different pressure reservoir and different size of nozzles ranging from 50 μm to 300 μm are being used. By changing these two parameters, the flow rate and jet velocity can be altered. The reported drawback for this method is that the injection pressure is varied as the 4th power of the reverse of injection nozzle size [16]. The mass flow rate is obtained by equation 5 and as can be seen the velocity is inversely proportional to the nozzle size.

$$\dot{m} = \rho_l v_l A \quad (1-5)$$

A represents the surface area of the nozzle hole, where ρ_l and v_l denote liquid density and liquid velocity, respectively. The pressure drop is calculated by Bernoulli equation (equation 6) and is proportional to the square of the velocity. For instance by decreasing one-third of the nozzle size from 150 μm to 50μm, the pressure must be increased 81 times from 0.5 MPa to 40.5 MPa in order to have the same mass flow rate [16].

$$\Delta p = \frac{1}{2}\rho_l v_l^2 \quad (1-6)$$

Based on the Weber number of suspension jet, different breakup regimes happens in the plasma jet and subsequently the formation of ligaments and small droplets. The another method for mechanical injection is a magneto-strictive rod. In this method the rod is positioned at the backside of the nozzle and superimpose pressure pulses at different frequencies (up to 222 kHz) [16]. Cotler et al. [31] made a novel self-cleaning apparatus for mechanical injection which allows to reduce the clogging and agglomeration problems.

The advantage of mechanical injection method is that less plasma jet perturbation takes place for this method. In addition, less deviation on generated droplet size and trajectory in the plasma jet can be observed compared with spray atomization. Furthermore, this method allows to have drops at the specific location of plasma jet [14].

- **Spray atomization**

In this method, the injection of suspension take places in the form of atomization. A twin-fluid atomizer containing of gas and suspension is commonly being used for spray atomization. Atomization of suspension jet requires an external energy that can provide by pressure of gas. The interaction between gas and suspension (either inside the nozzle or outside the nozzle) results in disintegration of suspension into fine droplets. The desired droplets size and velocity can be generated by changing the spray conditions and nozzle geometry. The size and velocity of disintegrated droplets are affected by relative velocity between gas and liquid, the ratio of the gas to liquid (both mass ratio ALR and volume ratio RGS are reported), the nozzle design and the liquid properties (density, surface tension, viscosity) [16]. More atomization of suspension can occur by increasing the mass ratio, however higher amount of air causes cooling down of plasma flow. Rampon et al. [32]

injected a suspension of stabilized zirconia into the plasma jet by using an internal mixing twin-fluid atomizer at different ALR (Figure 1-13).

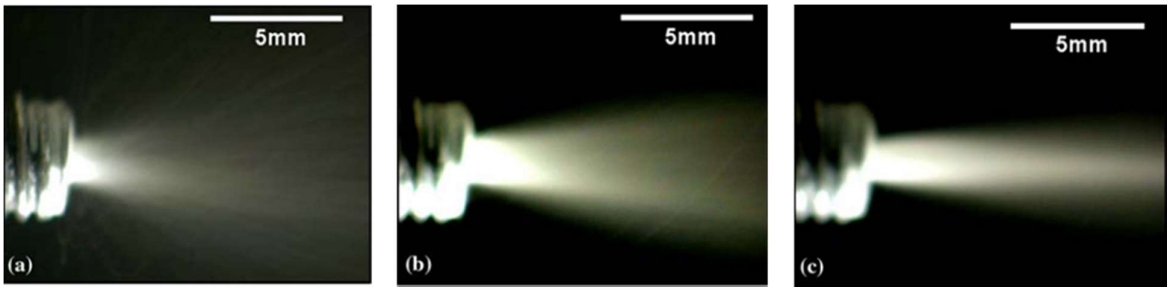

Figure 1-13. The spray pattern of zirconia suspension at We=6 for different ALR (a) 0.6 (b) 0.3 (c) 0.15 [32].

Toma et al. [30] showed that the coating thickness per pass decreased from 4 to 6 μm per pass for mechanical injection method to 1.5 to 2 μm per pass for spray atomization. However, they could not find significant differences in the microstructures of coatings for the different suspension injection method.

Lathka [8] discussed that less unmelted particles generated in atomization injection mode in comparison with continuous stream injection mode. In addition, the possibility of clogging will be reduced in injection mode and the atomization injection mode prevents agglomeration in nozzle. One main disadvantage of using atomization mode is the injection of cool air into the plasma plume and cooling it down. Mauer et al. [33] showed that the plasma temperature decreased by 500 K at axial distance of 50 mm, in the case of only air injection compared with no injection condition. Air injection not only cools down the plasma jet but also leads to a drastic plasma perturbation. Fauchais [34] presented a 3D models to treat correctly the perturbation of the plasma jet by the cold carrier gas. Another disadvantage of spray mode is the wide angle of the generated spray. Kassener et al. [35] discussed that commercial two-phase atomizers usually have the spray angles of up to 60^0 that results in deviation of particles to the plasma jet fringes or into the colder regions.

1.1.2 The current limitations on SPS

The SPS process method which employs suspension of small particles as feedstock, can enhance the mechanical and thermal properties of the coating compared with conventional coatings. In addition, the ability to use small particles, even those less than 100 nm in size, and to fabricate coatings with different microstructures are the main advantages of SPS techniques compared to other thermal spray methods [9], [13]. However, the solid feed rate and deposition efficiency in SPS are two or three times lower than other conventional plasma spray techniques [36]. In addition, there are some limitations of using water-based suspension. The poor atomization and resistance against evaporation are two disadvantages that should be considered when using water-based suspension.

- **Poor atomization of water-based suspension**

Water and ethanol are usually used as a solvent to make a suspension. Water has high resistance to fragmentation owing to high surface tension ($\sigma_{water}/\sigma_{ethanol} = 1.5$) and also high mass density ($\rho_{water}/\rho_{ethanol} = 1.5$). Therefore, poor atomization of water leads to droplets with large mean diameter ranging from 70 to 120 μm, comparisions with ethanol droplets that have diameter between 18 to 110 μm [13]. The lower surface tension in ethanol results in higher Waber number in same conditions and consequently better breakup in the plasma jet. Fauchais et al. [11] evaluated the penetration of pure ethanol jet (with We=563) and pure water jet (with We=170) inside the plasma jet and showed that no drops larger than 5 μm could be detected 9 mm downstream of torch for pure ethanol (Figure 1-14a). However, many drops more than 5 μm could be found 13 mm from downstream of the torch for pure water (Figure 1-14b). The first 2 mm were masked by the injector support. In addition, Siegert [37] showed that the deposition efficiency (the ratio of deposited powder to amount of powder sprayed toward the substrate) is double when switching water-based YSZ suspension. with ethanol-based suspension.

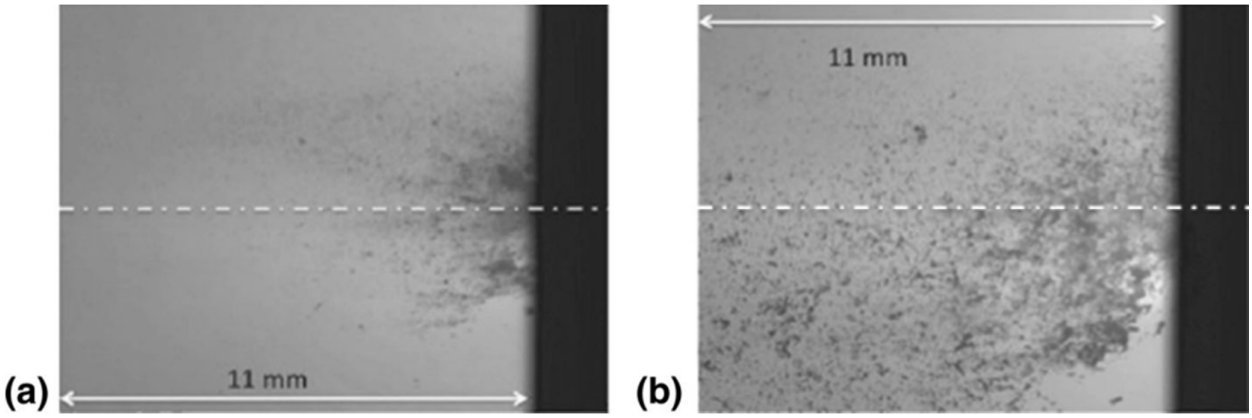

Figure 1-14. Penetration of a liquid jet injected into the plasma jet (a) pure ethanol (We=563) (b) pure water (We=170) [11].

- **High cost of energy for evaporation of water**

Water evaporation in the plasma jet consumes plasma energy that results in cooling down the plasma jet and reducing the temperature during the process. The evaporation of water requires 2.63 MJ/kg against 1.01 MJ/kg for ethanol owing to high evaporation enthalpy of water ($h_{water}/h_{ethanol} = 2.8$) [13]. Fauchais et al. [11] measured the plasma temperature distribution for two conditions of with and without water injection for two different distances of 5 and 15 mm from downstream of nozzle torch (Figure 1-15). It was observed that at distance of 15 mm the plasma temperature dropped from 11,300 to 9,800 K and also the length of plasma core decreased about 10 mm.

High cost of energy for water evaporation leads to lower available energy for particles melting and ultimately higher amount of unmelted particles would be appeared in the coatings. These unmelted particles may produce more porosity in the coatings. On the contrary, ethanol requires less heat to vaporize than water, and ethanol can also improve the thermal conductivity of the plasma jet after vaporization. More energy is available to melt most of particles and coatings with dense structure can be achieved by using ethanol-based suspension.

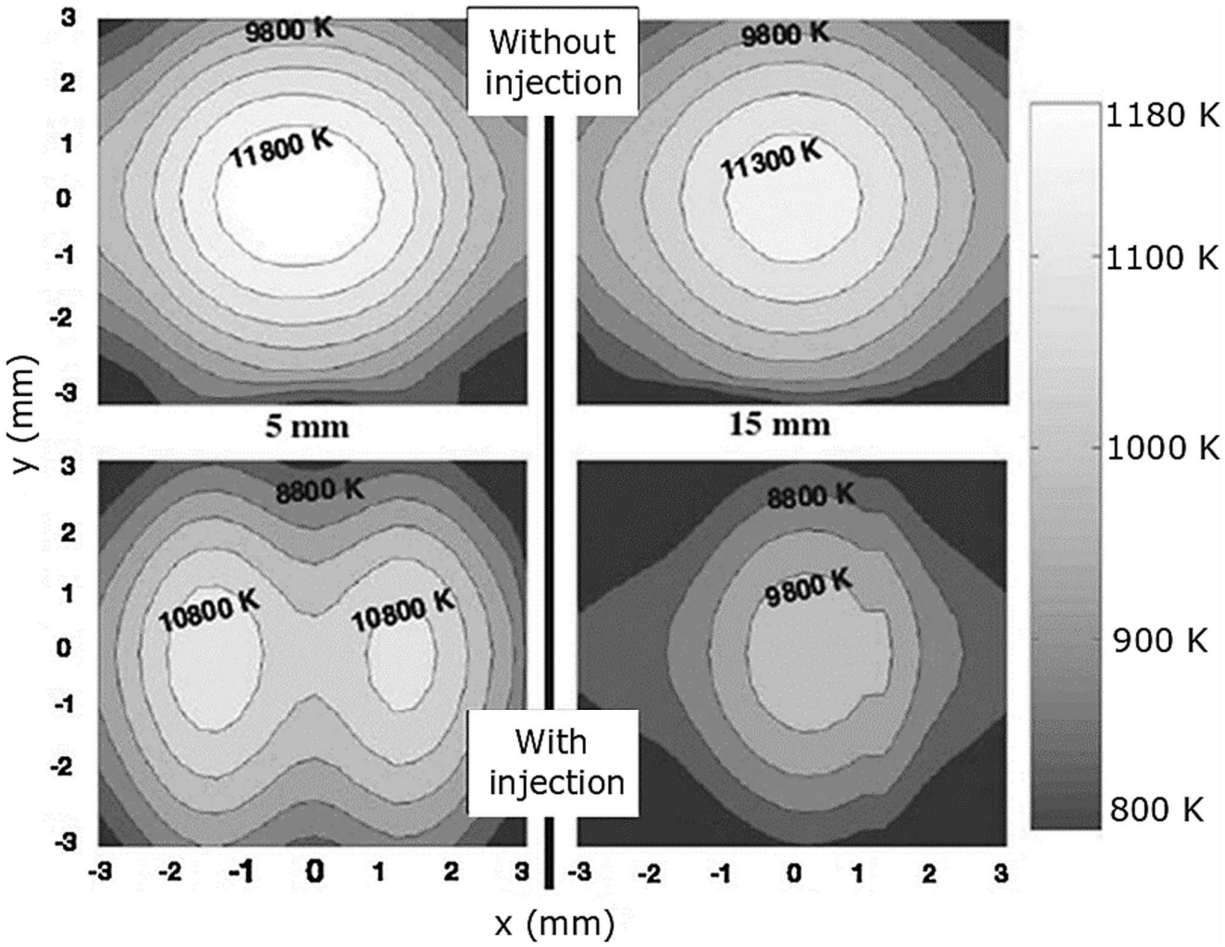

Figure 1-15. The plasma temperature distribution 5 and 15 mm downstream of torch with and without water injection [11].

Chen et al. [38] calculated that the amount of heat required to vaporize a suspension containing 75% ethanol and 25 % yttria-stabilized zirconia is 69 kJ against 183 kJ for water based suspension.

Joulia et al. [39] used two different solvents (water and ethanol) to produce suspensions (based on sub-micrometer sized of YSZ particles). They produced extremely dense coatings by applying ethanol as a solvent, whereas they obtained porous coatings with more defective layers for water-based suspension. In addition, they observed a uniform distribution of lamellae with diameters ranging from 1 to 5 μm for the ethanol case (Figure 1-16.a and b), whereas a mix of flattened lamellae and non-flattened lamellae could be found in the coating of water-based suspension (Figure 1-16.c and d). The non-flattened lamella was generated

due to non-melted YSZ particles. Figure 1-16 shows that the high amount of material would be deposited by increasing the enthalpy of plasma.

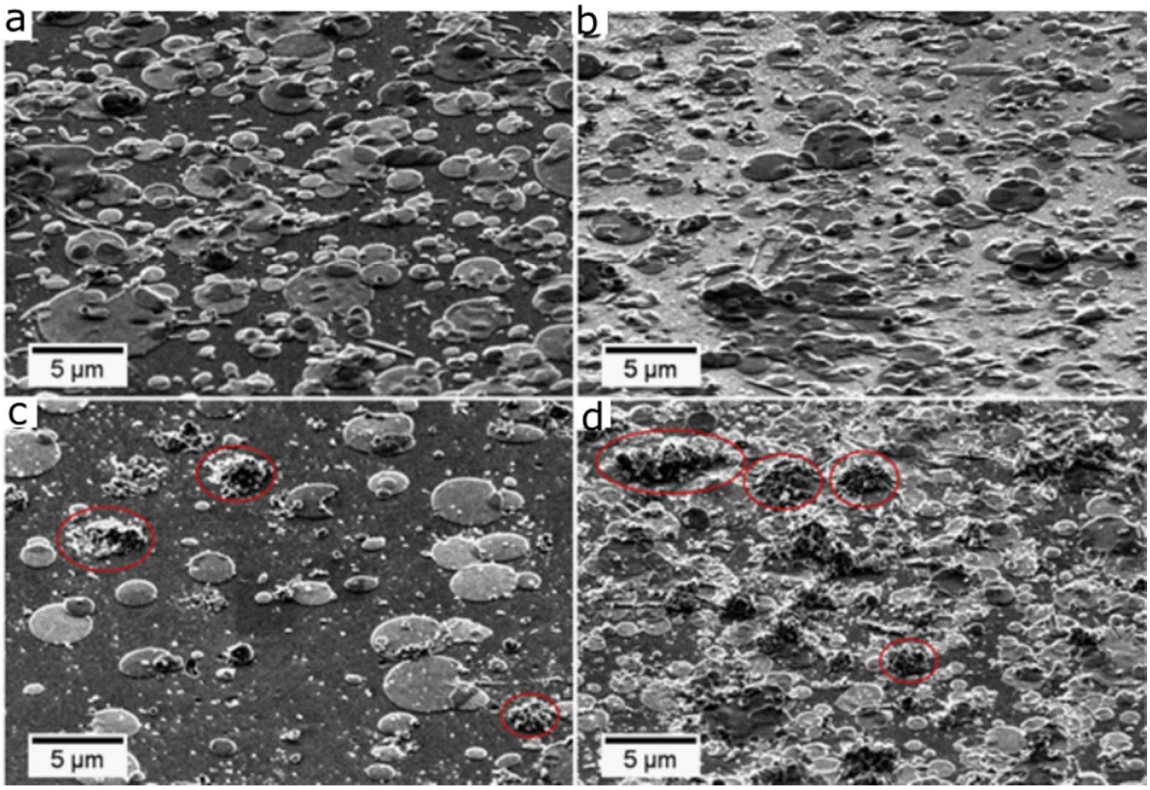

Figure 1-16. SEM micrographs of YSZ lamellae for (a) ethanol-based with low enthalpy condition (b) ethanol-based with high enthalpy condition (c) Water-based with low enthalpy condition (d) Water-based with high enthalpy condition [39].

1.2 Flash boiling atomization (FBA)

1.2.1 Thermodynamic concepts of FBA

Flash boiling atomization is an unstable thermodynamic process by which superheated liquid jet disintegrates to ligaments and small droplets. Superheated liquid is a liquid at temperature that is higher than boiling point at ambient pressure. Figure 1-17 illustrates the flash boiling process in two phase diagram, above the saturation line the equilibrium phase is liquid, and below it is vapor.

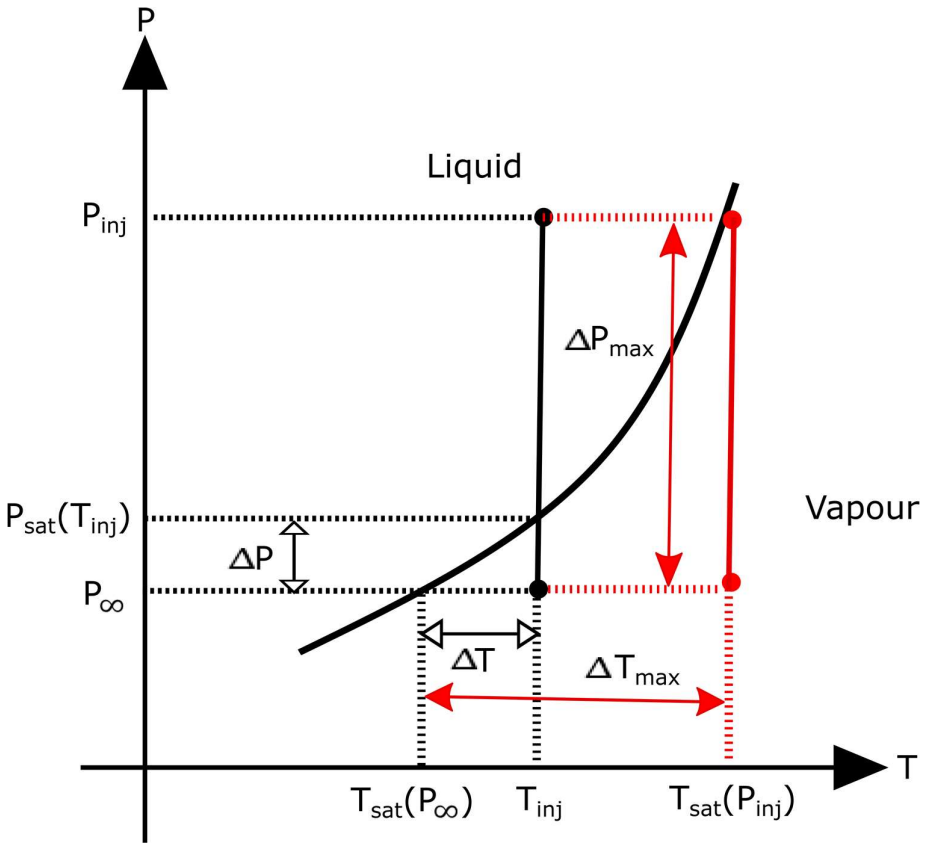

Figure 1-17. Superheated degree in flashing atomization [40].

Flash boiling is taking place when the pressure of superheated liquid (P_{inj}) drops suddenly to ambient pressure (P_{∞}) that is lower than saturation pressure of superheated liquid ($P_{sat}(T_{inj})$). In addition, the liquid temperature (T_{inj}) must be higher than saturation temperature of ambient pressure ($T_{sat}(P_{\infty})$) and also must be lower than saturation temperature of injection pressure ($T_{sat}(P_{inj})$) to avoid evaporation inside the tank. Finer droplets can be obtained under extreme injection pressures (P_{inj}) and a more rapid depressurization that lead to improving the quality of spray. Saury et al. [41], [42] investigated the influence of depressurization rate on flashing spray behavior such as temperature drop of superheated liquid, flashing time and evaporation rate.

When superheated liquid is injected to environment where the stable condition at this temperature is vapor, the unstable condition results in rapid evaporation. In other words, the

superheated liquid is in equilibrium condition and when injected to the environment, the excess energy cannot exist as a sensible energy, therefore it should be converted to latent heat of vaporization. The intensity of this process depends on the degree of superheat that can be defined either by pressure ratio R_p (ratio of saturation pressure to environment pressure) or temperature difference ($\Delta T^* = \frac{T_{inj} - T_{sat,p_\infty}}{T_{sat,p_{injection}} - T_{sat,p_\infty}}$, where T_{inj} is injection temperature, $T_{sat,p_{injection}}$ and T_{sat,p_∞} are saturation temperature at injection pressure and ambient pressure, respectively)

1.2.2 Nucleation types

Pressure-volume phase diagram typical for liquid-gas is shown in Figure 1-18. As can be seen, vapor can be produced either in isothermal decompression process (lines OB) or in isobaric heating (lines OA). In rapid depressurization, when the pressure is dropping and faced with liquid saturation curve, it is supposed that the phase change starts occurring and heterogeneous nuclei are emerging from the nucleation sites (dissolved gas, impurities, and roughness of surface). However, local equilibrium conditions can be achieved without any phase change at pressures lower than saturation pressure in the region which is named metastable zone by controlled laboratory conditions and by minimizing contact between superheated liquid and surface which is shown by gray area in Figure 1-18. In this condition, homogeneous nucleation or bulk motion of nucleation can be achieved by adding even small disturbance and fluctuation to the system which liquid starts to be evaporated explosively. In other words, homogeneous nucleation is associated with molecular process through the body of the superheated liquid and the heterogeneous nucleation is specified with liquid/solid surface interaction on the capillary surface of nozzle [43], [44]. The maximum attainable liquid superheat (boundary between metastable and unstable region) is reached by liquid spinodal curve (dashed line in Figure 1-18)

Furthermore, the homogeneous nucleation rate is noticeably higher than heterogeneous nucleation rate and also time scale for bubble growth in homogeneous case is significantly lower [45]. Sher et al. [46] captured the border between homogenous flashing water and heterogeneous jet and showed how the spray characteristics as well as nucleation rate would change in two regimes. In homogeneous nucleation, tensile force is trying to overcome to the molecular force of superheated liquid [47]. Vieira et al. [48] showed that how superheated iso-octane liquid can experience deep metastable level by imposing extreme low back pressure. Nucleation rate would be increased at high level of superheated degree. The maximum level of superheated degree that can be reached is specified by spinodal line in the pressure-volume thermodynamic diagram. The dp/dv would be zero at this point.

The flash boiling is always taking place somewhere between saturation line and the spinodal line and it depends on initial condition, the purity level of liquid and how fast the process of flash boiling is. Elias et al. [49] presented a model to predict the pressure at the flashing inception point by solving mass and energy equation and also considering bubble nucleation correlation. Empirical heterogeneous nucleation coefficient was defined for considering the effect of impurities and dissolved gases. The difference between saturation and minimum pressure is known pressure undershoot that depends on initial temperature, depressurization rate [50], [51] and also mechanical features of opening [51].

Bartak [52] reported the pressure undershoot data as a function of initial temperature and showed that the initial pressure has no significant influence on pressure undershoot. The author tested varying temperatures ranging from 130 to 300 ^0C and different pressures from 8 to 12.5 MPa. It was showed that for initial temperatures less than 240 ^0C the pressure undershoot would be negligible. Alamgir [53] presented a correlation for the pressure undershoot as a function of initial temperature and depressurization rate. When the pressure of superheated liquid decreased to pressures lower than saturation line, sufficient energy

might be provided by nucleation sites (such as crack and roughness of surface) to pull apart all molecules around the sites until phase change occurred in the liquid.

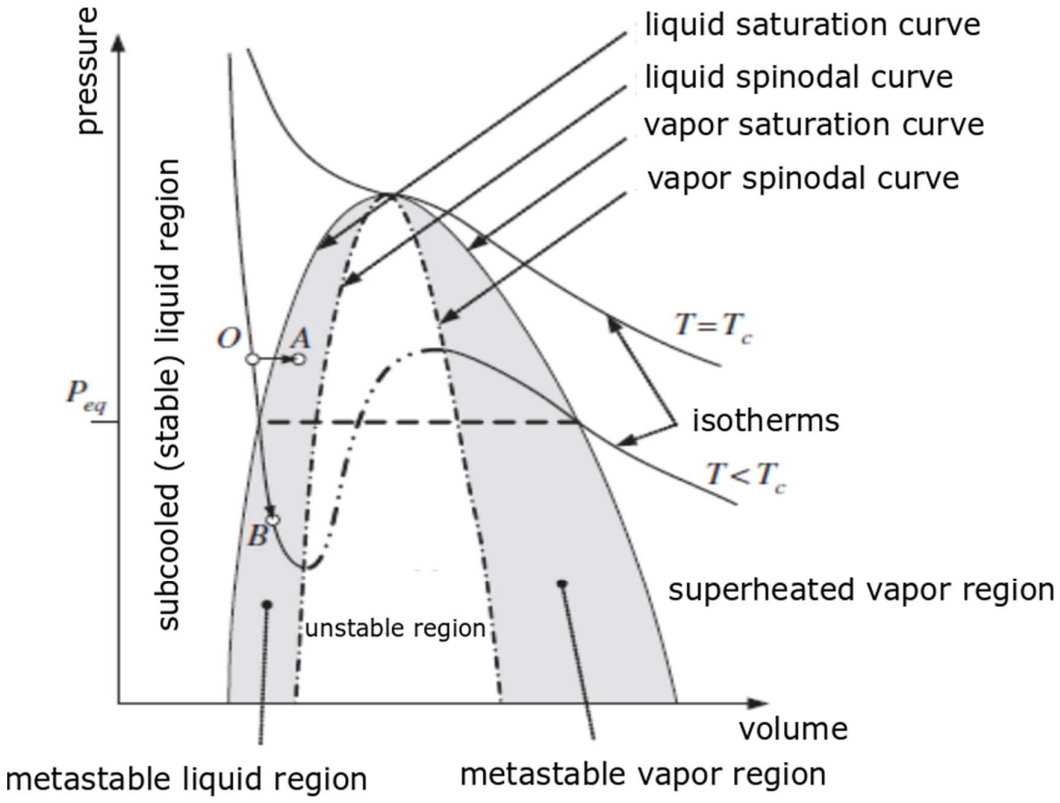

Figure 1-18. Schematics of pressure-volume isotherms for a pure fluid [46].

Based on the initial conditions, level of superheated degree, surface roughness and also the geometry of the nozzle (L/D), heterogeneous nucleation can be produced either on the wall of nozzle (internal flashing) or outside of the nozzle (external flashing). In external flashing that is usually occurring at lower superheated degree and short nozzles, droplets would be rejected from the liquid surface due to interaction between superheated liquid jet and ambient gas. However, in internal flashing, mixture of liquid and nucleation exist at the nozzle exit and it is associated with producing finer droplets and relatively higher spray angle. It has experimentally confirmed that the number of bubble nuclei increased by increasing superheated degree [54]. Reitz [55] studied external flash boiling atomization (with liquid

pressure of 697 KPa, air ambient pressure, temperatures from 300 to 427 K, orifice diameter 0.34 mm, length 1.37 mm) and observed the intact liquid core that drops are expelled from its surface. It was discussed that the length of penetration would be decreased by increasing the level of superheated degree and also mass flow rate would be decreased by increasing temperature. Wirth et al. [56] discussed and showed how internal flow can promote atomization by doing experiments at different pressures and temperatures for two different types of steel nozzle with sharp inlet and glass nozzle with rounded inlet. At the same pressure and temperature, bubble manifested at the exit steel nozzle however external flashing with intact liquid jet can be observed at glass nozzle exit.

1.2.3 Phenomena sequences of FBA

- **Bubble growth**

The vapor bubbles emerging either from heterogeneous nucleation sites or liquid intestinal (homogenous nucleation), which completely explained in the last section. Once the vapor bubbles appear in the superheated liquid, surface tension would be dominant and tries to destroy the nucleation and minimize the distance between molecules. While nucleation size overcomes the critical value which is introduced by Young-Laplace equation [40], [57]–[61] , it starts growing rapidly to remove excess energy from the superheated liquid that finally bursts and releases surface tension for shattering liquid jet into small droplets. Young-Laplace equation is used for equilibrium vapor bubble surrounded by superheated liquid at which a constant pressure would be applied.

$$P_v - P_\infty = \frac{2\sigma}{R_{cr}} \qquad (1-7)$$

In the above equation, P_v is the vapor pressure, P_∞ is the pressure of the surrounding liquid, σ is the surface tension and R_{cr} is the critical radius of vapor bubble. The well-known

correlation which introduces bubble growth in superheated liquid is Rayleigh-Plesset equation that has been used commonly in CFD simulations.

$$R\ddot{R} + \frac{3}{2}\dot{R}^2 = \frac{1}{\rho_l}\left(P_v - P_\infty - \frac{2\sigma}{R} - \frac{4\mu}{R}\dot{R}\right) \quad (1-8)$$

In this equation, the first term from the right hand side ($P_v - P_\infty$) explains the evolution of the bubbles in the superheated liquid. The second term is the contribution of surface tension and the last term shows the adverse effect of viscosity (μ) on bubble growing.

Two parameters of inertia and thermal diffusion at boundary conditions between liquid and vapor control the bubble growth in both cavitation and flash boiling. In cavitation and flash boiling at low level of superheated degree, inertia would be dominant parameter and control bubble growth in liquid. In this situation, vapor bubble is exposed to liquid pressure, vapor pressure inside the bubble and surface tension [62]. However, thermal diffusion compared to inertia, plays a key role in flash boiling especially in high level of superheated degree.

- **Two-Phase flow regimes inside the nozzle**

Different types of two-phase flow patterns such as bubbly, slug and annular flow can be observed inside the nozzle in flash boiling atomization that defiantly impact flashing spray characteristics outside the nozzle (Figure 1-19 and Figure 1-20). In bubbly flow regime, vapor bubbles are dispersed in superheated liquid over the whole nozzle. It takes place at low superheated degree that finally bubbles are growing at the exit nozzle and collapsing in the superheated jet and disintegrating it into ligaments and small droplets. By increasing the rate of generating bubbles at relatively high superheat, bubbles coalescence in the capillary of nozzle may become the dominant process to generate slug flow which has pulsating behavior in the exit nozzle [63]. Under high superheated degree condition, the annular regime can be observed in the nozzle in which there is a vapor core and liquid is formed in the periphery. It was discussed that very similarities can be found between internal flashing atomization and

effervescent atomization where two parameters of void fraction (or ALR) at the exit nozzle and flow state (bubbly, annular, droplet-dispersed, etc.) are important to specify spray characteristics.

Park et al. [64] used relatively long nozzle to investigate internal and external flashing flows at different superheated degree. They observed that bubbly flow is governing inside the flashing jet that associated with long intact core and drops are formed in the surface of the jet (Figure 1-19 a and Figure 1-20 a). It was shown that by increasing the level of superheated degree the drops coalesce to each other and bubbly flow changes to slug flow. The intact liquid core would become shorter in this case (Figure 1-19 b and Figure 1-20 b). However, annular regime would be in high superheated degree that generated uniform spray with fine droplets (Figure 1-19 c and Figure 1-20 c). This regime is taking place in flow with high superheated degree and also flow in long nozzles with low pressure that gives bubbles sufficient time to coalesce each other's. They used two nozzles with different aspect ratios (L/D) 29 and 7.27 to measure droplet size and spray angle. They observed that droplet size would be diminished by increasing the length of nozzle and spray angle increased because more nucleation would be activated in the long nozzle.

Nucleation starts manifesting at earlier distance in high initial temperature that there would be sufficient time for growing bubbles in this situation and bubble coalescence may take place to change bubbly regime to slug and even annular regime. Therefore, it would be obvious that evaporation rate is increased by increasing initial temperature and by changing bubbly flow to slug and annular flow in which collapsing flashing jet would take place more violently. Fine spray can be obtained in the annular regime [65].

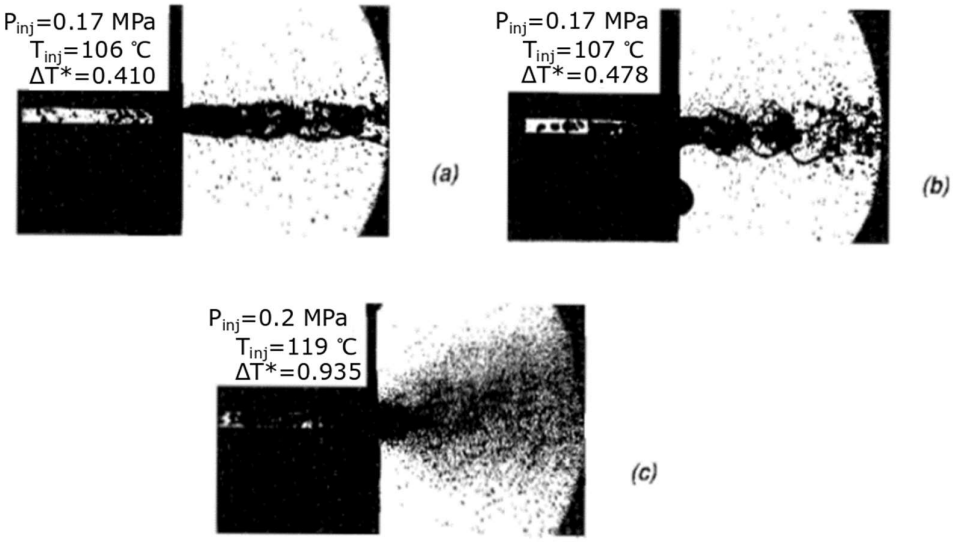

Figure 1-19. Different two-phase flow regime before exit; (a) bubbly flow; (b) slug flow; (c) annular flow [64].

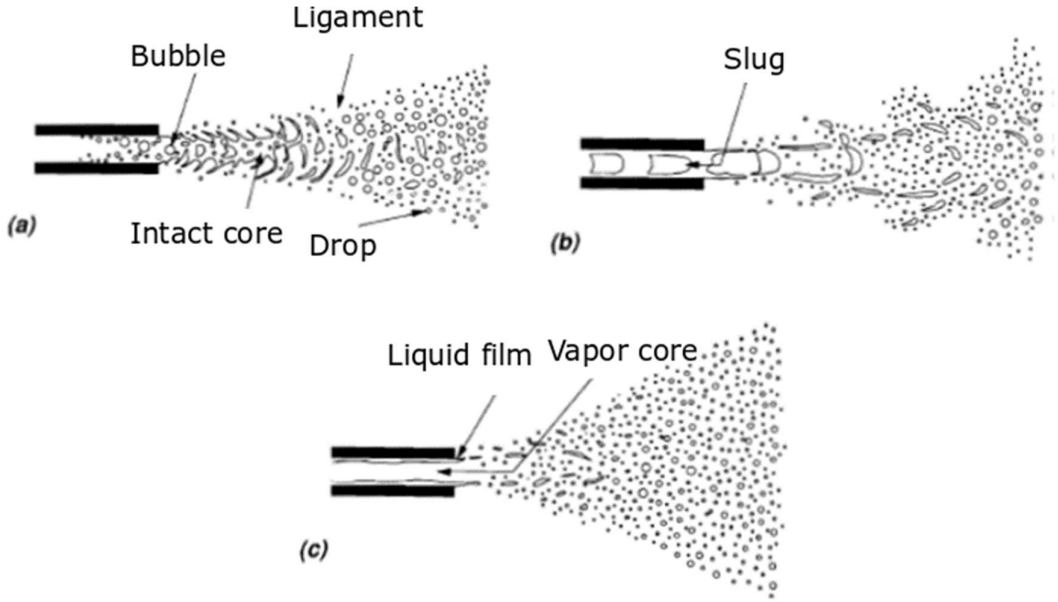

Figure 1-20. Different two-phase flow regime before exit; (a) bubbly flow; (b) slug flow; (c) annular flow [64].

- **Different breakup regimes outside the nozzle**

It was verified that by increasing the degree of superheat, flash boiling atomization would be enhanced. Gunther et al. [43] investigated the effect of fluid temperature on spray morphology at nozzle outlet. Figure 1-21 illustrates variation of flashing spray pattern with

increasing superheated degree for liquid water. At no superheating condition (T=25℃), no liquid breakup takes place. By increasing the temperature to higher than boiling point of ambient pressure, flash boiling can be observed even at low level of superheated condition (110-120℃). However, jet disintegration and evaporation rate is increased noticeably at temperature 130℃ and extremely violent breakup were observed at high level of superheated degree (150℃). Additionally, as demonstrated at a temperature of 110 ℃, it is observed that the broader the spray becomes with increased superheating.

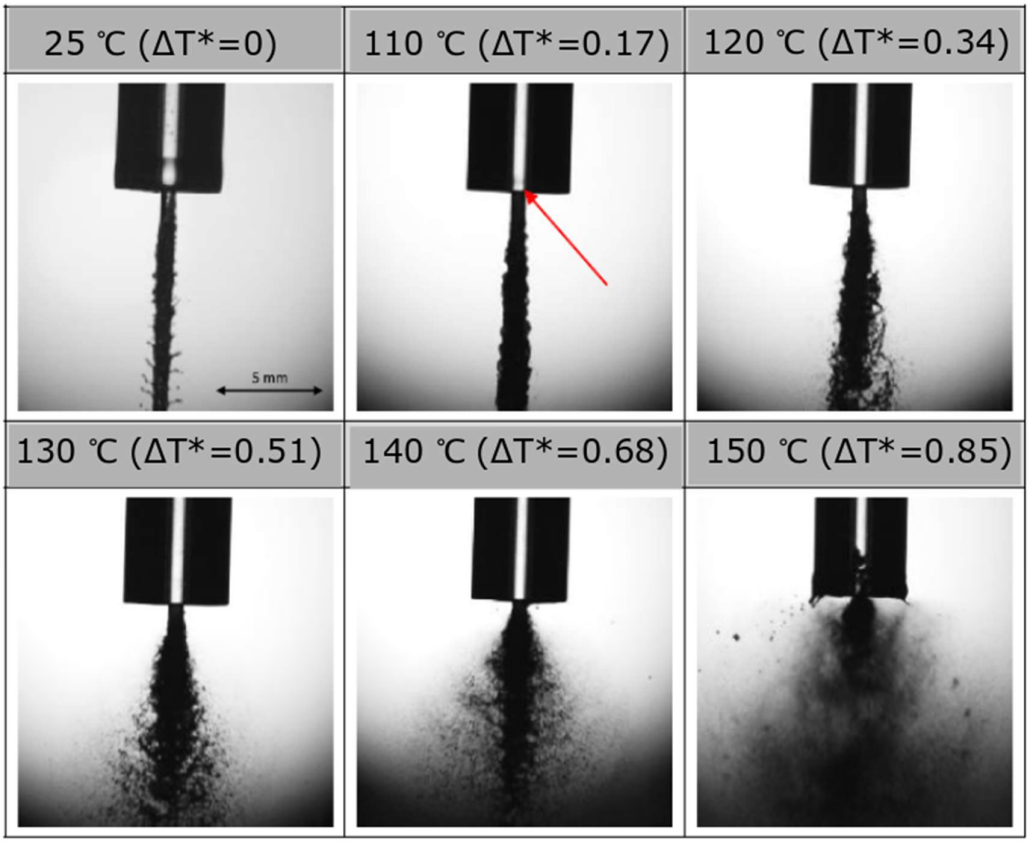

Figure 1-21. Spray structure at nozzle exit. $P_{inj} = 6\ bar$; Glass nozzle; $L/D = 20$; D=0.9 mm [43].

In flash boiling atomization, two processes of aerodynamic instability on surface of superheated liquid jet and thermodynamic instability in liquid are dominant phenomena in disintegrating jet to finer droplets [66]. The three breakup regimes, mechanical breakup, transition regimes and fully flashing atomization are known at the nozzle exit in flash boiling. At low level of superheated degree, the mechanical breakup would be dominant. In this kind

of breakup, at critical wavelength, the disturbance on the liquid surface tends to be increased which results in the detachment of small droplets from the liquid surface. When the superheated degree is increasing, both mechanical and thermal instabilities could be comparable and transition regime is taking place. However, fully flashing atomization can be seen in high superheated degree where bubble growth control the flashing jet. Moreover, by increasing the level of superheated degree, the intact liquid core which is clearly visible in mechanical breakup would be narrow and diminished completely in fully flashing atomization because the liquid already evaporated inside the capillary of the nozzle.

Weber number (We) and Jakob number (Ja) (which is defined as the ratio of sensible heat that is available to latent heat during the phase change h_{fg}) are appropriate parameters to find the transient between these regimes. It was verified that flash boiling commences (transient regime) at [66]–[69]:

$$Ja\varphi = 55We^{-1/7} \qquad (1-9)$$

With

$$\varphi = 1 - \exp(-2300(\rho_v/\rho_l)).$$

Also, the complete flash boiling starts at:

$$Ja\varphi = 150We^{-1/7} \qquad (1-10)$$

Therefore, it is obvious that by increasing Weber number the level of superheated degree for transient from mechanical breakup to transient regime and from transient to flashing breakup would be decreased. Lamanna et al. [66] showed the transition threshold from mechanical breakup to fully flashing at different levels of superheated degree. It was discussed that high spray angle (even higher than 160 ℃) can be observed due to fully flashing atomization however it cannot exceed 20℃ by considering aerodynamic framework solely. Their result

for flashing superheated acetone at different levels of superheated degree R_p is shown in Figure 1-22.

Corn et al. [70] identified three regimes of shear-atomized (mechanical breakup) with intact core which is approximately equal to orifice diameter, transient and fully flash atomization in the case of injecting superheated fuel jet into an unheated crossflow of air. They discussed that the crossflow result in bending and flattening of jet in mechanical breakup. In this condition, surface wave emerges and grows until primary breakup is taking place.

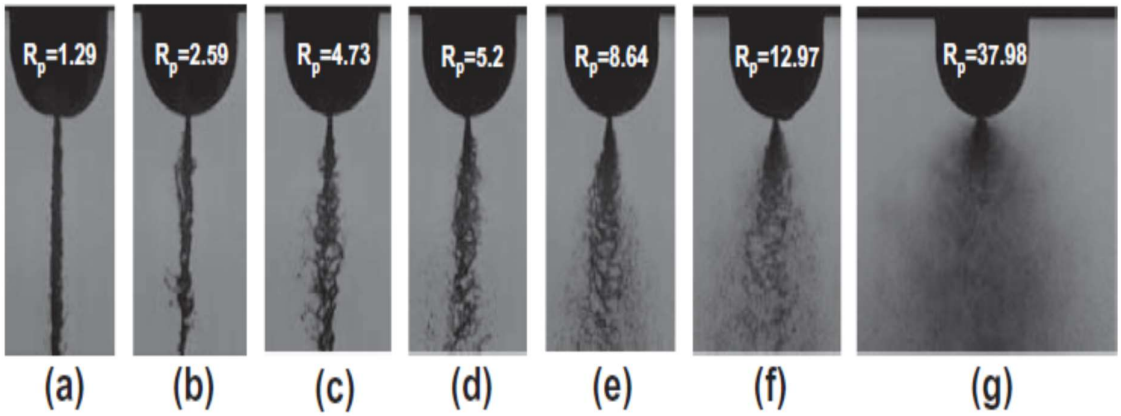

Figure 1-22. Variation of spray pattern with increasing superheat: (a) mechanical breakup; (b-d) external flashing; (e-f) transition regime; (g) fully flashing mode [66].

They defined a critical temperature (240 ℃) for transient between a shear-atomized to a transient regime for fuel Jet-A. In the viewpoint of mechanical breakup, the flow velocity in the nozzle exit is proportional to square root of pressure difference between sources and ambient, therefore Reynolds number would be increased and flow may be turbulent in high pressure difference. Consequently, turbulent flow especially at liquid surface can promote collapsing liquid jet to ligaments and small droplets. They observed that the penetration would be decreased significantly in transition regime in comparison with shear-atomized regime. They also illustrated the spray penetration as a function of axial distance for two shear-atomized and flash–atomized spray. In addition, they showed the droplet SMD, axial velocity for two temperature 309 K and 505 K fuel jets in shear-atomized regime.

1.2.4 Spray characteristics of flash boiling atomization

Flash boiling atomization is associated with the specific characteristics like large spray angle, low penetration depth, fast evaporation, large momentum transfer and fine droplet that would be useful in different fields of liquid atomization [71]. These characteristics have been measured by many researchers to better understand the behavior of this phenomenon.

- **Droplet size distribution**

The droplet size distribution has been studied by many researchers experimentally and theoretically. It was seen that droplet size can be a function of many parameters such as initial condition (pressure and temperature), the level of superheated degree, the roughness and the geometry of nozzle. It also can be varied at different axial and radial distance from the nozzle exit. It is demonstrated that the size of droplet that is generated in flash boiling is inversely proportional to level of superheated degree [45]. In addition, it was shown that the droplet size decreased by decreasing the ambient pressure and also increasing the injection pressure [71].

Gunther et al. [43] investigated the droplet size in glass nozzle and steel nozzle and discussed that larger droplet can be seen in glass nozzle with smaller roughness, therefore less evaporation rate with lowered jet disintegration and fragmentation are corresponded to glass nozzle. Shen et al. [72] showed that larger fuel droplets can be found further away from the exit nozzle because of the collision and coalescence of the droplets. In addition, more uniform and smaller fuel droplets were seen in more intensified flash boiling. Yildiz et al. [73] investigated the effect of pressure, temperature, orifice diameter and aspect ratio (l/d) on mean droplet size (D_{10}, D_{32}) of R134A completely. They evaluated droplet size distribution at different axial and radial direction and showed larger droplet can be seen in the center of jet comparison with periphery and also in further distances from the nozzle exit. They observed that by increasing temperature the droplet size would be decreased dramatically and

also become mono-dispersed. They also concluded that by increasing aspect ratio (L/D) the droplet size would be decreased.

- **Droplet velocity**

Droplet velocity is an important characteristic usually reported by researchers. Gunther et al. [63] measured droplet velocity at the center of spray in different distance from the nozzle outlet for two glass and steel nozzles. By increasing the superheated degree, the evaporation rate would be intensified and driven droplets would be at higher velocity. They reported droplet velocity of water for glass and steel nozzle at temperature 130 and 150 ℃ and pressure 5 bar as a function of distance from the spray axis. It was discussed that the droplet velocity would be decreased by further radial distance. Allen [74] employed Laser Doppler Anemometry (LDA) to measure the velocity of flashing propone at different axial and radial distance. He observed that the droplet velocity would be decreased by further distance from exit nozzle and also Gaussian manner was seen in radial direction which means maximum velocity is taking place in the centerline and decreased with further distance from centerline. Calay et al. [75] investigated the droplet velocity numerically as a function of axial distance from exit nozzle and showed velocity would be decreased sharply at closer distance from nozzle. Levy et al. [45] showed temperature can enhance droplet velocity.

- **Spray angle**

Level of superheated degree, pressure injection and configuration of nozzle are important parameters that affect the jet angles [76]. It would be increased in the dense nucleation concentration. Moreover, high spray angle can be seen in the high level of superheated liquid jet where phase change usually occurred violently [40], [46], [73], [76]. Zuo et al. [77] discussed that high spray angle is corresponded to sudden phase change and rapid depressurization of superheated liquid at the nozzle exit. Sher et al. [46] investigated the spray angle of flashing water jet in two different regimes of homogeneous and heterogeneous.

They observed that spray angle would be increased by enhancement of pressure and temperature. It was observed that spray angle was reduced in homogeneous case. Lamanna et al. [66] studied the spray angle as a function of axial distance, back pressures and superheated degree for different fluids. High level superheated degree corresponds to high nucleation rate and wider spray angle. Most of the work mentioned above pertains to pure water. Further investigation is necessary to explore suspensions and show the potential differences in these parameters between pure water and suspensions.

1.3 Objectives

The main goal of this study is to apply flash boiling atomization (FBA) as a new method of suspension injection in suspension plasma spraying (SPS), in order to inject suspension with high solid content to fabricate SPS coatings. The objectives of this thesis are as follows:

- Experimental and analytical studies of FBA for suspension to investigate the important parameters affecting the spray of the suspensions
- Development of a versatile FBA system to inject suspension into plasma spray process
- Development of SPS coatings with FBA technique and investigate its advantages in terms of coating properties and process efficiency.

1.4 Thesis organization

This thesis is organized into six chapters. Each chapter is briefly explained herein. Chapter 1 discusses the fundamental phenomena associated with SPS, different coating microstructures which are in SPS, different current suspension injection techniques in the SPS and the current limitations for the SPS. Afterwards, this chapter provides the fundamental concepts of FBA such as thermodynamic concepts which are relevant to FBA and all phenomena sequences

associated with FBA. In addition, a literature review for SPS and FBA were done in this chapter. At the end, the research objectives and thesis structure are presented.

Chapter 2 provides a detailed explanation of the experimental methodology used in this study. This includes the injection setup, visualization measurements, suspension, and coating characterization. The chapter also discusses technical and safety issues related to the FBA setup.

Chapter 3 investigates the preliminary results and observations of the FBA of titanium dioxide suspension. The effect of experimental conditions such as injection temperature and solid concentrations on spray structure were investigated. The FBA process was explained completely in the T-S diagram and some experimental studies were done to investigate the isentropic assumption for FBA. The results of this chapter, especially the spray structure for suspension, are very useful and vital to design a novel experimental injection setup for SPS to generate coatings by using FBA.

In Chapter 4, the FBA technique has been implemented as a new method of suspension injection in SPS, to fabricate coatings. The coating properties were compared with conventional coatings generated with mechanical injection. This chapter presents that FBA method enables the injection of suspensions with high solids concentration (up to 70 wt.%). The effect of different solid concentrations on coating thickness per pass, deposition weight per pass and coating microstructure were investigated.

In Chapter 5, the effect of power torches were examined on coating properties. At high solid concentration (70 wt.%), the coating microstructure is switched from high pores coating for low power torch of 33 kW to very dense coating for high power torch of 110 kW. The results of XRD analysis for all generated coatings were presented in this chapter. The anatase percentage varied from 35.7 to 66.9% based on power torches and solids concentration. The

typical thickness per pass in SPS is 1.5-2 μm, however, high thickness per pass up to 14 μm can be obtained by applying FBA method and using suspension with high concentration and at high power torches. In addition, the typical deposition efficiency for SPS is low and is between 15-20%, however, high deposition efficiency up to 60% can be achieved by using FBA technique and in the case of using suspension with high feedstock concentration in water (>55 wt.%) and with high power torches.

Chapter 6 summarizes the findings, conclusions and contribution of this work and presents further recommendations for the future research.

2 Chapter 2: Experimental methodology

The main objective of this chapter is to provide a detailed description of the experimental procedure employed in this work. The experimental methodology has been divided into three sections, including the injection setup, suspension and coating characterization, and, lastly, visualization measurements.

2.1 Injection setup

In this project, the primary setup was designed to increase the suspension temperature to superheated conditions, resulting in flash boiling atomization outside the nozzle. This primary setup is depicted in Figure 2-1. A 6-liter reservoir was specifically chosen for the experiment to withstand the necessary pressure and temperature requirements. This pressure vessel was bought from Cole-Parmer and is made from 316 stainless steel, capable of withstanding a maximum pressure of 125 psi (0.82 MPa) and a maximum temperature of 149 °C. When conducting experiments involving suspension, the container was placed on a magnetic stirrer table (1) to maintain continuous agitation using a magnetic stirrer (Thermo Fisher Scientific, USA). This method prevented sedimentation and minimized the production of agglomerations during the experiments as much as possible.

To achieve suspension superheating, two heaters were employed: a blanket heater (2) and an immersed heater (3). The blanket heater was a silicone heating blanket with a controller, which was wrapped around the surface of the pressure vessel. This blanket heater had a power of 720 watts and was also bought from Cole-Parmer company. To aid in the heating process, an additional immersed heater was added into the setup. This heater was a compact screw-plug immersion heater made from 316 stainless steel, securely screwed to the female outlet of the pressure vessel. The male thread type was NPT with a size of 1/4, matching the female outlet size of the pressure vessel. This heating element had a power of 250 watts and was obtained from McMaster-Carr company.

To continuously monitor the suspension temperature, a threaded thermocouple probe (5) was threaded into the female outlet of the pressure vessel. This thermocouple has an NPT male probe with a 1/4-inch connection, matching the female size of the pressure vessel. It's a K-type thermocouple with an accuracy of ±0.75% and can display temperatures up to 900℃. This thermocouple was connected to a thermometer for real-time temperature monitoring and was bought from McMaster-Carr.

To pressurize the tank, a pressure line was connected to the pressure vessel. Initially, a threaded on/off valve was securely screwed to the female outlet of the pressure vessel, and then a high-temperature push-to-connect fitting was used to connect the pressure line tube to the valve. The male part of the push-to-connect was threaded into the female section of the valve, while the releasing ring part of the push-to-connect was connected to the pressure line tube. It's crucial to emphasize the importance of using a high-temperature push-to-connect capable of withstanding temperatures up to 150 ℃ for safety reasons. In the course of the experiments, injection pressures ranging from a minimum of 0.27 MPa to a maximum of 0.68 MPa were tested with this experimental setup. It is vital to note that maintaining the injection temperature below the saturation temperature of the injection pressure is very important for safety reasons. Failure to do so could result in the suspension undergoing evaporation inside the tank, potentially leading to extremely unsafe conditions.

Whenever a superheated suspension reached a desired temperature, it should be directed to the nozzle for injection. So, one female outlet of pressure vessel should be allocated for superheated suspension. For this purpose, initially, a threaded on/off valve was securely screwed to the mentioned female outlet of the pressure vessel, and then a high-temperature push-to-connect was used to connect the flexible plastic tube to the female section of valve. It is worth to mention that all tube that are used for this experimental setup has specific features. They are transparent, semi-flexible and can tolerate temperatures up to 200 ℃.

These specific tubes were provided from McMaster-Carr company. To connect the tube to the threaded male nozzle, first tube should be connected to the push-to-connect and then the 316 stainless steel threaded connector was used to connect the male part of push-to-connect to the male section of nozzle.

It is worth mentioning that high-density thread sealant tape was used to cover all connection to avoid penetration of air to the suspension. This specific tape can tolerate high temperature up to 200 ℃ and was bought from McMaster-Carr company. Using regular tape for this setup can bring safety issues that regular tape may be melted at operated temperatures. The entire exit line from the valve on the pressure vessel to the nozzle was insulated with pipe insulation capable of withstanding temperatures up to 260°C. In this experimental setup, a stainless steel spray nozzle with a full cone condition was used, featuring various nozzle sizes: 0.1 mm, 0.15 mm, 0.2 mm, and 0.3 mm. The length of the nozzle is approximately 1.25 mm, and these types of nozzles were supplied by YBS Co., Ltd company.

There are several advantages and disadvantages to this experimental setup. The first limitation is that it takes 2 or 3 hours to reach the superheated temperatures because the entire setup, including pressure vessels and all connections, must be heated. The second limitation is that the superheated suspension cannot be measured by a flowmeter because passing superheated suspension through the flowmeter cools it down, and there are only a few flowmeters that can work at these high operating temperatures. However, the most significant advantage of this setup is its high level of controllability regarding injection temperature. The suspension temperature increases slowly, and it is possible to start the experiment at any exact temperature. This experimental setup was used to capture the spraying structure by using the high speed camera (7) and LED light (8).

One technical aspect of this setup is that there are four female exits on the pressure vessel, while there are five items that need to be connected (inlet pressure line, heater, thermocouple,

pressure relief valve, and exit line). To address this issue, a tee adapter (comprising one male part and two female sections) was employed to create an additional female space. The thermocouple and pressure relief valve were then connected to these additional female parts.

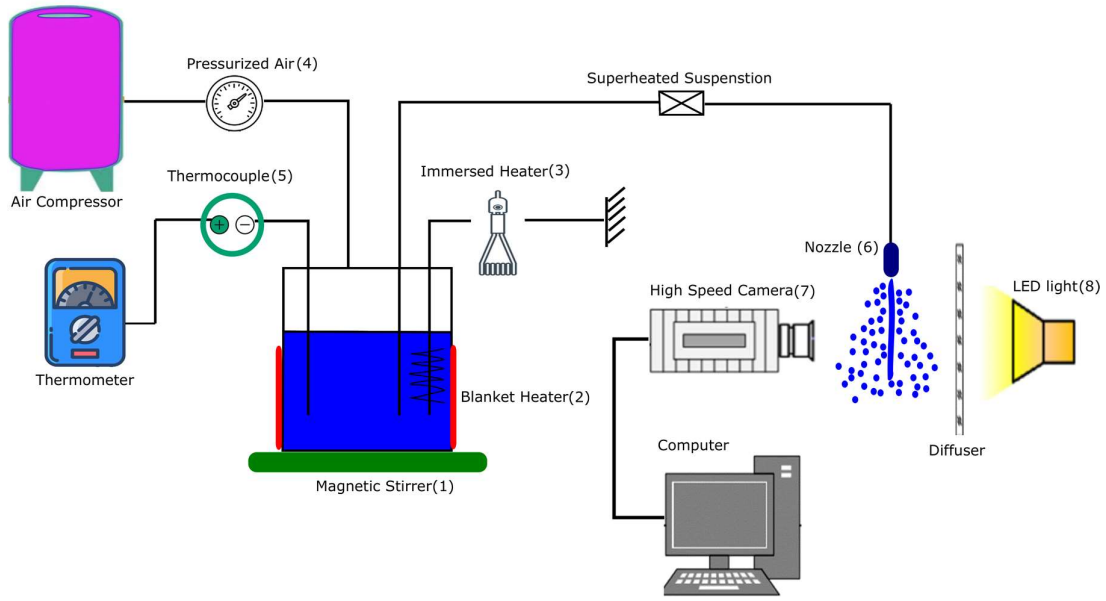

Figure 2-1.Schematic of the primary experimental setup.

Another experimental setup was designed for injecting suspension into the plasma jet for Suspension Plasma Spraying (SPS) (see Figure 2-2). Measuring the suspension flow rate is crucial in SPS, and it posed a limitation in the previous setup. Additionally, the experiment time can be significantly reduced from 2-3 hours to 10-15 minutes because the suspension is heated in-line instead of heating the entire suspension in a pressure vessel.

There are two pressure vessels, one for water (1) and the other for suspension (2). Since the water and suspension are maintained at room temperature, there is no need to use high-temperature push-to-connect fittings or specific high-temperature tape. Throughout the experiment, the pressure vessel for suspension was always placed on a magnetic stirrer table (3), which helps ensure a more uniform suspension and reduces the likelihood of agglomeration. The experiment begins with water, and once we reach the desired high

temperature (140°C) and observe the desired flash boiling spray, we switch the three-way valve (4) to the suspension direction, allowing us to introduce the suspension into the line. This approach minimizes suspension wastage. The injection pressure (5) is set at 0.69 MPa, which is the maximum operating pressure that the pressure vessel can withstand. Higher pressure enables us to achieve higher injection temperatures because, in flash boiling atomization, the temperature must exceed the saturation temperature of ambient temperature (100°C) while remaining below the saturation temperature of the injection pressure. Therefore, higher injection pressure allows us to attain higher injection temperatures.

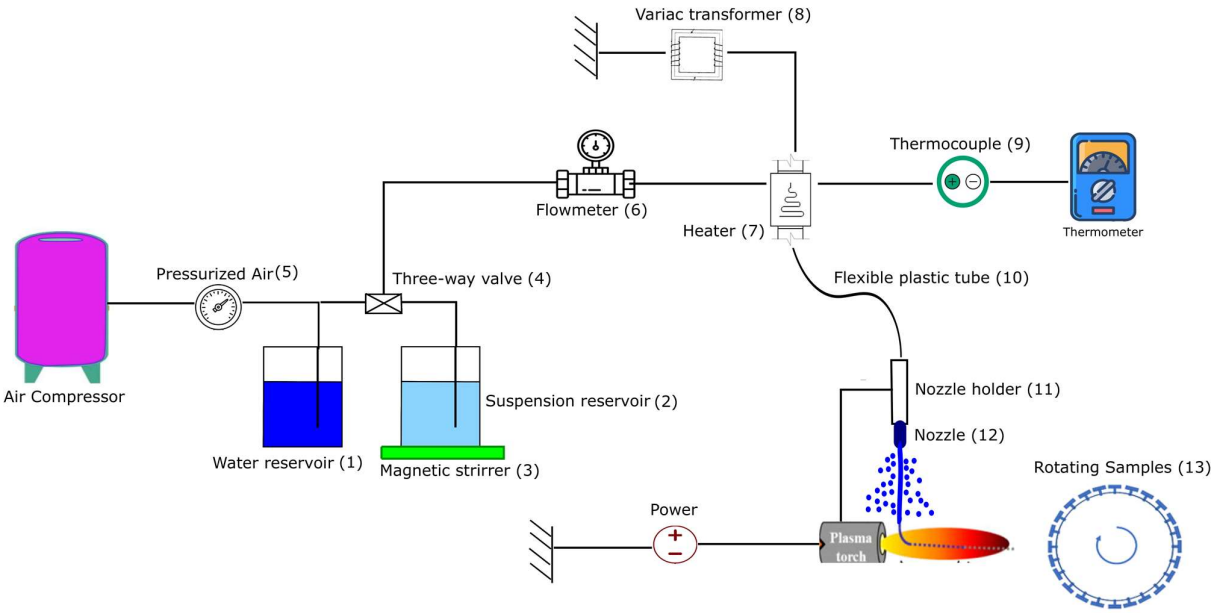

Figure 2-2. Schematic of the experimental setup for SPS.

The cooled suspension, before entering the inline duct heater, passes through a Coriolis flowmeter (6). It is then directed into the duct heater (7), constructed from 316 stainless steel and with a power rating of 1200 W, capable of withstanding temperatures up to 420 °C. This heater was purchased from the Omega company and is depicted in Figure 2-3. The duct heater is securely positioned near the plasma torch using strut channel, which is located at the top of the air ventilation system. To connect the heater to the strut channel, a metal ring was

placed on its outer surface. This heater is not directly plugged in; it is first connected to a Variac transformer (8), which gives us the ability to adjust the heater's power and, as a result, enables us to control the suspension temperature.

Figure 2-3. The inline duct heater.

To connect the tube to the inlet heater, a female-female straight reducer (3/8 inch to 1/4 inch) was threaded onto the male inlet of the heater. We used a high-temperature push-to-connect fitting to connect the suspension line to the adapter. At the heater's outlet, the suspension would reach temperatures of up to 140 ℃. To measure the suspension temperature, we installed a thermocouple at the heater outlet. To transport the superheated suspension, we used a right-angle tee adapter, which includes one male and two female connections. A male part was screwed to the female outlet of heater and one female was dedicated to the thermocouple (9), and the other female was used for the superheated suspension. We used threaded thermocouple probes (type K) in this experiment, capable of operating at temperatures up to 400 ℃, which were purchased from McMaster-Carr. Additionally, we utilized a flexible, high-temperature plastic tube (10) to direct the superheated suspension to the nozzle holder placed on a robotic arm. It's essential to keep this tube as short as possible to prevent cooling the superheated suspension and ensure it's adequately insulated. This tube should be connected to the nozzle, and a nozzle holder can then attach the nozzle to the torch. We couldn't use a long tube to give the robot's movement for full substrate coating, so we

kept the robot arm stationary, used the shortest possible tube for the superheated suspension to prevent cooling, and positioned rotating samples (13) directly in front of the plasma torch. The six stainless steel samples with size 50×25 mm were first blasted with 80 grit aluminum oxide particles (160 μm particle size) and then attached to the rotating samples.

Another experimental setup was designed to obtain coatings with full cover of substrates. This setup has been illustrated in Figure 2-4.

Figure 2-4. The redesigned experimental setup to generate coatings with full cover of substrate. (a) redesigned setup (b) coating covering the substrate completely .

The plasma torch was removed from the robot and fixed in one position with structural framing. The sample holder was attached to the robot instead the plasma torch. The smaller stainless steel substrates with size of 25×25 mm has been used in this experiments. The robot starts from the left of the torch and there are two movements from left to right for each pass.

In addition, another experimental setup was designed to thermodynamically study flash boiling atomization (Figure 2-5). This setup allows us to measure the inlet flow rate using a flowmeter (3), the atomized liquid flow rate (the amount of liquid that would be collected by a collector) (8), and thus the difference is the vapor generation rate. These parameters are crucial for determining the final position of the flash boiling atomization process on a temperature-entropy diagram. Pure water was used for these thermodynamic measurements

because a large amount of liquid (approximately 6 liters) is required to obtain measurable vapor, and it would have been challenging to prepare and superheat this quantity of suspension. In this experimental setup, a duct heater (4) was installed through the line before the injection system to increase the liquid temperature and create a superheated stream. The liquid temperature was continuously measured by a thermocouple (5) located at the outlet of the heater.

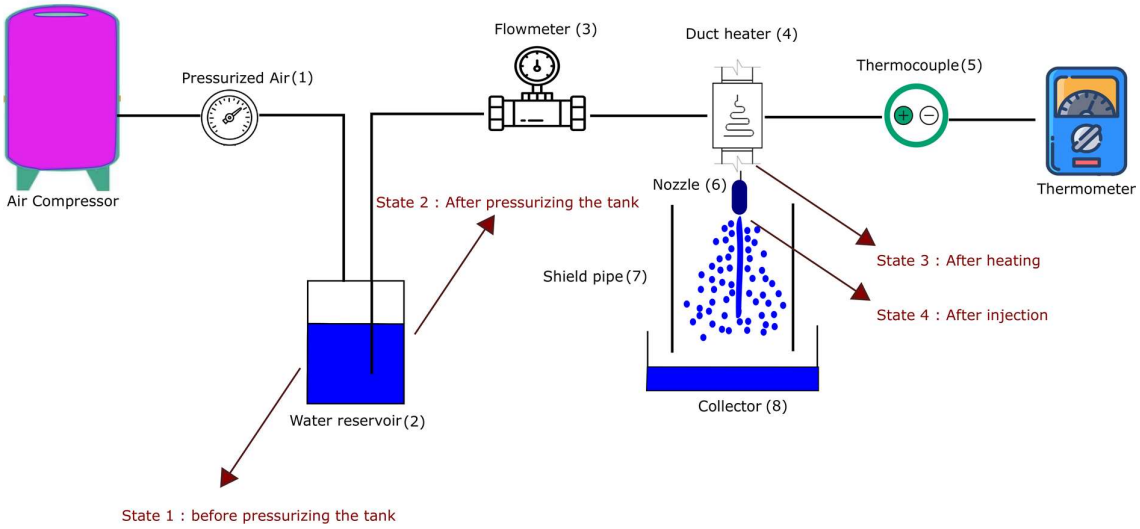

Figure 2-5 The experimental setup for thermodynamic measurements.

A variac transformer was connected to the duct heater to adjust the heater output anywhere from 0% to 100% load. The injection temperature was controlled by changing the transformer percentages. The flash atomization process can be divided into 4 states, all of which are explained in a temperature-entropy diagram presented in the next chapter.

2.2 Visualization measurements

Shadowgraphy is a valuable technique that was used in this research for capturing and analyzing flash boiling spray in various experimental conditions (Figure 2-6). By using this technique, we can provide insights into flash boiling spray characteristics like approximate droplet size, velocity and spray structure. By projecting a light source through the spray and capturing the resulting shadows with a high-speed camera, we can analyze the dynamics of

the spray, monitor the interaction of droplets with the surrounding environment, and optimize spray parameters for designing an efficient setup for suspension plasma spraying application. A 120 W LED light was used for illumination that was purchased from Delta Photonics company and a diffuser paper was placed in front of a light source to create uniform and diffused light. A Photron SA1.1 high-speed camera (Photron, California, USA), operating at 5000 frames per second (fps), was employed to capture the flash boiling spray. The minimum exposure time of 1 μs was used to capture the highest-quality image of the flash boiling spray, and the camera has a resolution of 1024×1024.

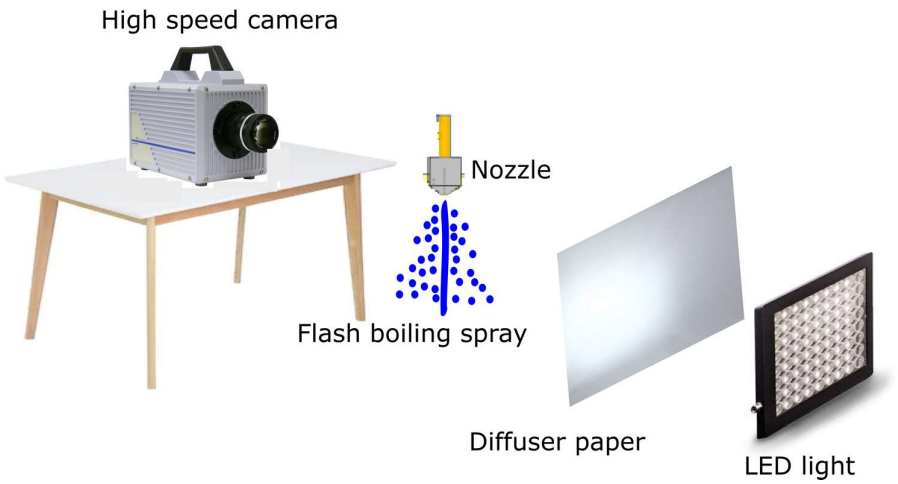

Figure 2-6 Experimental setup for the shadowgraph of the flash boiling spray.

In our experiments for fabricating coatings, an Accuraspray 4.0 sensor (Tecnar Automation Ltd., Canada) was utilized to monitor the trajectory and also measure the velocity of in-flight particles during spraying. We also used Accuraspray 4.0 to measure the in-flight particle temperature. However, we got unrealistic answers for in-flight particles temperature. It is important to note that the Accuraspray particle temperature measurements for radial injection SPS process are not typically accurate since the point of measurement (spray distance) falls within the plasma jet, which is a significant source of optical noise. As can be seen in Figure 2-7, the Accuraspray 4.0 device fixed in one position with structural framing that is perpendicular to the plasma spray axis.

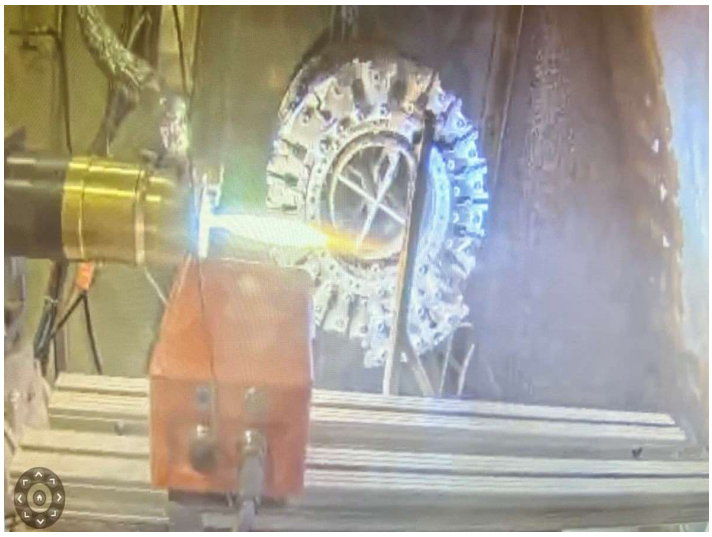

Figure 2-7. Measuring the velocity of in-flight particles with Accuraspray 4.0.

2.3 Suspension and coating characterization

In this study, suspensions with different solid concentrations (20%, 40%, 55%, and 70 wt.%) were utilized to fabricate TiO_2 coatings. The suspension contained commercial submicron-sized TiO_2 (TKB Trading, Oakland, CA) with an average particle size of 500 nm in deionized distilled water. It was prepared by magnetic stirring for various durations ranging from 30 minutes to 2 hours, depending on the suspension concentration. Simultaneously, the powder was dispersed using a 50 W sonicator. No dispersing agent was used in the suspension preparation.

It's worth mentioning that preparing a suspension with 70 wt.% can be challenging. The powder should be added to deionized water slowly, and the sonicator power should be increased gradually, in a few steps from 50 W to 80 W, to break down large agglomerates and ensure effective mixing.

Additionally, a Scanning Electron Microscope (SEM) S3400 from Hitachi, Japan, was employed to investigate the microstructure of the deposits at an accelerating voltage of 15 kV. SEM images were captured at various magnifications, ranging from 500x to 20,000x.

Moreover, the ImageJ software was used to assess the porosity of the deposits and to calculate the proportion of different regions within the deposits by generating binary images. The SEM images at 500x magnification were specifically utilized for porosity measurements.

3 Chapter 3: Investigation of flash boiling atomization of titanium dioxide suspensions

3.1 Objective

In this chapter, flash boiling atomization of titanium dioxide suspension has been investigated. The results of this chapter provide us with a better understanding of the FBA process, assisting in the successful design of an FBA system in the thermal spray laboratory or the fabrication of SPS coatings using the FBA method. In this chapter, we will discuss the flash boiling atomization process on the T-S diagram, providing us with fundamental insights into FBA. We focus on injecting superheated aqueous titanium dioxide (TiO_2) suspensions, which consist of sub-micron particles at varying concentrations, into atmospheric air. The choice of an aqueous TiO_2 suspension is based on its sustainability, accessibility, and cost-effectiveness. Additionally, we investigate and compare the effect of injection temperature on the spray structure of both the suspension and pure water.

3.2 Thermodynamics of flash boiling process

Flash boiling atomization can be analyzed as either an isenthalpic process or an isentropic phenomenon. However, this phenomenon is typically considered an isenthalpic process rather than an isentropic one. This means that during flash boiling, the enthalpy of the fluid remains constant, but the entropy may change due to the phase transition from liquid to vapor. Isenthalpic processes occur at constant enthalpy, ensuring that the total energy of the system remains constant throughout the process. To conduct a more accurate analysis with an isenthalpic assumption for flash boiling atomization, it is required to allow sufficient time to reach equilibrium conditions, usually by using a high L/D nozzle. However, in cases where there is not enough time to reach equilibrium conditions, such as pipe rupture carrying superheated liquid or a nozzle with low L/D, flash boiling atomization can be characterized as an isentropic process rather than an enthalpy constant phenomenon. In this case, flash

boiling happens quickly without time for heat transfer. In this research, it was assumed that flash boiling atomization is an isentropic phenomenon.

The flash boiling atomization process is sketched on the T-S diagram to gain a deeper comprehension of this phenomenon and the vapor mass fraction of the spray was attained from T-S diagram by considering an isentropic assumption for flash boiling atomization. In addition, the produced vapor mass fraction was obtained experimentally to verify the isentropic assumption for flash boiling. Pure water was used for this part, for greater simplicity and accuracy. Figure 3-1 shows a schematic representation of the flash boiling atomization process in a temperature-entropy (T-S) diagram. The operating state of the tank before pressurization was considered as state 1. Process 1-2 is an isentropic compression from the atmospheric pressure to the maximum pressure (here the absolute pressure is 650 kPa). In reality, the points 1 and 2 are very close and almost coincide with each other, but it has been exaggerated in the figure in order to show the process 1-2. The amount of specific work required for this compression is $w_{12} = h_2 - h_1$ (h is the specific enthalpy). The high-pressure water then passes through the flowmeter to measure the flow rate. The state of the water before entering the duct heater is equal to state 2, because it was assumed that the pressure loss through the pipe is negligible.

Process 2-3 is an isobaric heating process in which the liquid temperature increases from room temperature to the maximum temperature. The power of the heater is controlled by a transformer to obtain different injection temperatures and the temperature is continuously monitored by a thermocouple at the end of the heater. The $Q_{32} = h_3 - h_2$ is the amount of specific heat required to obtain the superheated state. State 3 (superheated liquid) has the higher entropy level in the T-S diagram compared to state 2 (non-superheated liquid). The increase in entropy during this heating process can be explained by Maxwell's equation:

$$Tds = dh - T\left(\frac{\partial V}{\partial T}\right)_p dP \qquad (3-1)$$

The pressure loss in the duct heater was assumed to be negligible, so the last term in Eq. 1 considered to be zero. Also, dh can be replaced by $C_p dT$. This simplified the equation to the form:

$$ds = C_p(dT/T) \qquad (3-2)$$

If C_p is assumed to be constant as the liquid temperature increases, the entropy changes during the heating process (from state 2 to 3) can be obtained by taking an integral from Eq. 2:

$$S_4 - S_3 = C_p \ln(T_4/T_3) \qquad (3-3)$$

At stage 3, the superheated water enters the capillary area of the nozzle where the steam bubbles begin to appear on the nozzle wall. These bubbles rapidly expand from high pressure to atmospheric pressure. The bubble growth converts the excess energy of the superheated water into the latent heat of vaporization. Process 3-4 was assumed to be isentropic expansion because the flash boiling process in our experiments leaves little time for heat transfer and can be assumed to be an adiabatic process. For example, the length of the nozzle used in these experiments is 1.25 mm, and the superheated water entering through the nozzle has an approximate velocity of ≈ 20 m⁄s. This means that the flashing process in our experiments takes place in the order of a few microseconds, making the isentropic assumption more realistic.

The enthalpy, entropy, and experimental conditions for all states are given in Table 3-2. The vapor mass fraction after injection (at state 4) can be calculated from the T-S diagram for different injection temperatures by making two assumptions: first, the mixture temperature after injection process is 100℃ (the thermocouple shows the mixture temperature at the exit

nozzle to be 90-95°C), and second, the entropy of state 4, which is equal to state 3 for the isentropic process, is known.

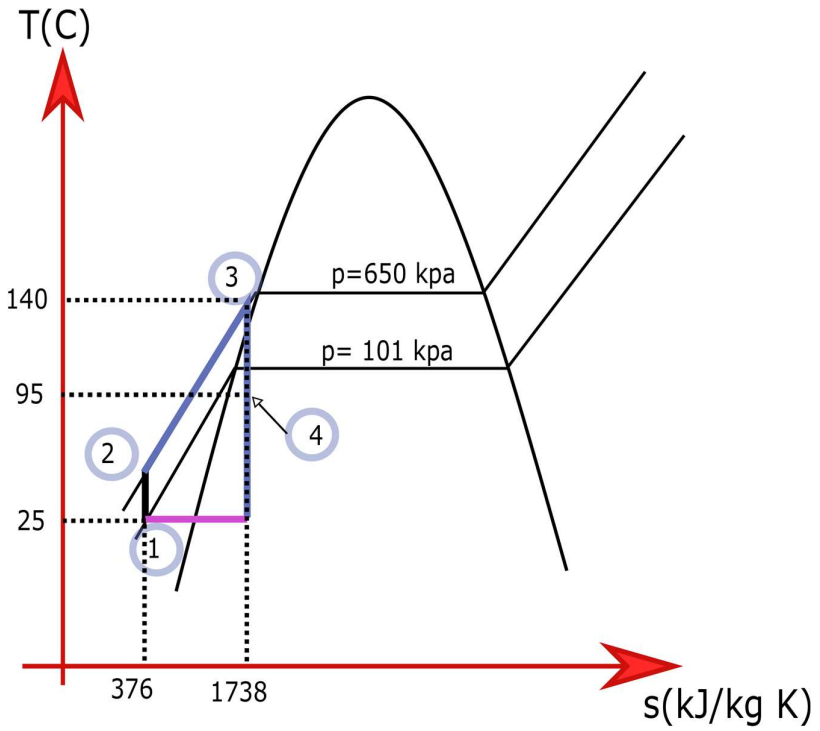

Figure 3-1. Flash boiling process in the T-S diagram.

Knowing the injection pressure and temperature, the entropy of state 3 can be determined. Also, the saturation temperature (100°C) and entropy of state 4 can be used to determine the vapor mass fraction. The steam mass fraction at different temperatures was shown in Table 3-2. As expected, the vapor mass fraction is increased by increasing the injection temperature, and more vapor would be produced at higher injection temperature.

Some experiments were performed to study the irreversibility of the flash boiling process and get the real vapor mass fraction. The flow rate was measured continuously during the experimental period by means of a flow meter installed through the pipe in front of a duct heater. After injection, the mixture contains vapor and an atomized water. The atomized water was directed to the collector through a shield pipe, and the vapor part goes out immediately from a shield pipe due to its low density. The amount of water collected (m_{liquid})

was measured after the experiments. The vapor mass fraction can be obtained from Eq. 4 by knowing the amount of vapor produced (m_{vapor}) as well as the amount of water collected.

$$x = \frac{m_{vapor}}{m_{liquid} + m_{vapor}} \qquad (3-4)$$

The results of the vapor mass fraction from the experiments were also shown in Table 3-2. No significant differences (~ 3%) were found between the vapor mass fraction calculated from the T-S diagram (isentropic process) and the vapor mass fraction obtained from the experimental results for high temperature condition. This means that an isentropic assumption can be applied to find the vapor mass fraction for different experimental conditions.

Table 3-1. The thermodynamic parameters at different states of flash boiling atomization.

State	Pressure (kPa)	Temperature (℃)	Enthalpy $(\boldsymbol{kJ/kg})$	Entropy (kJ/K)
1	101	24	100.7	0.35
2	653	24	101.2	0.35
3	653	140	589.3	1.73
4	101	90-95	577.9	1.73

Table 3-2. Vapor mass fraction at different temperatures.

Temperature (℃)	$\boldsymbol{x}$ (isentropic assumption)	$\boldsymbol{x}$ (experimental results)
110	3.5	2.4
125	6.1	3.1
140	8.6	8.9

3.3 Preliminary results and discussion

3.3.1 The effect of injection temperature on suspension spray structure

In our experimental setup, the suspension is initially stored under high pressure, and then the temperature is increased up to 150℃. When this superheated suspension flows through the pipeline and approaches the nozzle exit, the vapor bubble nuclei start to emerge at the nucleation sites (nozzle and/or particle surface) and create a two-phase flow at the nozzle exit. As this two-phase flow passes through the nozzle and encounters the surrounding environment, the vapor bubbles expand and disintegrate the suspension jet into smaller fractions. Figure 3-2 illustrates the structure of the flash-boiling spray at different temperatures. In the case of a non-superheated suspension jet (25℃) and a low degree of superheat (110℃), flash boiling does not occur; instead, aerodynamic instability controls the jet disintegration. In this condition, the interaction between the jet and the surrounding air generates surface waves on the suspension surface, resulting in the detachment of small droplets from the suspension column. In our experiments, the jet was observed to break up at a distance of approximately $250d_o$ (where $d_o$is the nozzle diameter).

By increasing the temperature from 110℃ to 120℃ and 130℃, the flashing inception can be observed, and the suspension droplets start to form at the periphery of the spray while the jet is ruptured to the large droplets at the center. When the suspension temperature is elevated, it leads to the generation of a greater number of vapor bubbles, thereby enhancing the atomization process as a result of their increased presence. In general, the steady-state rate N of formation of activated vapor nuclei with a radius R can be estimated by [78].

$$N = C.\exp\left(-\frac{\Delta A}{k.\Delta\theta}\right) \qquad (3-5)$$

$$\Delta A = \frac{4}{3}\pi R^2.\sigma \qquad (3-6)$$

$$\Delta\theta = \frac{T_{inj} - T_\infty}{T_{sat} - T_\infty} \qquad (3-7)$$

Where C represents the constant determined based on the density of bubble nuclei within the liquid, σ is the surface tension, $\Delta\theta$ is the superheat degree of the liquid, and k corresponds to Boltzmann constant. In Eq. 7, T_{sat} and T_∞ are the saturation temperature of the injection pressure and ambient temperature, respectively. This equation clearly explains that the number of vapor bubbles is directly proportional to the temperature. In addition, the vapor bubbles not only increase in number, but the bursting process is more intense at higher temperatures, resulting in droplets being thrown further away from the center [79].

In high level of superheating degree (140℃ and 150℃), the jet is broken to the large droplets at about $50\,d_o$ distance and a large number of small droplets is observed in the periphery. It is important to highlight that besides the impact of temperature on vapor bubble formation, the surface tension and viscosity of the suspension are notably decreased as the injection temperature rises [80]. This reduction further contributes to the improved disintegration of the jet. Eq. 5 also represents that the number of vapor bubbles is inversely proportional to the surface tension, it means that the number of activated vapor bubbles increases by decreasing the surface tension.

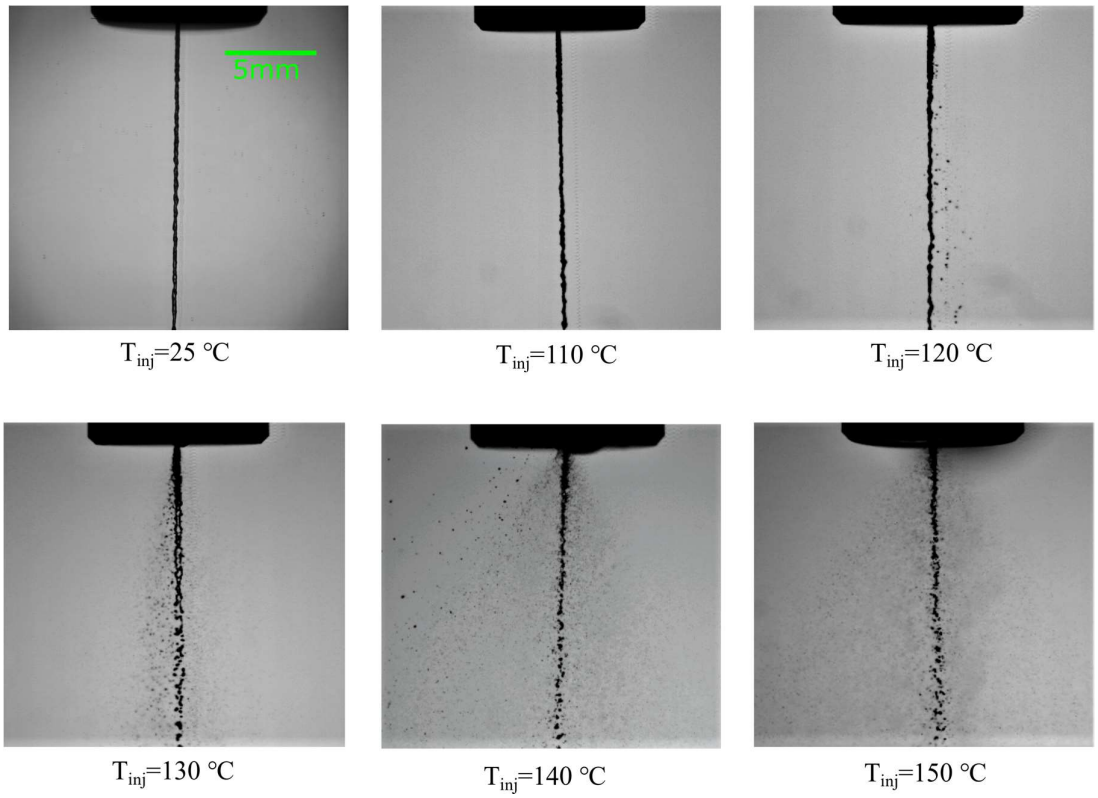

Figure 3-2. The effect of injection temperature on the structure of the suspension spray. Solid concentration and nozzle diameter were 5 wt.% and 200 µm, respectively.

3.3.2 The effect of suspension concentration on spray structure

Figure 3-3 illustrates the effect of different solid contents on the spray structure of flash boiling suspension at a high temperature ($T_{inj} = 150$℃). To investigate the impact of solid content, suspensions with three different solid contents of 5, 20, and 40 wt.% were prepared. As observed, the column of large droplets in the center disappears with increasing particle concentration, resulting in a more uniform spray pattern. This phenomenon can be attributed to two key factors:

First, the number of activated nucleation sites increases as the number of particles in the suspension increases, and based on nucleation theory, more vapor bubbles would be available to break the jet into smaller droplets [81]. During the flash boiling atomization, bubbles originate from the nucleation sites and grow in the water content of the suspension. There are

three potential nucleation sites, which can be divided into two types of homogeneous and heterogeneous. They are the interstitial water (homogeneous nucleation), the porosity on the surface of the particles (heterogeneous nucleation), and the roughness of the nozzle (heterogeneous nucleation) [81]. By increasing the solid contents, heterogeneous nucleation is much more likely to occur, and atomization would be promoted under this condition.

Second, as the particle concentration increases, the suspension becomes more viscous [82], which may result in a reduction in the flow rate.

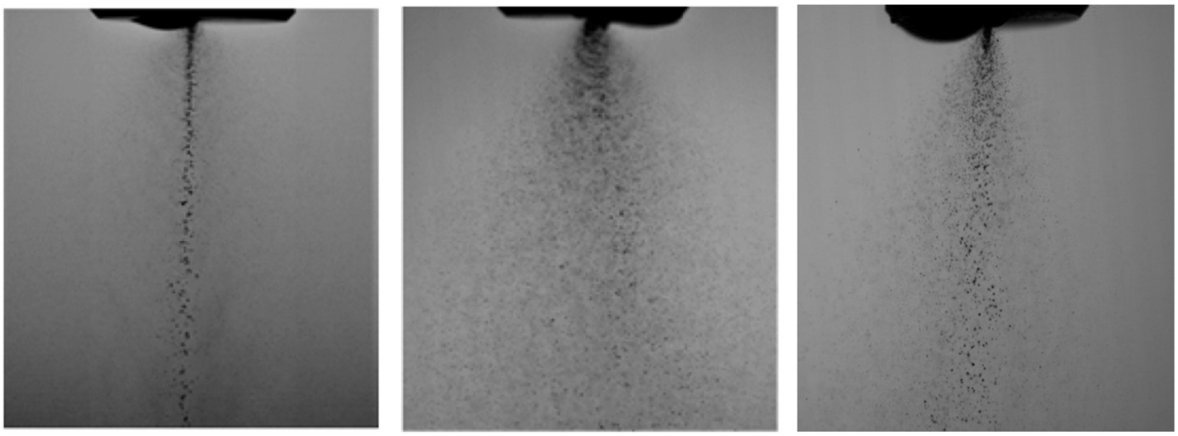

Figure 3-3. Suspension spray structures at injection temperature of 150℃ with a nozzle diameter of 0.2 mm and varying solid contents: (a) 5 wt.%, (b) 20 wt.%, and (c) 40 wt.%.

3.3.3 Difference between spray structure of pure water and suspension

Figure 3-4 shows the spray structure of flashing jets for distilled water and suspension at a high temperature ($T_{inj} = 150℃$). The particle concentration is changed from 0 (representing pure water) to 10 wt.%. At a high level of superheated degree (150℃), when the particle concentration is 0 (pure water), the spray forms a narrow structure, and the spray becomes like a willow tree mainly due to air entrainment. This entrainment behavior in flash boiling spray has been observed by many researchers and it has been studied both experimentally and numerically [40], [83], [84]. For pure water, the expansion and entrainment regions are detectable, as seen in Figure 3-4 (a). The vapor bubble explosion produces small droplets in

the capillary region of the nozzle (or near the nozzle exit). These small droplets rapidly expand into the environment as they leave the nozzle exit, forming the expansion region. The amount of expansion depends on the operating conditions (injection pressure and temperature), nozzle geometry and liquid properties [83]. Then, at a short distance from the nozzle exit, strong vortices are formed, and air as well as small droplets are sucked toward the spray axis. This region, where small droplets are pushed toward the spray axis, is called the entrainment region. It is noteworthy that as the injection temperature increases, the air entrainment effect becomes more important due to the reduction in droplet size.

On the contrary, the flashing suspension jet (see Figure 3-4 (b)) contains only the expansion region so that a triangular-shaped spray is formed. In other words, the spray boundary changes linearly with distance from the nozzle exit. The reason is that since the disintegrated suspension droplets, being heavier and larger than the water droplets, have a higher momentum, the aforementioned vortices are not able to push the droplets toward the spray axis (i.e., the disintegrated droplet trajectory does not change significantly). Therefore, the entrainment region cannot be observed here.

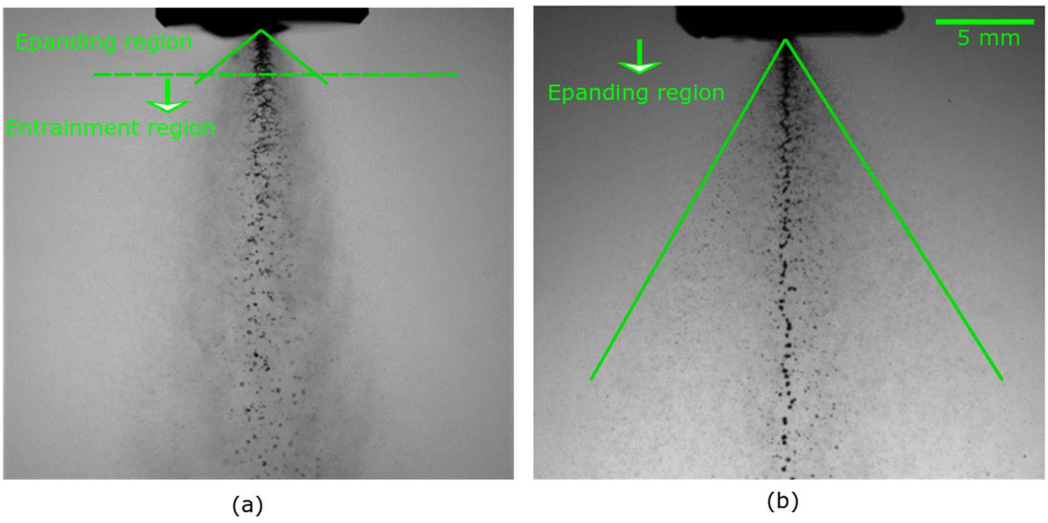

Figure 3-4. Flash boiling spray structure at injection temperature of 150℃ with a 300 μm nozzle diameter. (a) pure water and (b) a suspension with a particle concentration of 10 wt.%.

In this study, a quantitative comparison of the spray structure between distilled water and the suspension was conducted by measuring the spray angle at different injection temperatures. The spray angle is defined as the angle between two tangential lines connecting the nozzle tip and the points on the jet's periphery located 8 mm from nozzle exit (see Figure 3-5). To ensure accuracy, at least one hundred images were analyzed for each temperature to measure the spray angle, and the average value was considered as the representative spray angle. Figure 3-8 shows how the spray angle varies with injection temperature for both pure water and the suspension. As can be observed, the spray angle for pure water increases to a maximum value of 60° as the injection temperature rises to $T_{inj} = 130℃$. This is because increasing the injection temperature leads to a higher number of vapor bubbles that burst more vigorously, causing more disintegrated droplets to be ejected towards the spray periphery with greater radial velocity. After reaching its maximum value, the spray angle for pure water begins to decrease, reaching 40° at $T_{inj} = 150℃$. This decreasing behavior is linked to the air entrainment phenomenon.

Flash boiling atomization exhibits a threshold behavior, transitioning from partial flash boiling to complete flash boiling as the injection temperature increases to a specific threshold. In the complete flash boiling regime, the size of disintegrated droplets decreases significantly.. [44]. These small droplets can be easily affected by drag force and strong vortices around the jet, resulting in the movement of droplets from the periphery towards the center of the jet. The results indicate that the maximum spray angle for pure water occurs at the temperature between 130 ℃ to 140 ℃ with superheated level of $\Delta\theta = 0.82$ (for an injection pressure of 515 kPa). This up and down behavior for the spray angle of pure liquid has been observed by many researchers [64], [85]. Park et al. [64] demonstrated that this maximum spray angle occurs within the range of $0.45 < \Delta\theta < 0.85$, depending on different

injection pressures. Nagai et al. [85] reported $\Delta\theta = 0.55$ as the maximum spray angle (with an injection pressure exceeding 400 kPa).

However, a similar trend in spray angle cannot be seen for flash boiling atomization of the suspension. In the case of suspension injection, the narrowest spray angle is observed at the lowest injection temperature ($T_{inj} = 120℃$), and the spray angle increases to 60° as the injection temperature rises to $150℃$ without showing a decreasing trend. In this case, it seems that the air entrainment is not able to draw the droplets toward the center of the spray because the suspension droplets are larger and heavier than the water droplets.

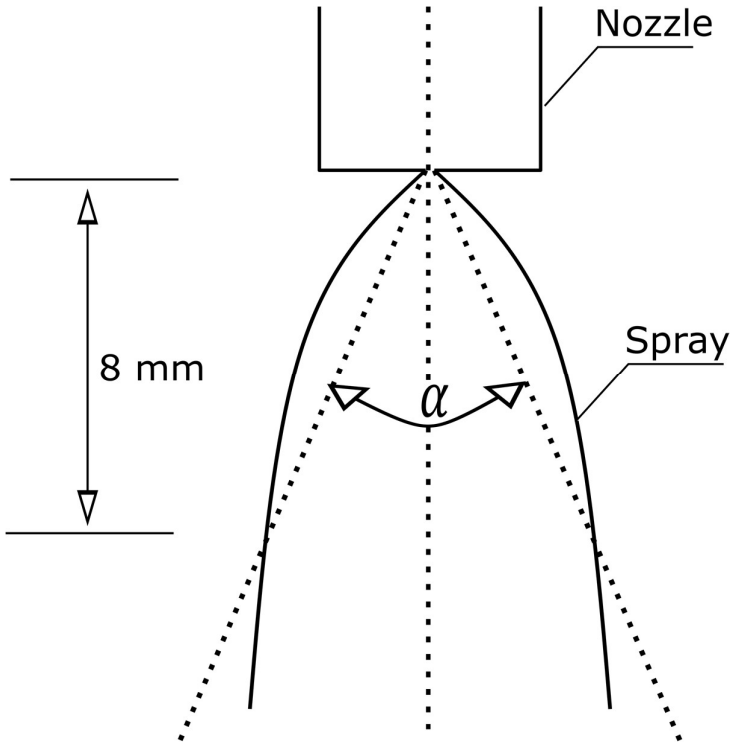

Figure 3-5. Definition of spray angle.

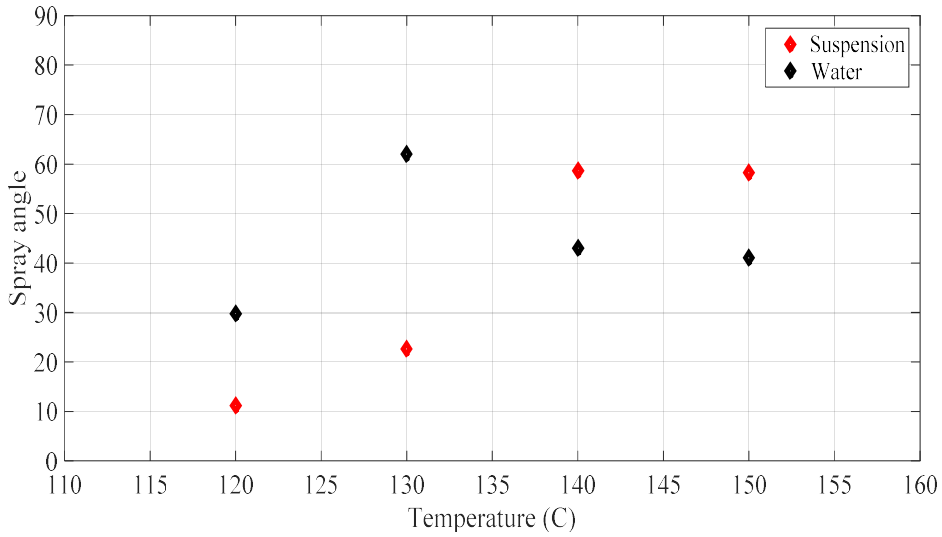

Figure 3-6. Spray angle comparison for flash boiling of pure water and suspension. Nozzle size: 0.2 mm, Solids concentration: 5 wt.%.

4 Chapter 4: Flash boiling atomization of high-concentration suspensions in suspension plasma spraying

4.1 Introduction

Suspension plasma spraying is defined as a type of plasma spraying in which submicron or nanoparticles are suspended in a liquid, such as water or ethanol, and then injected into the plasma plume under atmospheric conditions. This leads to fragmentation of the suspension into smaller droplets due to the very high shear stress caused by the plasma jet. Under the heat load of the plasma jet, the solvent would evaporate, and the small particles would melt and be accelerated to impact the substrate surface and form a coating. One advantage of SPS over conventional methods is that the finer powders can produce finer microstructures that can be porous, dense or columnar allowing for increased performance in several industrial applications [36], [86].

Suspension injection is an important process in SPS because it has a significant impact on the quality and performance of coatings. Radial and axial injection are two different approaches used in suspension plasma spraying. Radial injection involves injecting the suspension perpendicular to the plasma torch axis, while axial injection involves injecting the suspension parallel to the torch axis, each offering unique advantages in terms of coating properties and process efficiency [36]. A continuous jet or spray atomization are two methods commonly used to inject the suspension radially into the plasma plume. In the continuous jet method, the suspension is held in a pressurized container and passed through an injector of varying diameters to form a continuous jet. On the other hand, the spray atomization method disintegrates the suspension into an ensemble of droplets through atomization by gas expansion inside or outside the nozzle [87], [88]. Marchand et al. [88] injected yttria-stabilized zirconia (YSZ) into an atmospheric plasma jet using two different designs of two-fluid atomization nozzles (internal and external mixing). They found that by changing the design of the atomizing nozzle, different injection modes could be achieved, from a liquid jet to multiple sprays with a variety of drop size distributions. They observed that external

mixing nozzles produce a constant and rather low drop velocity, while internal mixing nozzles produce a higher drop velocity, which increases with the degree of atomization. The main disadvantage of using the spray atomization method is that injecting gas into the plasma can reduce evaporation inside the plasma jet, which, in turn, may affect particle melting. Lower deposition rate is another disadvantage of spray atomization method. Toma et al. [30] showed that the film thickness per pass decreased from 4-6 μm per pass for continuous jet method to 1.5-2 μm for spray atomization.

Regardless of the suspension injection modes, the feed rate of solid particles and deposition efficiency of the SPS process are approximately one-fourth to one-third lower than that of conventional plasma spraying [36]. Increasing the solid feedstock concentration increases the viscosity of the suspension, which decreases its flowability and ultimately may lead to clogging problems [82]. There are some approaches to inject high concentration into the plasma jet such as performing particle size distribution analysis, designing specific nozzle, continuous monitoring and cleaning. One effective way to reduce the viscosity of the suspension is to add a suitable dispersing agent to the suspension [89]. Surfactants can affect the rheological properties of the suspension, such as viscosity and surface tension. By modifying these properties, surfactants can improve the flow and atomization characteristics of the suspension, promoting better spray pattern and droplet formation during plasma spraying. Another way, which will be used in these experiments, is to raise the temperature of the suspension to achieve a superheated state, resulting in a flash boiling spray at the nozzle exit.

Flash boiling atomization is a thermodynamic instability that occurs when the pressure of a superheated liquid jet suddenly decreases and becomes less than its saturation pressure. Vapor bubbles begin to form at the nucleation sites when the pressure reaches saturation. These bubbles grow as the pressure decreases and eventually burst into the jet, breaking it

into small droplets. This thermodynamic process has significant industrial applications such as engine fuel injection [90], inhalation drug delivery in the pharmaceutical industry [91], desalination [79], fuel atomization in gas turbine engines [92], etc. Flash boiling atomization could improve the flowability of the suspension because the viscosity decreases with the increase of temperature. In addition, there are other unique potential advantages to flash boiling atomization. For example, unlike other atomization methods in SPS, this method does not cool the plasma jet by injecting gas into the plasma stream [7]. In this method, no external air is added to the suspension to break up the jet. In flash boiling atomization, the bursting vapor bubbles emerging from inside the jet are responsible for shattering the suspension jet.

In this work, a titanium dioxide suspension was injected into the plasma jet by two different methods: flash boiling atomization and continuous jet injection. The microstructure of the deposits, phase composition, deposition efficiency, deposition rate per pass, thickness per pass and width of the depositions were compared for a suspension concentration of 20 wt.%. Suspensions with high solids concentrations of 40, 55, and 70 wt.% were also injected by flash boiling atomization.

4.2 Experimental Methodology

4.2.1 Injection setup

A scheme of the experimental setup is shown in Figure 4-1. This suspension injection setup consists of two 6 L stainless steel vessels for water (1) and suspension (2). The suspension vessel was placed on the magnetic stirrer (3) to obtain a stable suspension during the experiments. In order to save the suspension, the experiment starts with water first to get a stable flash boiling spray. Then the plasma torch is ignited and the three-way valve (4) is opened to feed the suspension into the line. The injection pressure is 450 kPa for continuous jet method (5). It was observed that the flow rate is lower in flash boiling atomization, so the

injection pressure increased to 690 kPa to keep the flow rate constant. The suspension flow rate and density are measured by a Coriolis flow meter (6) through the line. The duct heater (7) is used to raise the temperature of the suspension to reach a superheated condition. The power of the heater can be controlled by a variac transformer (8) and can be regulated from 0 to a maximum power of 1.2 kW. The injection temperature is continuously measured by a thermocouple (9) located outside the duct heater (with an accuracy of ±0.75%). In this experiment, the maximum temperature is up to 140℃. A cylindrical stainless steel nozzle (12) with an exit diameter of 0.15 mm and a length of 1.25 mm is used in this experiment and attached to the plasma torch with a nozzle holder (11). The suspension feeding line is made of a flexible plastic tube (10) to give the robotic arm more flexibility for movement. Stainless steel substrates measuring 50×25 mm are mounted on the rotating sample holder (13).

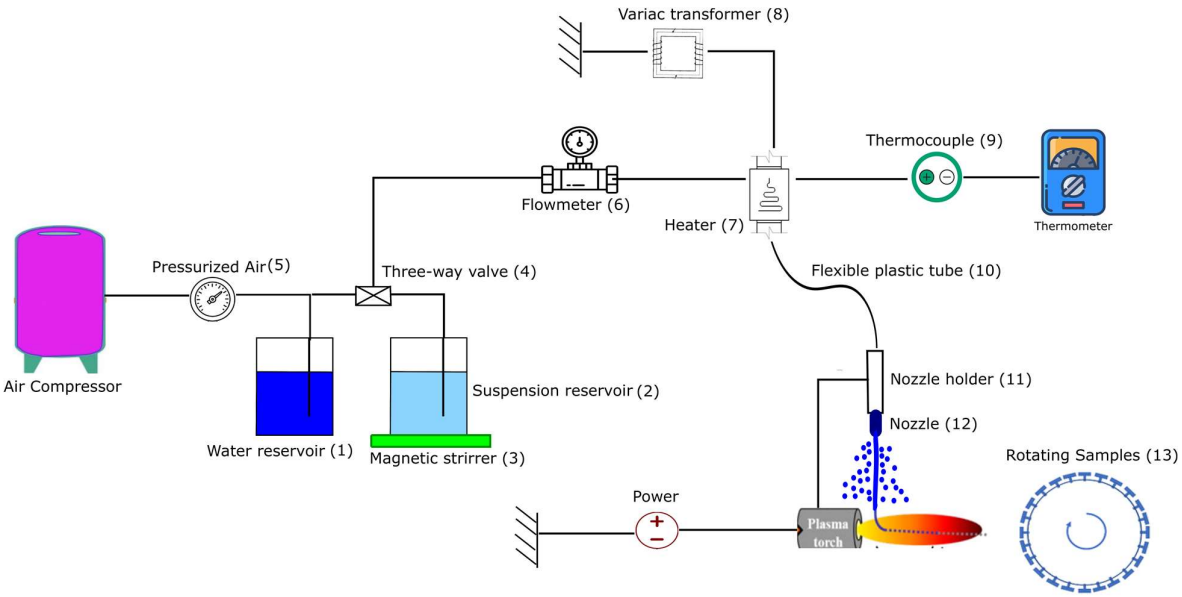

Figure 4-1. Schematic of the experimental setup.

4.2.2 Plasma spraying

The 3MB torch (Oerlikon-Metco, Westbury, USA) was used in this experiment, and the operating parameters of the plasma torch are summarized in Table 4-1. The stand-off distance

is 50 mm and the distance between the tip of the nozzle and the torch axis is 8 mm (the distance between the nozzle and the edge of plasma jet is approximately 4 mm). The maximum operation power of 33 kW was used with this torch. The radial injection was normal to the flow axis. Figure 4-2 shows the position of the 3MB gun towards the nozzle in a front view and a side view.

Table 4-1. Plasma torch operation parameters.

Injection type	Concentration (wt.%)	Plasma gas (SLPM)	Current (A)	Suspension flow rate (ml/min)	Gas pressure (kPa)	Temperature (℃)	Spray time (s)	Density (g/cm^3)
Flash boiling atomization	20	Ar+ H_2 (50,3.5)	600	34-36	690	140	45	1.19
	40			32-34			30	1.43
	55			30-32			15	1.77
	70			28-30			10	2.14
Continuous jet	20			34-36	450	25	45	1.19

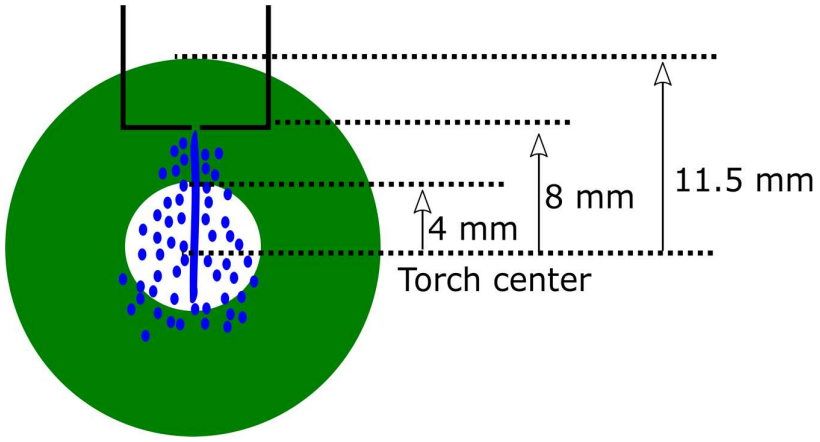

(a)

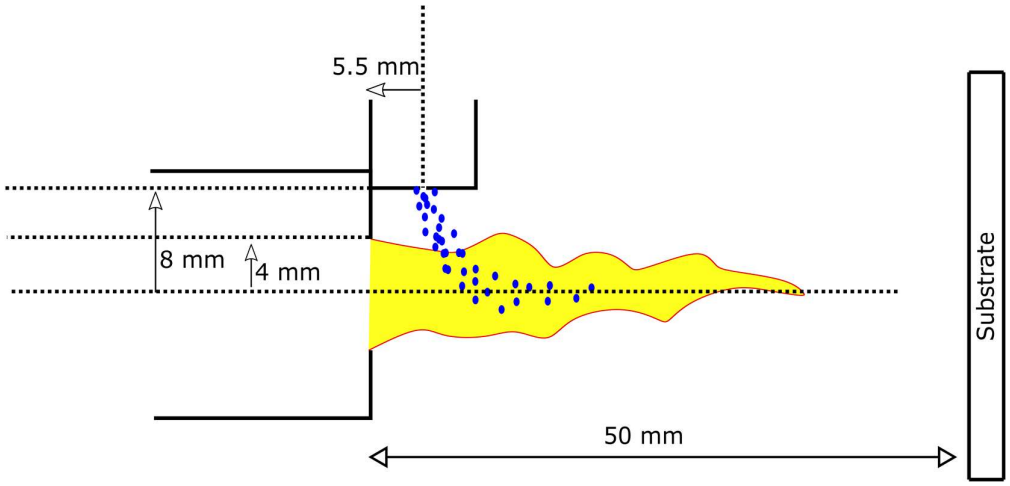

(b)

Figure 4-2. The position of 3MB gun to the exit nozzle, (a) in front view (b) side view.

4.2.3 Suspension and coating characterization

In this study, we chose to use TiO_2 suspension for several reasons. First, TiO_2 suspension is known for its sustainability as well as its accessibility and cost-effectiveness. For the SPS deposition process, suspensions of TiO_2 powder were prepared without adding any dispersion. The suspensions with different solids concentration of 20, 40, 55, 70 wt.% were prepared by adding the TiO_2 nanoparticles to water agitated with a magnetic stirrer and a probe sonicator.

In our experiments, we were unable to spray the entire surface of the substrate because we had to hold the torch stationary and use the rotating sample holder. The sample holder rotates at 60 rpm (with linear velocity of 1 m/s) in front of the plasma jet, allowing multiple passes on the same line of the substrates. Therefore, the deposits are characterized by the weight of material deposited per pass on this single line, the height and width of the deposits as well as their microstructures. All substrates were blasted with 80 grit aluminum oxide particles (i.e., 160 μm particle size). The roughness of the stainless steel substrates were measured with a Surftest SJ-210 roughness tester (Mitutoyo, Kawasaki, Japan). The approximate roughness of the substrates was 5-6 μm. The weight of the substrates was measured before and after the

deposition process, and the deposition net weight was divided by the number of passes to obtain the deposition weight per pass. In addition, the deposition efficiency is defined as the ratio of the net weight to the weight of TiO_2 powder used during spraying. The maximum thickness usually occurs at the center of the substrate, and this value is divided by the number of passes to determine the thickness per pass.

The deposits microstructure were observed by using a scanning electron microscope (SEM) S3400 (Hitachi, Japan) at accelerating voltage of 15 kV. In addition, the ImageJ software was used to evaluate the porosity of the deposits and also calculating the percentage of different regions within the deposits by generating binary images of the deposits. The SEM images at 500 magnification were used for porosity measurements. The phase identification (rutile and anatase distribution) of the coatings was measured by X-ray diffraction (XRD) using a X'Pert Pro; PANalytical (Philips, Netherlands). The Cu-Kα radiation is used and is in the range of 10-90°with a step size of 0.02°.

4.2.4 Visualization measurement

A shadowgraphy setup was used to analyze the spray behavior. A Photron SA1.1 high speed camera (Photron, California, USA) operating at 5000 fps was used to capture the atomization process accurately. The images were captured using the backlight method with a 120 W LED light and a diffuser. The resolution of the camera is 1024×1024 and the exposure time was 1 μs. In this study the velocity of in-flight particles in SPS was measured using the AccuraSpray 4.0 (Tecnar Automation Ltd., Canada).

4.3 Results and discussion

4.3.1 Spray structure for flash boiling atomization

The spray structure under continuous jet and flash boiling conditions is shown in Figure 4-3. In the continuous jet method (Figure 4-3.a), a single jet can be observed at constant room temperature. The suspension jet has a constant radius at the nozzle exit, but after a certain distance from the nozzle exit, Plateau-Rayleigh instability [93] starts to develop on the surface of the suspension jet as the surface tension tries to minimize the surface area (assuming the effect of viscosity is negligible). In this state, the suspension column will no longer have a constant diameter. Eventually, this instability will grow and the wavelength of this disturbance will become larger than the jet diameter, breaking the suspension jet into droplets that have diameters in the order of the nozzle size. In continuous jet method, the aerodynamic instability controls the jet breakup and the thermodynamic instability has no effect because the suspension is not superheated. However, flash boiling atomization is controlled by the thermodynamic instability.

In flash boiling atomization (Figure 4-3.b), the spray of superheated suspension can be observed. Under this condition, the superheated suspension at 140°C is accelerated through the injection nozzle and its pressure (690 kPa) begins to decrease in the capillary region of the nozzle to reach atmospheric pressure (101 kPa) at the nozzle outlet. When the pressure reaches the saturation pressure of water at 140°C (363 kPa), vapor bubbles begin to form inside the nozzle at nucleation sites and detach from the surface and move to the center of the nozzle. Most often, nucleation will occur on the nozzle surface, but bubble formation can be promoted on the surface of solid particles in the suspension. In this condition, vapor generation will take place and a two-phase flow consisting of vapor bubbles and liquid will form inside the nozzle. When this two-phase flow is injected into the environment, the excess energy is converted to the latent heat of vaporization, causing the vapor bubbles to grow

rapidly until they finally burst, breaking the suspension jet into small droplets. The injection temperature is an important parameter that affects the spray structure. As the injection temperature increases, more vapor bubbles are nucleated and begin to form earlier (upstream of the nozzle). They can coalesce to form large areas of vapor, which increases atomization [64].

Based on the results in Figure 4-3, the vertical distance of 8 mm was chosen between the nozzle exit and the torch axis for flash boiling atomization in order to increase the chance of droplets penetrating into the plasma jet. However, for continuous jet method, this distance is less of a concern because all the suspension jet is not divergent.

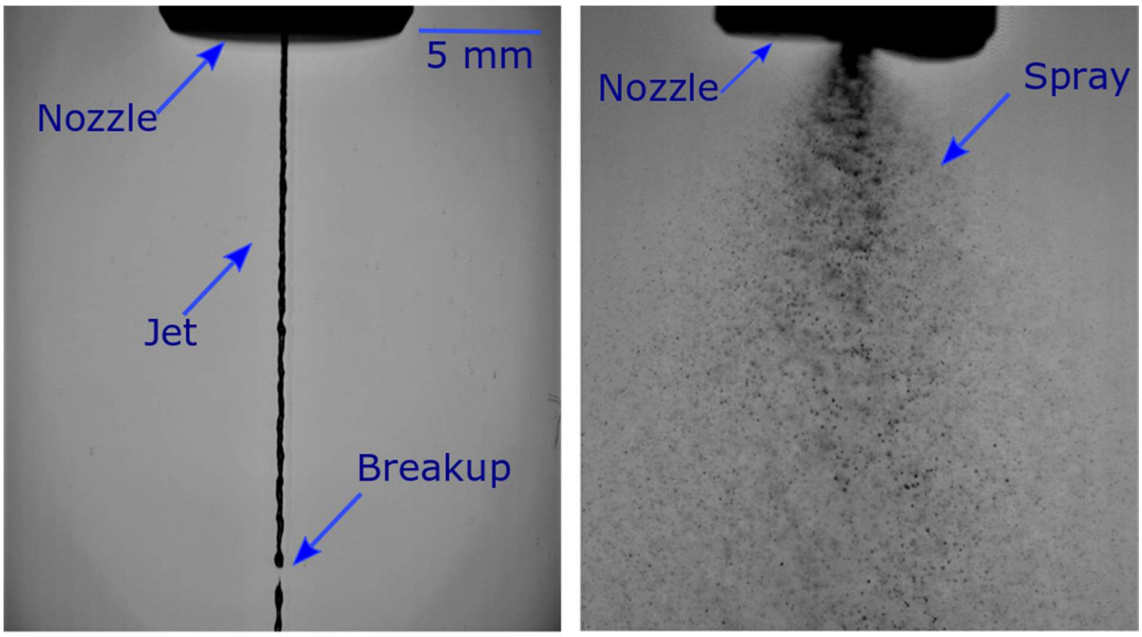

Figure 4-3. Spray structure of (a) continuous jet (b) flash boiling atomization.

4.3.2 Deposit properties with continuous jet and flash boiling atomization

In this section, the microstructure of the deposits, the deposition weight per pass, deposit thickness per pass, deposition efficiency and deposit width were investigated by comparing the deposits produced by continuous jet and flash boiling atomization. All experimental

conditions were kept the same for both methods. The only difference is the injection pressure. As discussed in the previous sections, the suspension flow rate in the flash boiling condition is lower than in the single jet condition for the same injection pressure. It is related to the physics of this phenomenon. Flash boiling atomization results in the formation of vapor bubbles within the suspension. These vapor bubbles occupy space within the nozzle, reducing the available volume for suspension flow. In addition, these vapor bubbles act as a barrier, hindering the smooth flow of suspension and reducing the flow rate. In order to compensate this reduction, the injection pressure is increased from 450 kPa for continuous jet to 690 kPa for flash boiling atomization. A spray time of 45 s (45 passes) was chosen to limit the deposit thickness and avoid delamination, as another series of experiments with the same conditions showed that delamination is a major challenge at higher spray times, as can be seen in Figure 4-4 for spray times of 90 s, 120 s and 180 s. The lower substrate temperature is likely the main reason for delamination during prolonged spray times producing think deposit. For this type of torch with the specified power, the maximum substrate temperature would be less than 300°C [94].

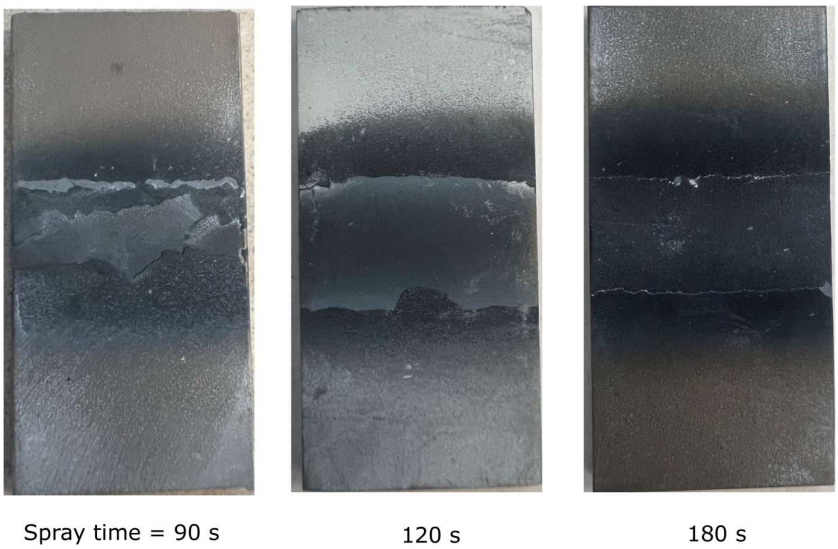

Figure 4-4. Deposit delamination on substrates after the different spray times.

The deposit weight per pass, deposition efficiency, and thickness per pass for both continuous jet and flash boiling atomization are presented in Table 4-2. The weight gain per pass for continuous jet remains relatively constant across all samples, at approximately 1.25 mg/pass. However, for flash boiling atomization, this value is more variable and differs from sample to sample, ranging from 1.35 mg/pass to 1.48 mg/pass, with an average of 1.42 mg/pass. The deposition weight per pass slightly increased with flash boiling atomization at the same flow rate.

In the single jet condition, a constant flow rate is introduced into the plasma jet, resulting in a consistent deposition weight per pass for all substrates. However, in flash boiling atomization, the distribution of large and small droplets changes over time, leading to an unsteady flow rate entering the plasma jet. This variation in flow rate accounts for the observed variability in deposition weight per pass on the substrates. Nevertheless, the deposition efficiency increased from 34% in the continuous jet to 38.8% with flash boiling atomization, and the thickness per pass increased from 0.88 μm/pass in the continuous jet to 1.16 μm/pass with flash boiling atomization.

Table 4-2. The deposition and thickness per pass for continuous jet and flash boiling atomization.

	Thickness per pass (**μm**)	Weight per pass (mg)	Standard deviation (mg)	Deposition efficiency (%)	Standard deviation (%)
Continuous jet	0.88	1.25	0.01	34.0	0.2
Flash boiling atomization	1.16	1.42	0.03	38.8	1.2

The deposit width for both injection methods is shown in Figure 4-5. The mass distribution is different for continuous jet and flash boiling atomization. In continuous jet, the whole suspension jet is injected towards the plasma torch axis, whereas in flash boiling, the

atomized suspension droplets follow divergent trajectories hitting not only the center of the plasma jet but also its outer edges. Therefore, it would be expected to obtain a larger deposit width for flash boiling atomization compared to continuous jet ($L_F > L_M$), which is confirmed via Figure 4-5.

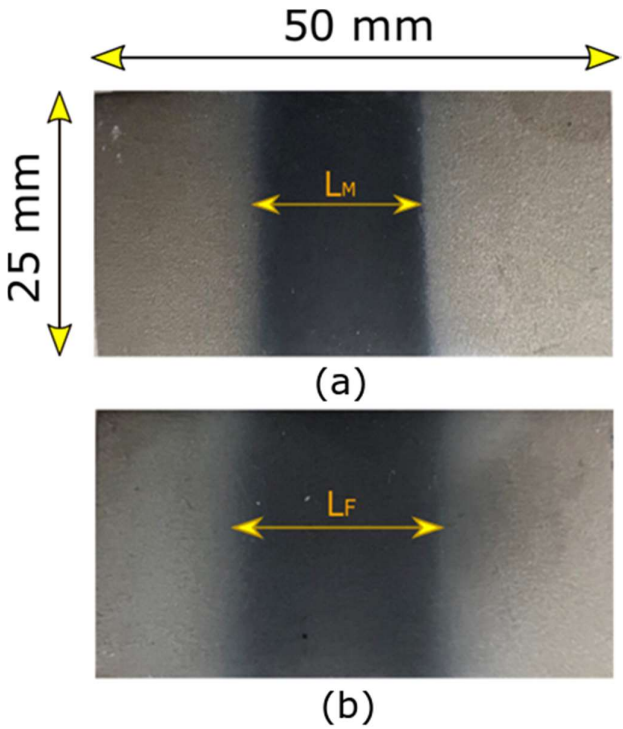

Figure 4-5. Deposit width for (a) continuous jet, L_M, (b) flash boiling atomization, L_F.

Figure 4-6 shows cross-sectional SEM micrographs of TiO_2 deposits produced on stainless steel substrates by two injection methods continuous jet and flash boiling atomization. The images were taken in the center of the deposit, where the thickness is maximum. The deposits consisted of three regions of well-melted particles with a light color in the deposits, non-melted particles with a gray color, and the porosity region with a dark color. All deposits were dense and the dark area (porosity region) was negligible (less than 5% porous area). Some particles have enough mass and momentum to penetrate the hot regions of the plasma jet. These particles are sufficiently melted under the high temperature conditions to produce dense splats, the light color regions of the deposit. However, some suspension droplets did not penetrate the plasma jet sufficiently and remain at the outer zones of the plasma jet. This

results in the deposition of unmelted particles that are found in the gray regions in the deposit. These regions are less dense than the dense splats and, consequently, appear darker in the SEM images [94]. Figure 4-7 shows a higher magnification cross-sectional SEM image from the different regions observed on the coatings.

Table 4-3 shows the distribution of the different regions in the TiO_2 deposits. The results show that the percentage of unmelted particles in the total area is the same for both methods, i.e. between 33-35%. The percentage of well-melted particles is also the same, between 65-67%. In addition, as seen in Fig. 6, the concentration of unmelted particles in the area close to the substrate tends to be higher than in the upper areas of the deposits. The main reason for this is expected to be the low substrate temperature at the beginning of the deposition process. The unmelted particles are deposited when some suspension droplets reach the substrate. When the substrate temperature is low, the presence of water on the substrate surface is expected to reduce the probability of sticking of the fully melted TiO_2 particles. After a few passes, the substrate temperature increases making it possible to vaporize more rapidly the water coming from the impact of the suspension droplets impinging on the substrate surface and thus increasing the probability of deposition of the fully molten TiO_2 particles.

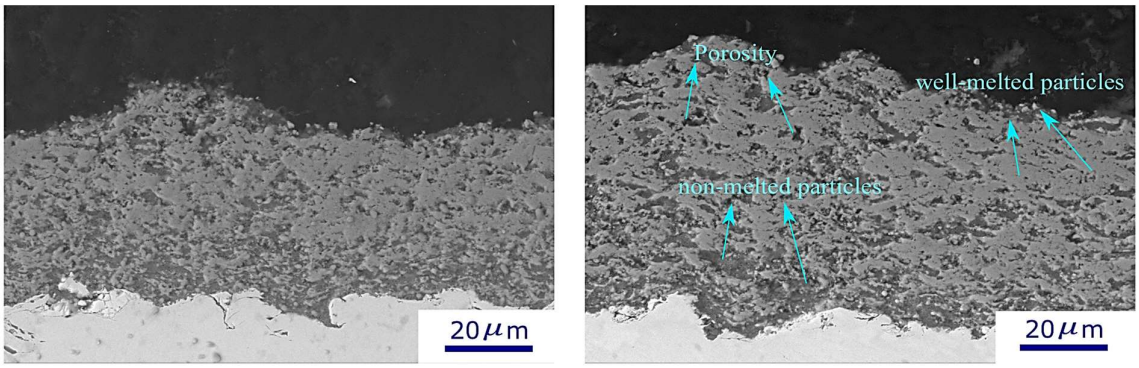

(a) (b)

Figure 4-6. Cross-sectional back-scattered SEM micrographs for (a) continuous jet (b) flash boiling atomization.

Table 4-3. Distribution of different regions of the TiO_2 deposits.

	Light area distribution (well-melted particles)	Gray area distribution (non-melted particles)
Continuous jet	65-67 %	33-35 %
Flash boiling atomization	65-67 %	33-35 %

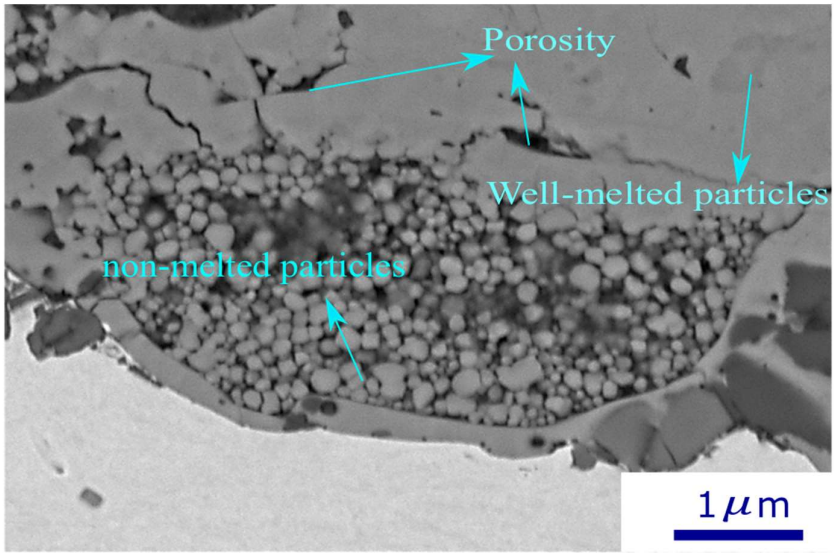

Figure 4-7. High-magnification cross-sectional SEM micrograph showing different regions on the TiO_2 coatings.

In addition, the AccuraSpray system was used to measure the in-flight velocity particle inside the plasma jet (Figure 4-8). The particles velocities are 251 m/s for continuous jet and 290 m/s for flash boiling atomization. One main reason for the higher deposition weight per pass observed in the flash boiling atomization method, compared to the continuous jet method, can be attributed to the higher particle in-flight velocity. Additionally, the suspension jet is already atomized into droplets, eliminating the need for the plasma jet to consume more energy on primary breakup within the plasma jet itself. Moreover, the droplets within the flash boiling spray are at a temperature close to the water boiling point (approximately 95°C), and the plasma jet only needs to provide latent heat for complete solvent evaporation. This

implies that approximately 20% of the total energy required for complete solvent evaporation can be saved, as around 80% is utilized for latent heat.

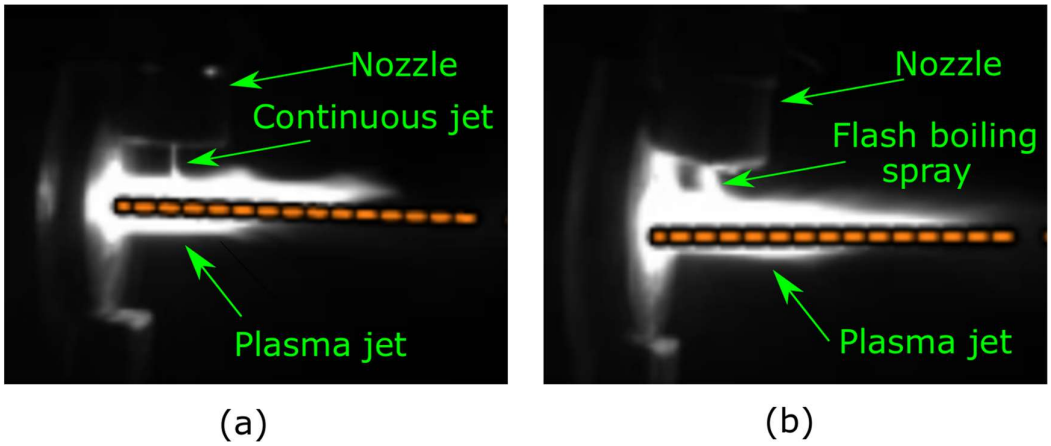

Figure 4-8. AccuraSpray results for both injection methods (a) continuous jet (b) flash boiling atomization.

4.3.3 Water-Based suspension with higher solid contents

A major advantage of using flash boiling atomization is the injection of suspensions with high solid content. The use of suspensions with concentrations higher than 60 wt.% would be challenging for continuous jet method in SPS [11]. Clogging problem is the main limitation to injecting suspensions with high particle concentrations, which is related to the high viscosity and low flowability. The flow of suspension through pipes, flow meters and nozzles would be very slow and more difficult for suspension with high viscosity. The suspension density is also affected by increasing the solid content. It is approximately doubled by increasing the concentration from 20 to 70 wt,%.

Suspension viscosity increases with increasing solid content because the effective space between the particles is reduced and therefore the resistance to particle movement due to shear stress is increased. In particular, Garmeh [95] obtained the stress-strain rate curves for the same TiO_2 suspensions at different concentrations of 30, 50 and 70 wt.% and observed that the suspension viscosity increased significantly once the suspension concentration increased from 50 to 70 wt.%. In addition, Waldbillig et. al [82] showed that viscosity does

not have a linear relationship with concentration and that the suspension viscosity increases by a factor of 5 as the solid content is increased from 5 to 20 vol%. Furthermore, the suspension viscosity decreases by increasing the suspension temperature [82] because the particles can get more energy to overcome the attractive forces between each other. Thus, it seems that an efficient way to prevent the nozzle from clogging is to reduce the viscosity by increasing the suspension temperature.

In this experiment, the suspension is superheated to 140°C and we could observe that the clogging issue is reduced. We have found that immediate clogging was a significant challenge at suspension concentrations above 40% for continuous jet method. In addition, in order to avoid sedimentation in high concentration suspensions, the container was placed on the stirrer. Additionally, a lower number of passes (spray time) was chosen when injecting high concentration suspensions to avoid delamination on the substrate.

Figure 4-9 shows cross-sectional backscattered SEM images of deposits with different concentrations of TiO_2 particles in the water-based suspensions (20, 40, 55, and 70 wt.%). As discussed earlier for the microstructure of the TiO_2 deposit, there are three different regions of light area (well-melted particles), gray area (non-melted and partially melted particles), and dark area (porosity). Many regions of unmelted particles can be seen in the deposit microstructure achieved with the 70 wt.% suspension. In general, the quality of deposits decreases with increasing the suspension concentration. Indeed not only does the area of unmelted particles increase with increasing suspension concentration, but many cracks appear at the interface between the unmelted and well-melted particle zones, as shown in Fig. 10. Table 4-4 shows that the percentage of non-melted particles in the deposits increases from about one-third at 20 wt.% suspension to an estimated half at 70 wt.% suspension.

Table 4-4. Distribution of different regions of the TiO_2 deposits at different concentrations.

Concentration of TiO_2 (wt.%)	Light area distribution (well-melted particles)	Gray area distribution (non-melted particles)
20	65-67 %	33-35 %
40	60-62 %	38-40 %
55	60-62 %	38-40 %
70	50-52%	48-50 %

Two reasons can be suggested for the poor quality of deposits with the high solid concentration. Suspensions with high solid fractions may result in poor atomization (i.e., in the form of large droplets) [80], and agglomeration in these large droplets could easily result in large unmelted zones in the deposit. Another possibility is that the power provided by the 3MB plasma torch to produce the deposits (33 kW) is not sufficient for these high solid content suspensions. Producing coatings with higher power plasma torches would permit to efficiently atomize the high-concentration suspensions and subsequently melt the ceramics particles. Our calculations estimate that the total energy required for complete water evaporation and complete particle melting in a suspension with 20 wt.% is approximately 140 kW. However, this power requirement increases to 390 kW for a suspension with 70 wt.%.

The deposition weight and thickness per pass for these samples are shown in Table 4-5, and it can be observed that they increase with increasing solid concentration. This is important because high thicknesses per pass and high deposition rates can provide technical advantages related to increasing the efficiency of SPS and ultimately economic advantages due to less energy consumption.

Deposition efficiency is also shown in Table 4-5. As the suspension concentration increases, the deposition efficiency decreases. For example, at a concentration of 20%, the deposition

efficiency is 38%, while at a concentration of 40%, it drops to 26%, and at a concentration of 55%, it drops further to 25%. The deposition efficiency reaches its lowest point of 21.3% at a high concentration of 70%. However, despite the lower deposition efficiency, increasing the concentration results in a greater amount of material being deposited on the substrate.

Table 4-5. Deposition weight and thickness per pass for different concentrations

Concentration (wt.%)	Thickness per pass (µm)	Deposition per pass (mg)	Deposition efficiency (%)
20	1.23	1.42	38.1
40	3.83	2.21	26.1
55	6.67	3.46	25.7
70	7.1	4.15	21.3

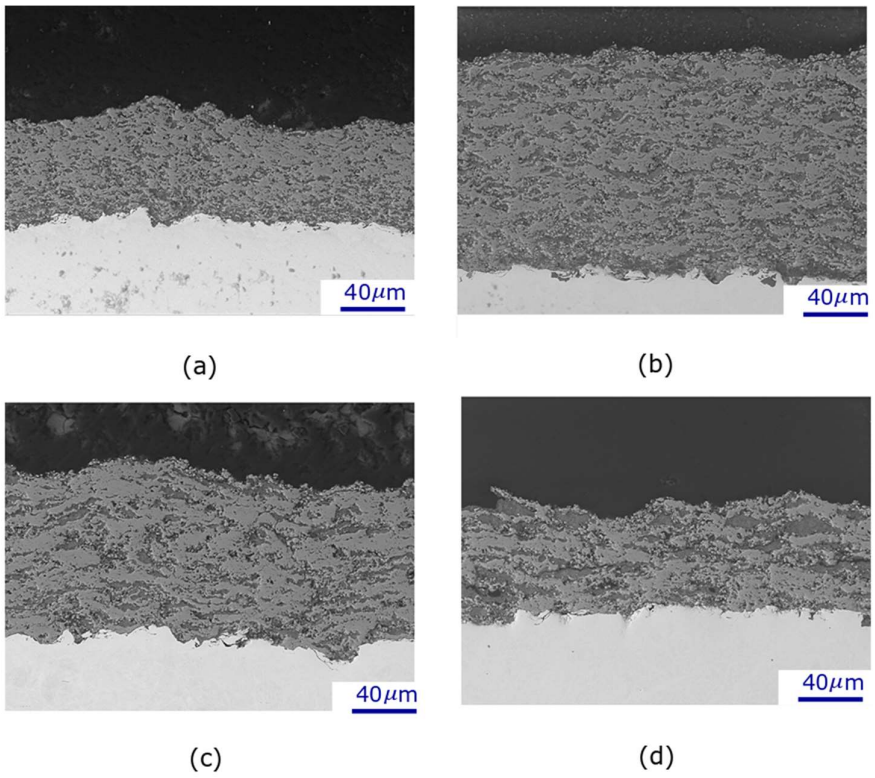

Figure 4-9. Cross-sectional back-scattered SEM micrographs for suspensions injected via flash boiling atomization with TiO_2 concentrations of (a) 20 wt.% (b) 40 wt.% (c) 55 wt.% (d) 70 wt.%.

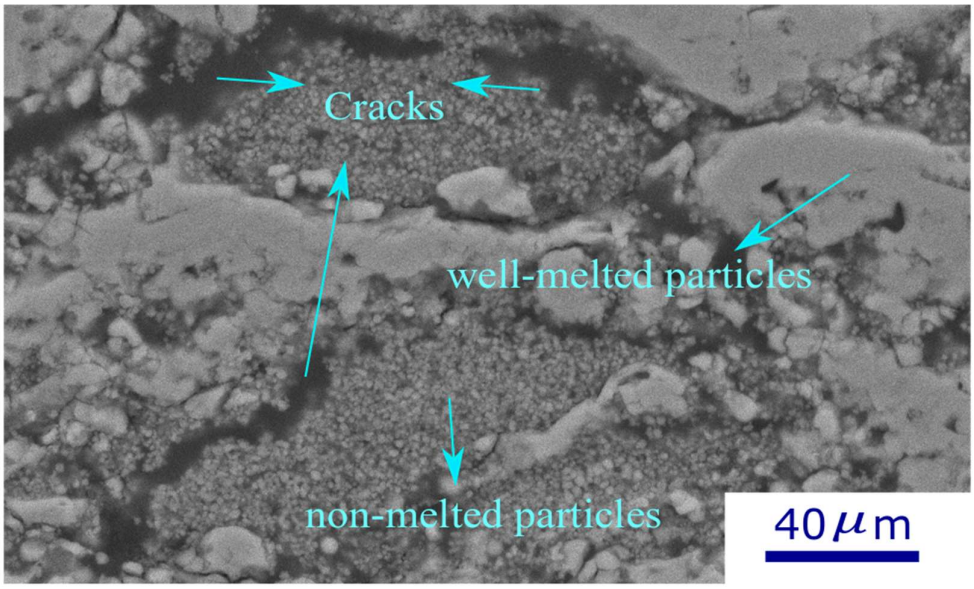

Figure 4-10. High-magnification SEM micrograph showing cracks along boundaries between two regions; coatings with 70 wt.%.

4.3.4 Phase composition

Figure 4-11 shows the XRD patterns of the deposits produced by flash boiling atomization and continuous jet. The percentage of each phase was determined based on relative peak intensity and is listed in Table 4-6. As expected, the phase composition is relatively similar because, as discussed in previous sections, the distribution of unmelted and melted particles through the deposits is approximately the same for the two methods. In thermal spray coatings, this can be explained by the general observation that anatase corresponds to the partially and unmelted particles, while the rutile phase is attributed to the fully melted particles [96].

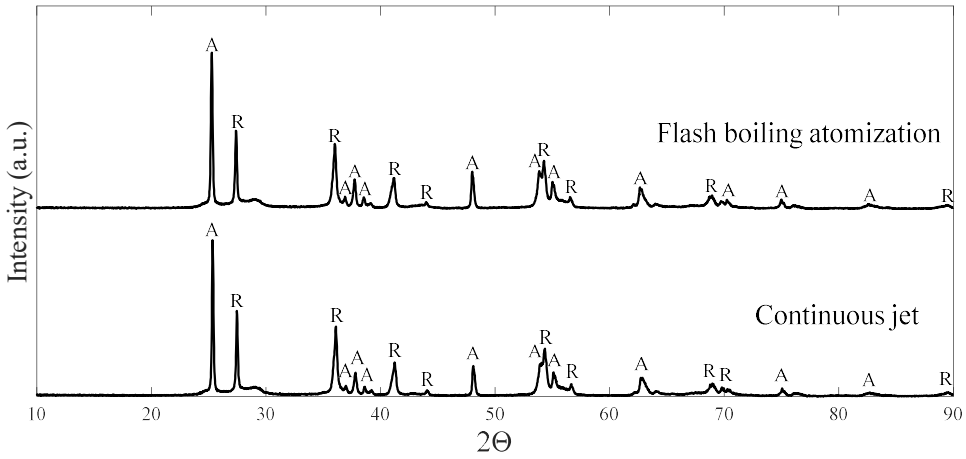

Figure 4-11. XRD patterns of the TiO_2 deposits for flash boiling atomization, and continuous jet.

Table 4-6. Phase composition for flash boiling atomization, and continuous jet.

	Anatase (%)	Rutile (%)
Continuous jet	56.9	43.1
Flash boiling atomization	59.4	40.6

The XRD analysis of the TiO_2 deposits at different suspension concentrations is shown in Figure 4-12. As listed in Table 4-7, all deposits contain more anatase phase than rutile phase. In this study, low power torch (33 kW) was used to create the deposits and more anatase phase can be explained by the fact that the heat treatment between the plasma jet and the particles takes place at lower plasma temperatures. The deposit produced with suspension concentration 70 wt.% contains approximately a 2:1 ratio of anatase to rutile, which is the largest fraction of anatase to rutile in this study. This may eventually be useful for photocatalytic applications, as the anatase phase has been shown to have higher photocatalytic activity compared to the rutile phase [97].

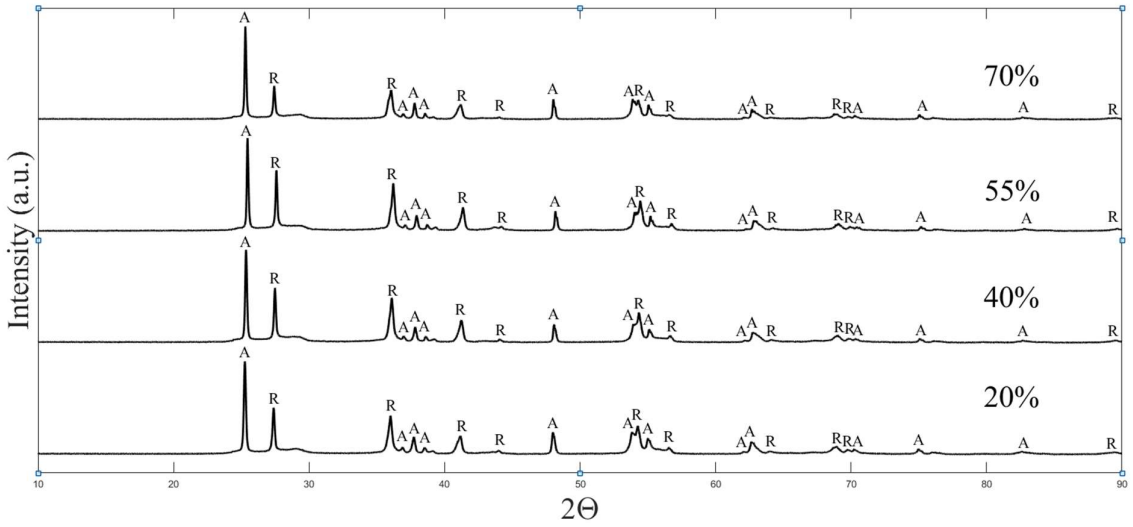

Figure 4-12. XRD patterns of the TiO_2 deposits for flash boiling atomization method with suspension concentrations of 20, 40, 55 and 70 wt.%.

Table 4-7. Phase composition of deposits produced at different solids concentrations.

Concentration (wt.%)	**Anatase (%)**	**Rutile (%)**
20	59.4	40.6
40	52.8	47.2
55	50.3	49.7
70	66.9	33.1

4.4 Conclusions

In this study, flash boiling atomization was used as a novel method to inject a water-based TiO2 suspension into a plasma jet. The deposits produced were compared with those produced by conventional injection methods (i.e., continuous jet) by examining the microstructure of the deposits, their deposition weight and deposit thickness per pass, deposition efficiency and the width of the deposits. No significant differences were found in the microstructure of the deposits between the two methods using a low power plasma gun. On the other hand, the deposition weight per pass increased slightly compared to the conventional method at the same flow rates. Greater variability was observed in the

deposition weight per pass with flash boiling atomization, which can be attributed to the unsteady flow rate entering the plasma jet. Wider deposits were also observed as one of the characteristics of this type of injection.

At concentrations above 40 wt.%, the suspension becomes highly viscous. This makes it difficult for the conventional method to effectively inject and deliver the particles into the plasma jet. This study also helped to highlight the possibility of injecting suspensions with higher solid content using flash boiling atomization compared to previous reports using continuous jet. It has been shown that the deposit weight and thickness per pass are dramatically increased by increasing the solid concentration from 20 to 70 wt.%. However, the deposition efficiency and the quality of the deposits seems to decrease as the distribution of unmelted particles increases with solid concentration, and a larger distribution of cracks seems to appear at the boundary between unmelted and well-melted zones of these deposits. The anatase and rutile distributions were examined for all deposits and it was observed that a high anatase phase can be found in the 70 wt.% deposit which confirms limited melting degree of the deposits. Our future work will focus on the use of a high powder plasma torch to cope with the higher spray rate when high concentration suspensions are used. This should have a positive impact on the actual coating structure and deposition efficiency.

Acknowledgements

The authors would like to thank the financial support of Natural Sciences and Engineering Research Council Canada (NSERC) and the Canada Research Chairs Program.

5 Chapter 5: Microstructure of deposits sprayed by a high power torch with flash boiling atomization of high-concentration suspensions

5.1 Introduction

Suspension plasma spraying (SPS) is a form of plasma spraying that allows the injection of nano-sized or submicron-sized powders into the plasma jet. These small particles are dispersed in a solvent to give them enough momentum to enter the plasma jet. The solvent is rapidly vaporized when exposed to the plasma stream and the small particles are melted, accelerated and directed to impact the substrate and form a coating. A unique coating microstructure can be created with this method, and both the mechanical and thermal behavior of coatings can be improved by using SPS compared to conventional air plasma spray (APS) coatings [6], [7]. However, the feed rate of the powders and deposition efficiency in SPS are typically two to three times lower than in APS [36]. The use of suspension with higher particle concentration is one way to improve the deposition of the feedstock. However, clogging can be an obstacle to injecting higher concentration suspensions (above 40 wt.%) because increasing the particle concentration increases the suspension viscosity, which leads to a decrease in suspension flowability. Nevertheless, flash boiling atomization has been found to be an effective method for transferring and injecting high viscosity fluids in various industries [98], [99].

Flash boiling is the thermodynamic phenomenon that occurs when a pressurized superheated liquid (i.e., a liquid heated to temperatures above its boiling point without boiling) is exposed to an environment where the ambient pressure is lower than the saturation pressure of the liquid. Flash boiling atomization has various applications ranging from fuel injection in combustion chambers [100] to distillation [101], spray drying [91] or pharmaceutical industry [102]. Since high temperatures help to reduce the viscosity of liquids or solutions, this method is also used to spray highly viscous liquids. Karami [103] used flash boiling atomization to spray black liquor (pulpwood to paper pulp byproduct) and studied the spray parameters, such as the spray pattern, at different injection temperatures. The viscosity of

black liquor at 70 wt.% solids and 127 ℃ is 88 times higher than the viscosity of water at room temperature [103]. Gunther et al. [104] used flash boiling to spray a polyvinylpyrrolidone solution and investigated the spray characteristics at different temperatures, nozzle geometries and fluid properties. This type of polymer has a viscosity 25 times greater than water at a solids concentration of 20 wt.%.

Suspension injection in SPS can be either axial or radial. In axial injection, the suspension is fragmented inside the torch by interaction with the atomizing gas, and the fragmented droplets are then exposed to the plasma jet. In radial injection, the suspension is injected into the plasma stream from outside the torch. Radial injection allows more control over injection parameters such as injection angle or adjusting the distance between the nozzle tip and the plasma jet. Mechanical injection and spray atomization are two different radial injection methods currently used in SPS.

In mechanical injection, a single continuous jet is injected into the plasma jet using a pressurized gas, and different jet breakup regimes occur in the plasma jet based on the Weber number of the gas (defined as the ratio between inertial forces and surface tension forces). In spray atomization, the suspension is injected as droplets generated by an atomizer. Toma et al. [30] used two different injection methods, mechanical injection and spray atomization (using an inert gas for atomization), to inject fine TiO_2 particles for the preparation of photocatalytic titania coatings. They showed that the microstructure of the coatings did not change for the different suspension injection methods. However, they found that the deposit thickness per pass decreased from 4-6 μm for mechanical injection to 1.5-2 μm for spray atomization. Three disadvantages of spray atomization over mechanical injection have been reported in the literature: First, gas atomization spraying creates disturbances in the plasma jet. Second, it would be more difficult to achieve precise injection of the feedstock at the

chosen location of the plasma jet with this spraying method. Third, there is a dispersion of droplet trajectories, sizes and velocities when working with spray atomization [10].

In mechanical injection, the injection pressure is the most important injection parameter that can affect the deposition efficiency rate, coating properties and microstructure. Meillot et al. [15] studied the feedstock penetration at different injection pressures for two different injection modes (up-to-down and down-to-up). They found that the feedstock required an optimal high pressure to reach the plasma center, while a very high pressure would lead to a decreasing deposition efficiency. Fauchais et al. [105] studied the effect of injection pressure and concluded that by increasing the pressure, the suspension can penetrate deeper to reach the hot region within the plasma jet. In spray atomization, in addition to injection pressure, other parameters such as nozzle design [88] and ALR (gas-to-liquid mass ratio) [32] can affect the size and velocity of the droplets and the properties of the coating. Marchand et al. [88] designed two different internal and external two-fluid nozzles to spray yttria stabilized zirconia (YSZ) into the plasma jet. They achieved different sprays with different droplet size and velocity distributions by changing the design of the atomizing nozzle. Rampon et al. [32] showed different spray patterns of yttria partially stabilized zirconia (Y-PSZ) suspension for three ALR values (0.15, 0.3 and 0.6). It was observed that better atomization occurred at higher ALR. However, the injection of atomizing gas into the plasma jet leads to a decrease in plasma temperature and consequently reduces the heat transfer to the suspension droplets. In flash boiling atomization, no gas is required for atomization and vapor bubbles are responsible for breaking the suspension jet into small droplets, so this method can overcome the adverse effects of using atomization gas on the plasma flow, such as plasma cooling and plasma disturbance.

In flash boiling atomization, not only is no atomization gas added to the plasma jet which contributes to the plasma cooling, but also the disintegrated droplets at the nozzle exit can

reach temperatures close to the water boiling point. This indicates that approximately 20% of the energy required for water evaporation with the plasma jet can be saved, as 80% of the required energy for water evaporation is associated with latent heat. In our pervious work [106], we compared two different coatings fabricated using flash boiling atomization and a single jet method. Our results demonstrate that flash boiling atomization can achieve slightly higher deposition with wider deposits compared to the conventional single jet method.

This study focuses on the preparation and injection of a high concentration submicron-sized titania suspension into the high-power plasma jet to develop SPS deposits. The spray parameters were selected to ensure stable plasma conditions and a controlled deposition process. To investigate the influence of increasing suspension concentration on coating microstructure, thickness, and deposition weight, four different solid concentrations were used, 20, 40, 55, and 70 wt%. The effect of torch power on the microstructure of the deposits as well as on the deposition efficiency of the process was investigated by using three different power levels, 33, 70, and 110 kW. The effect of torch power and solid concentration on the phase composition of the deposits was conducted by XRD analysis.

5.2 Materials and Methods

5.2.1 Experimental setup and SPS conditions

The experimental setup is shown in Figure 5-1. Two tanks were used, one for water (1) and the other for suspension (2). To avoid using more suspension, the experiment started by initially introducing water to the line to generate a consistent flash boiling spray. Then, the plasma torch was activated, and the three-way valve (4) was opened to introduce the suspension into the line. Water was also used to clean the line after each injection. The suspension was continuously agitated with a magnetic stirrer (3) during the experiment to prevent sedimentation. The air injection pressure (5) was 0.69 MPa. The flow rate of the

suspension was measured by a Coriolis flow meter (6) placed before a heater. This type of flow meter (Proline Promass 83, Endress+Hauser, Switzerland) can monitor the suspension feed rate and density of the suspension. The suspension was then superheated to 140 °C in the duct heater (7) but remained in the liquid phase because it was pressurized. The power of the heater can be regulated from 0 to 1.2 kW by connecting it to a variac transformer (8), and the desired temperature can be obtained by changing the power. The temperature was continuously monitored by a thermocouple (9) inserted at the outlet of the heater. The heater was connected to the torch nozzle holder (11) by a flexible plastic tube (10). This tube allows for more flexibility in the movement of the robotic arm. The cylindrical stainless-steel nozzle (12) with a diameter of 0.15 mm and a length of 1.25 mm was used attached to the robot arm with a nozzle holder.

In this experimental setup, the movement of the robotic arm was limited and didn't allow the entire substrate to be coated. The torch was attached to the robotic arm and held stationary in front of a rotating sample holder (13). The stand-off distance (distance between the torch exit and the substrate) was 50 mm. Stainless-steel substrates with dimensions of 25 mm × 50 mm were grit blasted with 80-grit alumina particles (i.e. particle size of 160 μm) and then were mounted on the rotating sample holder. Two different rotational speeds of 60 and 180 rpm (with linear velocities of 1 and 3 m/s, respectively) were used for the sample holder. Different spray times were chosen based on the suspension concentration because it was observed that delamination can occur at spray times longer than one minute.

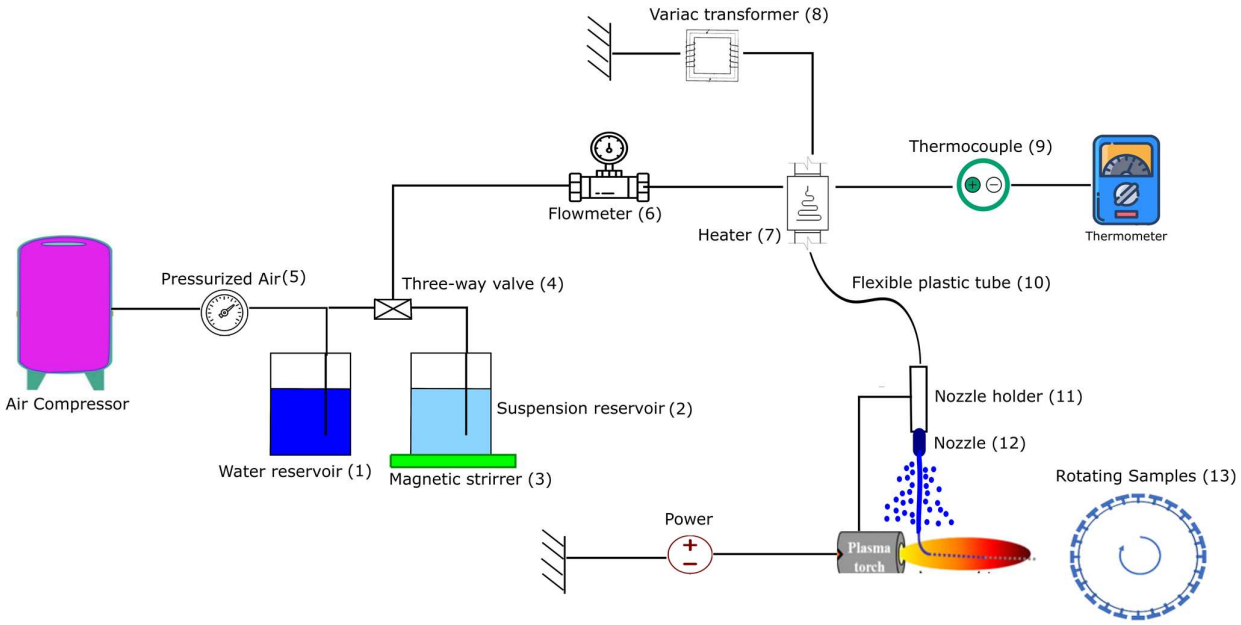

Figure 5-1. Schematic of the experimental setup

The 3MB torch (Oerlikon-Metco, Pfaffikon, Switzerland) and the Mettech Axial III torch (Northwest Mettech Corp., North Vancouver, BC, Canada) were utilized to produce deposits using low and high plasma powers, respectfully. In both cases, the suspension was injected radially in the plasma jet downstream the torch nozzle exit. Spray conditions for the 3MB and Axial III torches are shown in Table 1 and Table 2, respectively. The Axial III torch is designed for axial injection, therefore, some modifications were required to allow radial injection. The plasma power was 33 kW for the 3MB torch and two plasma powers 70 kW and 110 kW were used for the Axial III torch. The vertical distance between the nozzle tip and the center of the plasma jet was 8 mm for the 3MB torch and 15 mm for the Axial III torch.

The substrate temperature was not measured directly, but based on several previous experiments, it was known that sample temperatures cannot exceed 300°C [94] for the 3MB torch and 450°C for the Axial III torch when using a rotating sample and not preheating the

substrates[107]. The repeatability of experiments was confirmed by repeating each experiment two or three times, depending on the experimental conditions.

Table 5-1. Spray conditions for the 3MB torch.

Sample	Plasma power (kW)	Gas flow rate (SLPM)	Current (A)	Suspension concentration (wt.%)	Feed rate (mL/min)	Density (g/cm^3)	Spray time (s)	Rotating sample holder speed (RPM)	Coating thickness (μm)
C1	33	Ar/H_2 (50,3.5)	600	20	34-36	1.19	45	60	55
C2				40	32-34	1.43	30		115
C3				55	30-32	1.76	15		100
C4				70	28-30	2.14	10		70

Table 5-2. Spray conditions for the Axial III torch.

Sample	Plasma power (kW)	Gas flow rate (SLPM)	Total gas flow rate (SLPM)	Suspension concentration (wt.%)	Flow rate (mL/min)	Density (g/cm^3)	Spray time (s)	Rotating sample holder speed (RPM)	Coating thickness (μm)
C5	70	$Ar/N_2/H_2$ 45/45/10	180	55	30-33	1.7	10	60	140
C6	110	$Ar/N_2/H_2$ 45/45/10	220	20	34-36	1.17	30	180	55
C7				70	28-30	2.14	10		120

5.2.2 Suspension and feed material

The suspension was prepared by dispersing submicron-sized titanium dioxide particles (TKB Trading, Oakland, CA) with an average size of 500 nm in deionized water. A SEM micrograph of the SPS feedstock powder is presented in Figure 5-2. The particle concentrations were 20, 40, 55 and 70 wt.%. To produce uniform suspensions, especially at high concentrations (more than 70 wt.%), the particles were added slowly to the water and mixed simultaneously using a magnetic stirrer and an ultrasonic liquid mixer (QSonica,

USA). The suspension injection conditions used in this study are detailed in Tables 5-1 and 5-2.

In this research, nano titanium dioxide powder was chosen for its long-term sustainability, accessibility, and cost-effectiveness. Titanium dioxide (TiO_2) coatings are mostly recognized for their photocatalytic properties, and they are widely used in photocatalytic applications such as air and water purification, wastewater treatment, and self-cleaning surfaces across various industries.

The viscosity of the suspension increases significantly with increasing solid concentration [82], and the fluidity of the suspension also decreases in this condition. For this specific powder, Garmeh [95] conducted experiments to generate stress-strain rate curves for identical TiO_2 suspensions with varying concentrations of 30, 50, and 70 wt.%. The findings showed a notable rise in suspension viscosity when the concentration increased from 50% to 70%. In a highly viscous suspension, due to the presence of more solid particles, the interaction between the particles would be increased and agglomeration occurs. An efficient method for decreasing the viscosity of the suspension involves using an appropriate dispersing agent into the mixture [89]. An alternative approach, chosen for this experiment, entails increasing the temperature of the suspension until it reaches a superheated condition. The viscosity of a suspension is inversely proportional to the temperature and the viscosity decreases significantly at high temperatures and also the flowability would be improved in this condition [104]. It has been observed that suspensions with high TiO_2 concentration can be injected with this method for a longer injection time without clogging.

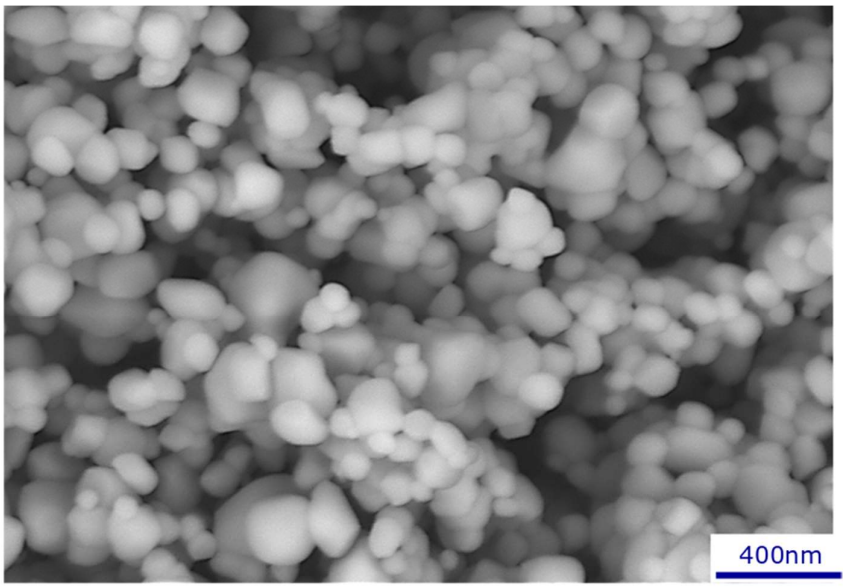

Figure 5-2. SEM micrograph of SPS feedstock TiO_2 powder.

5.2.3 Visualization and characterization measurements

The flash boiling spray was captured using the shadowgraph technique with a high-speed camera. The vertical distance between the suspension injector tip and the plasma jet was chosen based on these shadowgraph results. This vertical distance is important to ensure that most disintegrated droplets can penetrate to the plasma jet. The microstructure of the generated deposits was observed by scanning electron microscopy (SEM) (Hitachi S3400, Japan) at different magnifications. In addition, the phase identification (rutile and anatase distribution) of the deposits was measured by X-ray diffraction (XRD) using a X'Pert Pro; PANalytical (Philips, Netherlands). The Cu-Kα radiation was used and the 2θ angle ranged from 10 to 90°with a step size of 0.02°.

5.2.4 Flash boiling atomization condition

Flash boiling atomization is a thermodynamic process that can produce a spray of droplets. When a pressurized suspension (at a pressure of 0.69 MPa) passes through the duct heater, its temperature rises from room temperature to over 140°C, which has become a superheated

suspension. In this state, the suspension can be kept in the liquid phase due to its high pressure, but the maximum temperature must be kept below the boiling temperature of the injection pressure (the boiling temperature at 0.69 MPa is 169℃) because the suspension may evaporate inside the heater. When the superheated suspension passes through a nozzle, it experiences a rapid pressure drop from injection pressure to atmospheric pressure (0.1 MPa). At the time of pressure reduction, when the pressure reaches the saturation pressure of the injection temperature (a saturation pressure at 140℃ is 0.27 MPa), the suspension cannot be maintained as a liquid phase, and the phase change begins.

The onset of phase change occurs at nucleation sites, and the vapor bubbles begin to emerge from these sites. In pure water without impurities and dissolved gas, the wall of the nozzle is the main nucleation site. In suspension, in addition to the wall roughness, the surface of TiO_2 particles can promote the formation of steam bubbles. These vapor bubbles start growing rapidly, eventually reaching a point of expansion where they finally burst, breaking the suspension jet into smaller droplets. The flash boiling atomized spray jet of titanium dioxide suspension is shown in Figure 5-3.

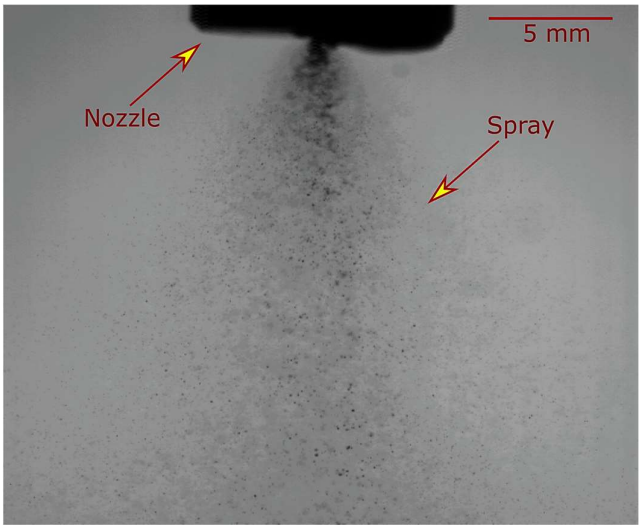

Figure 5-3. Spray jet morphology of the flash boiling atomization of the TiO_2 suspension. Suspension concentration: 20 wt.% (condition C1).

In the flash boiling spray jet, larger droplets remain in the center while smaller droplets are visible at the edge of the spray jet. The larger droplets at the center of the spray have enough momentum and also the right direction to reach the hot region of the plasma jet and can create a well-melted zone in the deposit microstructure. However, small droplets at the edge of the spray may be driven away by the plasma flow or may only penetrate to the outer zones of the lower temperature plasma flow, creating an unmelted zone in the deposits.

5.3 Results and discussion

5.3.1 Microstructure of TiO_2 deposits fabricated with different torch powers

The cross-sectional microstructure of the TiO_2 deposit obtained through flash boiling spray with a high-power torch (110 kW) and low solids concentration, is illustrated in Figure 5-4. A bimodal microstructure can be observed for the deposit: fully melted particles (light region) and unmelted particles (gray region). In addition, some dark areas correspond to the porosity observed in the deposit, which is negligible compared to other sections.

In our earlier investigation [106], we presented the deposit formed under conditions C1, characterized by lower power (3MB torch at 33 kW, solid concentration of 20 wt.%), which exhibited a high amount of unmelted areas mixed with well-melted particles. Notably, there was an observable gradient of unmelted particles within the deposit, with a high concentration near the deposit-substrate interface. This may be related to a rapid cooling rate between the stainless-steel substrate and the high-temperature particles. In our experimental setup (Figure 5-1), it is not possible to preheat the substrates because it takes several minutes to obtain the desired flash boiling spray jet, and the torch cannot be ignited in the meantime.

In contrast, the deposit formed under conditions C6 (Figure 5-4), produced at higher power (Axial III torch, solid concentration of 20 wt.%), exhibited a more uniform deposit with a

higher proportion of well-melted particles. By increasing the power of the torch from 33 kW to 110 kW, more energy is available for liquid evaporation and particle melting. Under these conditions, unmelted particles are not only concentrated near the substrate, but mixtures of well-melted and unmelted particles are also distributed throughout the entire deposit.

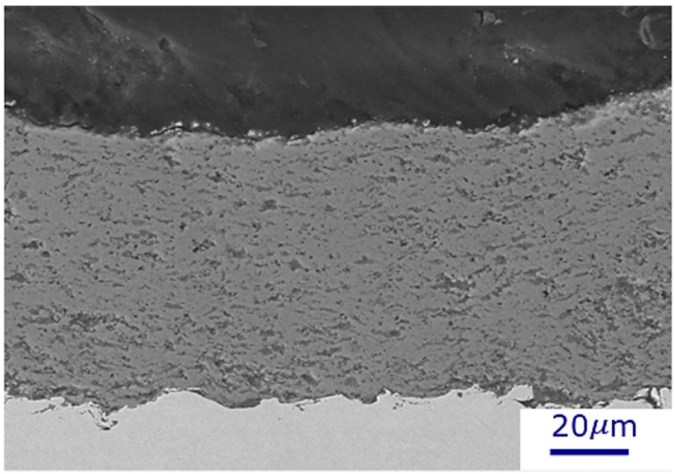

Figure 5-4. SEM micrographs of TiO_2 deposits obtained by flash boiling atomization for suspension concentration 20 wt.% and plasma power of 110 kW (condition C6).

Figure 5-5 shows higher magnification image of TiO_2 deposit under condition C6. The deposit comprises distinct zones: some are formed from the solidified splats resulting from the impact of fully melted particles, while others consist of unmelted particles coming from the suspension itself, with diameters ranging from 100 nm to 300 nm. A comparison between the unmelted particles within the deposits and the starting powder reveals that certain initial particles remain unmelted and are unable to reach the hot region in the plasma jet. In radial injection unlike the case of axial injection, the heat transfer between the plasma jet and the TiO_2 particles is not sufficient to provide the particle melting energy. As a result, the deposit produced with radial suspension injection and lower torch power is mainly built up by unmelted particles impacting the substrate. The non-melted zones have a weaker bond strength, which can be easily removed from the deposit with less abrasion [108]. In addition, the concentration of unmelted particles at the deposit-substrate interface for low power torch

can lead to weak deposit adhesion, and tolerance for thick deposits would not be supported. This delamination is the primary failure mode observed for deposits produced at low torch power and long spray times (greater than one minute at 60 rpm).

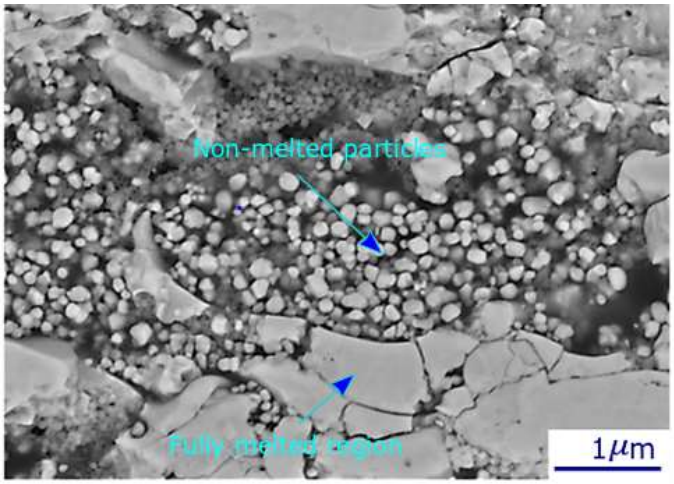

Figure 5-5. High magnification SEM micrograph showing non-melted particles and fully melted regions in a TiO2 deposit (condition 6).

5.3.2 Deposits fabricated with high solid content suspensions

Figure 5-6 shows deposit microstructures produced by using suspensions containing 70 wt.% of TiO2 particles and spraying at two different torch powers (33 kW and 110 kW): these are deposits C4 (Figure 5-6. a) and C7 (Figure 5-6. b). At low torch power, a significant amount of unmelted particles can be observed by increasing the solids concentration from low suspension concentrations to the 70 wt.% (Figure 5-6. a). And each region in the picture was determined by the contrast differences between them. In addition to the lower power available for particle melting, two other reasons could explain this high amount of unmelted particles. First, in suspensions with high solid concentrations, there is high particle interaction, which tends to facilitate particle agglomeration. These agglomerates, as well as larger particles, remain partially or completely unmelted in the plasma jet, and a higher plasma torch is required to melt these agglomerates: therefore, many unmelted particles are

obtained at low power conditions [109]. This is illustrated in Figure 5-7, which shows a magnified cross section of a 70 wt.% suspension deposit, showing a large number of agglomerates in the deposit microstructure. Suspension agglomeration may happen at each suspension conditions however when the suspension concentration is high, there is a greater chance for particles to come into close proximity, leading to increased agglomeration. In addition, the higher concentration means more solid particles are present in a specific volume of suspension, increasing the chance of collision to make an agglomeration.

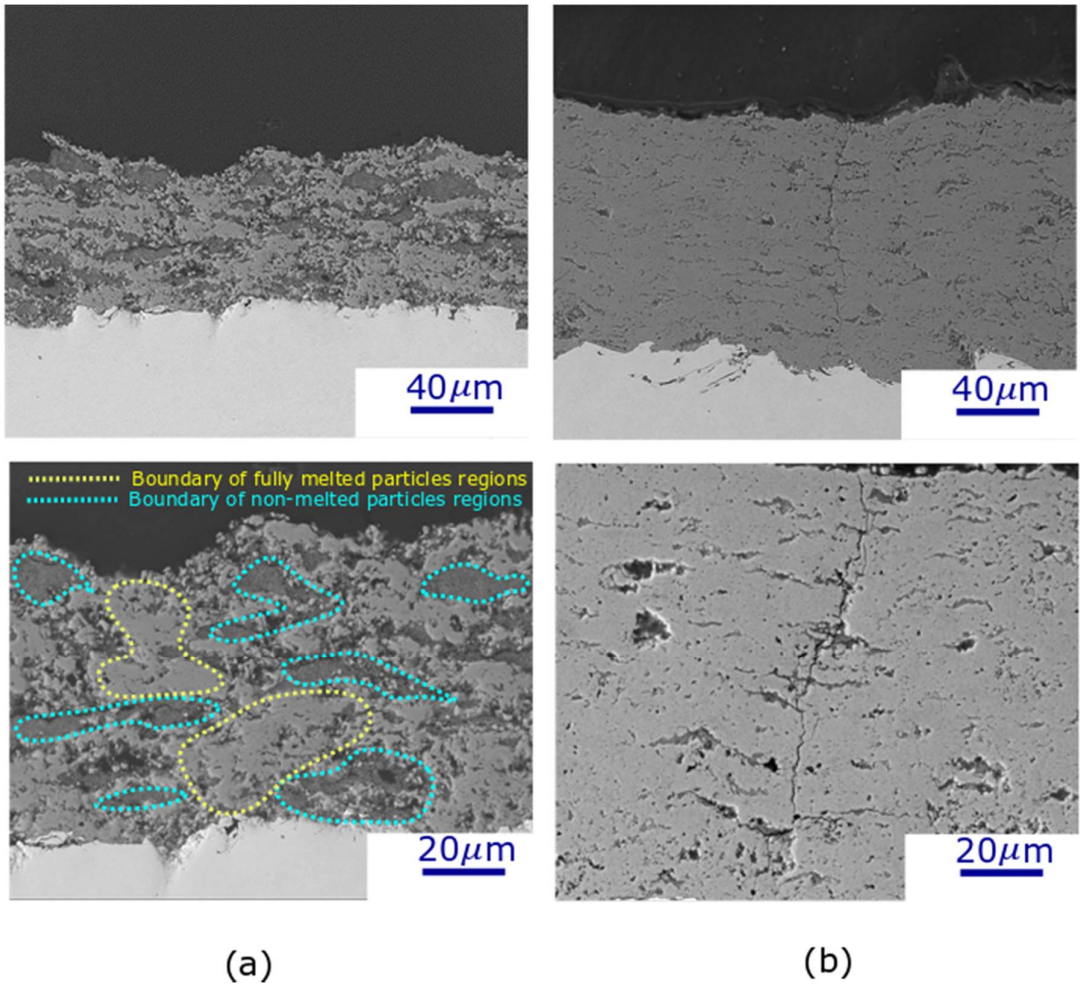

Figure 5-6. SEM micrographs of TiO2 deposits obtained by flash boiling atomization at different torch powers and solids content concentrations (a) C4 [18] (b) C7.

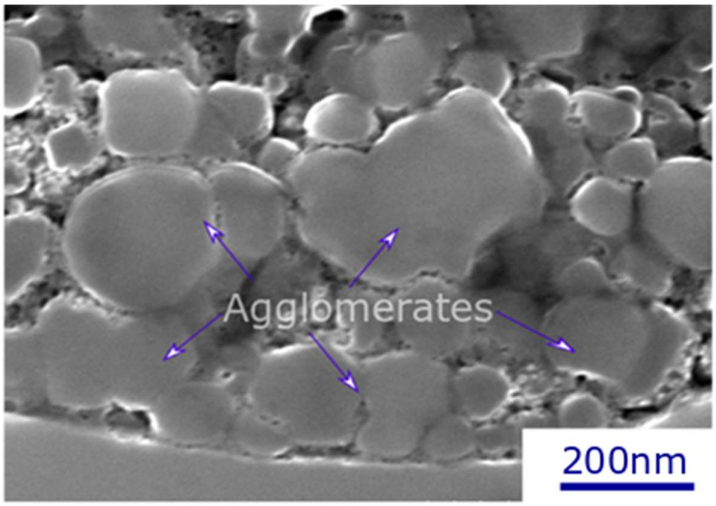

Figure 5-7. High magnification SEM micrograph of agglomerated particles in a TiO_2 deposit obtained with a 70 wt.% (condition C4).

Second, flash boiling atomization produces less spray atomization (primary atomization) with larger droplet size distribution in high viscosity suspension because the high viscosity hinders bubble growth and bubble bursting inside the suspension [104]. In addition, the surface tension of the suspension would increase with the solid concentration, leading to a decrease in the Weber number (equation 2) and consequently less secondary breakup of large droplets occurs inside the plasma jet. The fragmentation of the suspension inside the plasma jet is strongly dependent on the Weber number, and complete breakup usually occurs at high Weber numbers [11]. Less primary and secondary fragmentation results in the presence of larger suspension droplets inside the plasma jet and ultimately a higher amount of unmelted particles in the microstructure of deposits.

$$We = \frac{\rho_g \times u_r^2 \times d_l}{\sigma_l} \qquad (5-1)$$

Where ρ_g is the gas density (kg/m3), u_r is the relative velocity between the gas and liquid (m/s), d_l is the drop or liquid jet diameter (m) and σ_l is the liquid surface tension (N/m).

However, a dense deposit microstructure can be achieved at high solid concentrations and high torch power (110 kW) (Figure 5-6. b). The heat transfer increases by increasing the torch power and more energy is available for particle and agglomerate melting. In addition, the gas velocity and momentum are increased with higher torch power [82], and the Weber number is proportional to the square of the velocity, resulting in increased breakup within the plasma stream. In contrast to low torch power, high torch power produces a denser deposit by increasing the solid concentration from low suspension concentrations to 70 wt.%. Vicent et al. [110] calculated the power required to plasma spray water suspensions of alumina/titania by SPS at different solid contents of the suspension feedstock and showed that this power is reduced by increasing the solid concentration. Therefore, by increasing the concentration, a smaller amount of water is injected along the plasma flow and the energy consumption related to water evaporation during the plasma jet would be reduced.

Regardless of the torch power, no cracks are observed in the deposits produced with low solid concentrations . However, many horizontal and vertical cracks can be found at the boundaries between unmelted and well-melted particles in the high concentration, low torch power deposits (Figure 5-6. a) because these sections are the weakest part of the deposits. In addition, vertical cracks appeared in the high solid concentration, high torch power deposits (Figure 5-6. b). These vertical cracks can enhance the strain tolerance of the coatings. When the coating is subjected to mechanical stresses or strains, these cracks help distribute the stress more evenly by deflecting and absorbing energy. Additionally, they provide pathways for the dissipation of mechanical energy.

In these experiments, poor quality deposits with many cracks were obtained when spraying under C5 conditions, i.e. with solids concentrations above 55 wt.%, torch power above 70 kW and a lower speed of 60 rpm (Figure 5-8). This could be explained by the high solid deposition per pass at low rotational speeds, and thus the thermal expansion of the molten

particles as well as the thermal stress caused by the large temperature differences between the deposited feedstock and the substrate can destroy the deposit structure [111]. At high solid concentrations/high torch power, the rotational speed was tripled to avoid destruction of the deposits.

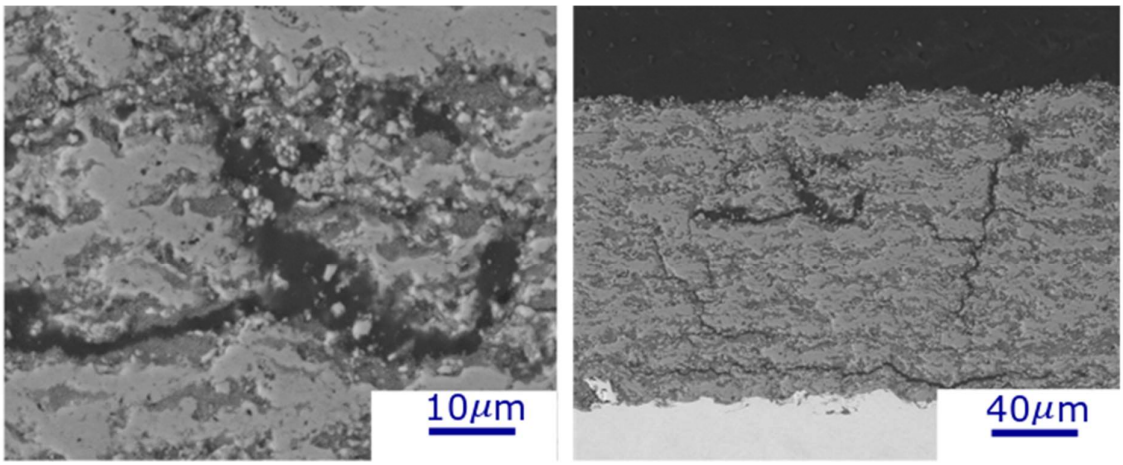

Figure 5-8. SEM micrographs of TiO_2 deposits obtained with high solid concentrations (> 55 wt.%), high torch power (> 70kW) and low rotating sample holder speed (60 RPM) (condition C5).

5.3.3 Deposition efficiency

In our experiments, flash boiling atomization efficiently injects high solids concentrations into the plasma jet without clogging. Suspensions with high concentrations yield a significant number of particles injected.

Figure 5-9 illustrates the amount of TiO_2 powder injected toward the substrate under various plasma spraying conditions. Comparing the injected particles under different spray conditions reveals a significant increase in the amount of injected particles with an increasing solids concentration. This relationship is not linear; for instance, the amount of injected particles per second for C4 (70 wt.%) is approximately five times higher than that for 20 wt.% solids content.

Figure 5-10 shows the deposition efficiency of deposits produced by flash boiling atomization under different conditions. The deposition efficiency is defined by dividing the change in weight of the substrates before and after spraying by the weight of TiO_2 powder used during spraying. The deposition efficiency for condition C1 (20 wt.% at 33 kW torch power) is 35% and decreases with increasing solid concentration at low torch power (33 kW) to reach 26 % for C2 (40 wt.%), 25% for C3 (55 wt.%), and finally 21% for C4 (70 wt.%).This behavior has also been observed by other researchers; when the plasma enthalpy is low, injecting more material into the plasma jet reduces the deposition efficiency [112], [113].

Therefore, it appears that as a direct result of increasing the solid concentration at low torch power, less energy is available from the plasma jet to melt individual particles, resulting in lower deposition efficiencies.

However, it was also observed that increasing the solid content at high torch power would increase the deposition efficiency (Figure 5-10). In particular, the deposition efficiency increased from 46% for C6 (20 wt.% at 110 kW torch power) to 60% for C7 deposit (70 wt.%). This is consistent with the findings of Curry et al. [114] who also showed that increasing the solids content at a high torch power of 105 kW would increase the deposition efficiency. In addition, the deposition efficiency was significantly improved by increasing the torch power at constant solids concentration. For example, the deposition efficiency is 25% for deposit C3 (33 kW) and increases to 61% for deposit C5 (70 kW power) (Figure 5-10). The reason for these high deposition efficiencies can be related to the higher input power, which not only compensates for the energy lost in water evaporation, but also allows for more complete particle melting.

The deposition efficiency of SPS is about 20%, while conventional spray techniques can reach 55-80%. Water-based suspensions have half the efficiency of ethanol-based ones due to

water's high evaporation heat [115]. However, employing flash boiling atomization in SPS, especially with high concentration suspensions, high-power torches, and fast rotational speeds of sample holders, can achieve efficiencies up to 60%, highlighting its significant advantage.

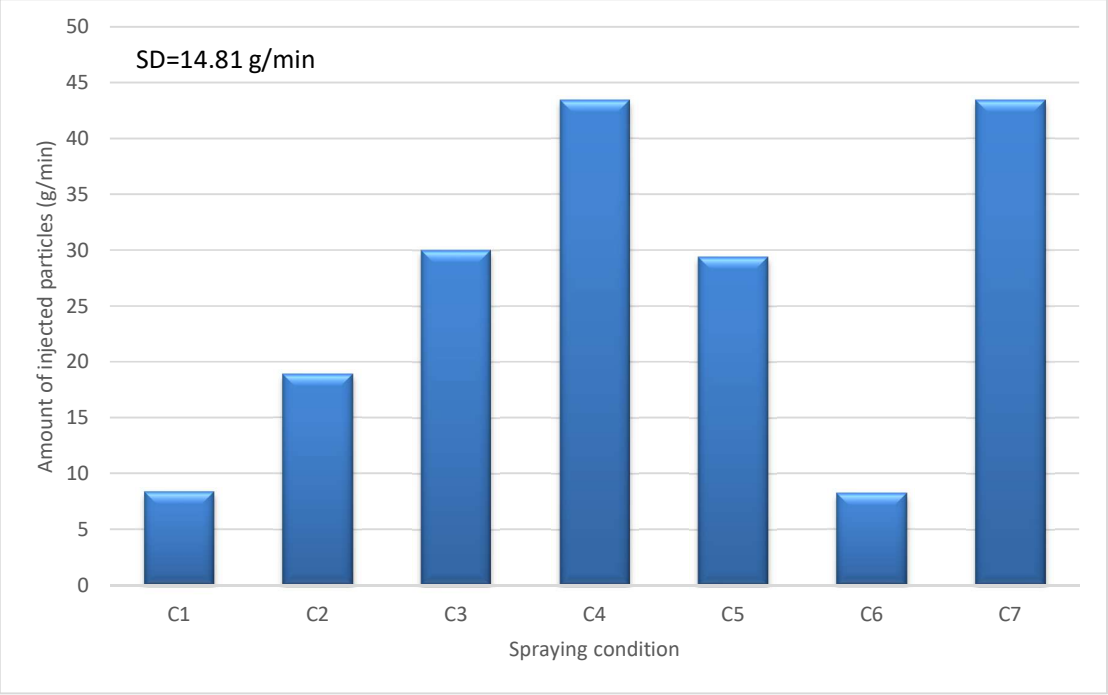

Figure 5-9. Amount of injected particles (g/min) for different spraying conditions.

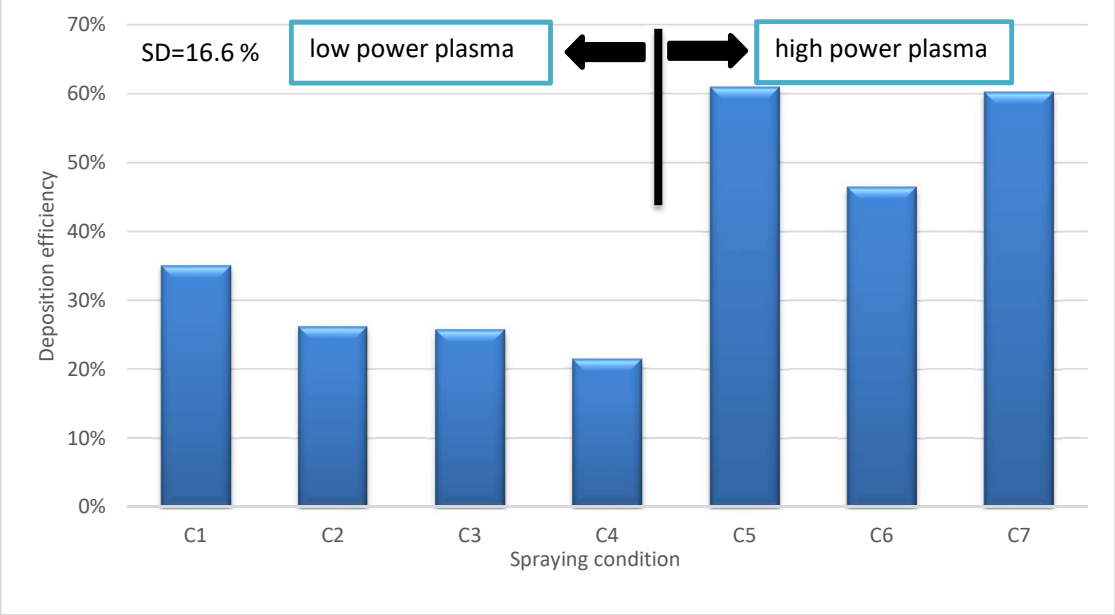

Figure 5-10. Deposition efficiency for different spraying conditions.

5.3.4 Phase composition

The XRD analysis of the TiO_2 deposits under various spraying conditions is depicted in Figure 5-11. This figure illustrates the XRD pattern for all deposits generated at high torch powers (Axial III torch at 70 & 110 kW). All deposits were identified as mixtures of rutile and anatase phases. The percentage of each phase for both low and high-power torches was determined using the relative peak intensity and is listed in Table 5-3. The percentage of the anatase phase varies from 35.7% to 66.9% depending on the suspension properties and plasma conditions chosen. The coatings produced under low torch power settings (C1 to C4) exhibit a higher concentration of anatase in comparison to rutile, as indicated in Table 3. This disparity can be attributed to the lower plasma power and subsequently lower plasma temperatures.

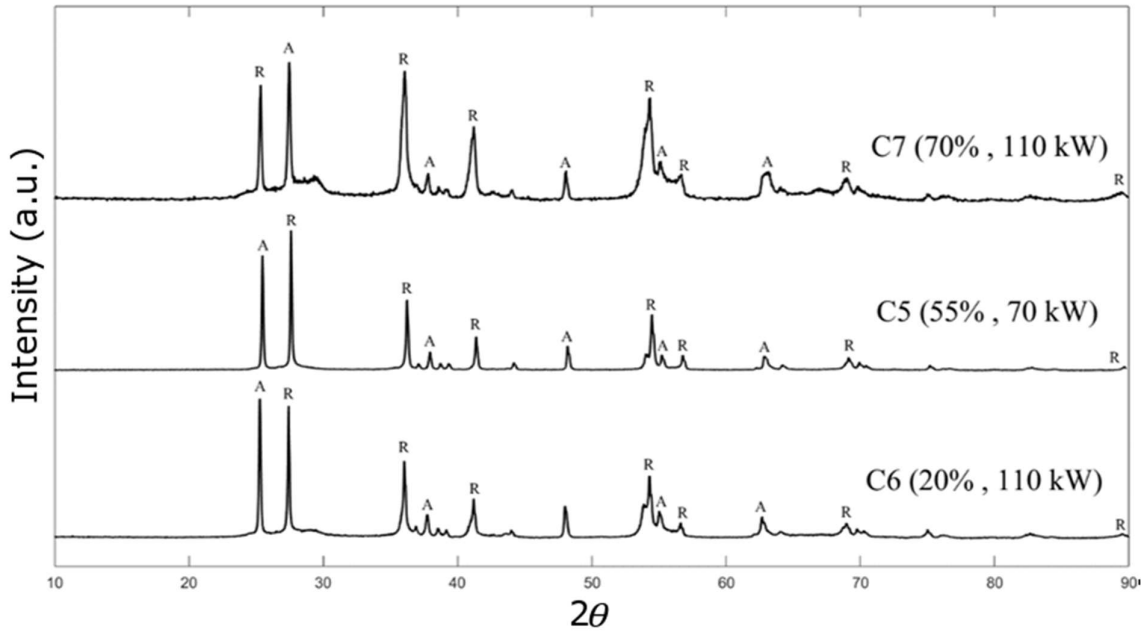

Figure 5-11. XRD patterns of the TiO_2 deposits for conditions C5 to C7 (plasma power of 70 & 110 kW).

At low torch power, more anatase phase would be formed by increasing the solid content, and the anatase distribution was increased from 59.4% for C1 (solid concentration is 20 wt.%) to 66.9% for C4 (solid concentration is 70 wt.%). Also, it seems that when the anatase phase of TiO2 nanoparticles was higher, a large amount of unmelted particles were observed in the

deposit microstructure, which can be observed in the SEM images (Fig. 6a). There's a suggestion that anatase phase is linked to partially and unmelted particles, whereas the rutile phase is ascribed to particles that have undergone complete melting [96], [116].

Table 5-3. Percentage of anatase and rutile phases for the deposits produced with conditions C1 to C7.

Samples	Anatase (%)	Rutile (%)
C1	59.4	40.6
C2	52.8	47.2
C3	50.3	49.7
C4	66.9	33.1
C5	35.7	64.2
C6	48.1	51.9
C7	38.2	63.9

Our measurements revealed that the main peak for the anatase phase at low power torch can be found between 2θ=25.2° and 2θ=25.4° depending on the different solid concentrations, which is in agreement with the peak values reported in the literature [117]. This can be explained by the low torch power, for which there is no significant change in the peak intensities related to the anatase and rutile phases. The main peak for the rutile phase occurs at 2θ=27.8° at low plasma temperature. Under conditions C4, the deposit formed shows an anatase-to-rutile ratio of approximately 2:1, the highest proportion of anatase to rutile through all other conditions. This could prove valuable for photocatalytic utilization, because the anatase phase can exhibit greater photocatalytic behaviour compared with the rutile phase [97].

In contrast to the low torch power, the rutile phase is predominantly formed, and the irreversible phase transformation of TiO_2 nanoparticles from anatase to rutile is more

prevalent. This can be explained by the high plasma temperature, which is sufficient to cause excessive heating of the particles, which can promote this phase transformation. In contrast to the lower power torch, where increasing the solid concentration resulted in less rutile and more anatase formation, the higher power torch resulted in an increase of the rutile phase from 51.9% for deposit C6 (20 wt.%) to 63.9% for deposit C7 (70 wt.%). A high solid concentration in the suspension promotes agglomeration of particles injected into the plasma jet. The heat transfer rate between the plasma flow and the agglomerates would be much lower than the heat transfer rate with the nanoparticles, so depending on their size, the agglomerates may not be melted or even partially melted inside the plasma jet. Thus, the higher power torch is required to convert the agglomerates from the anatase phase to the rutile phase. The rutile content for sample C4 (70 wt.% and 33 kW torch power) is 33.1% and this amount is approximately doubled to 63.9% for sample C7 (70 wt.% and 110 kW torch power).

On the other hand, at low solid content (20 wt.%), no significant increase in rutile phase was observed by increasing the torch power, from 40.6% for sample C1 (33 kW) to 51.9% for sample C6 (110 kW). When using flash boiling atomization for SPS, the droplets generated from the suspension should reach the core region of the plasma jet (hot zone) to achieve successful deposit deposition. This condition is more easily achieved for suspensions with high solids concentrations (e.g., 70 wt.%) because their density and momentum can be up to twice that of suspensions with lower solids content (Table 5-1).

5.4 Conclusion

Flash boiling atomization was applied as a new method of suspension injection in suspension plasma spraying to inject suspensions with high solid content. In this study, a water-based TiO2 suspension with a particle size of 500 nm was used with different solid concentrations

(20, 40, 55 and 70 wt.%). In this method, a pressurized suspension is first superheated to temperatures above 140 ℃ via a duct heater, then injected through a 0.15 mm stainless steel nozzle, and the spray jet of disintegrated droplets penetrates into the plasma jet. Unlike other spraying methods, no additional gas is added to the suspension for atomization, and the vapor bubbles created in the capillary area of the nozzle by rapid depressurization are responsible for atomization. A low power torch at maximum power (33 kW) and a high power torch at two power levels (70 & 110 kW) were used to investigate the effect of torch power on deposit properties such as deposit microstructure, deposition efficiency and phase composition. The key findings from our experimental investigation were presented below:

1) Remarkably high deposition rates could be achieved with the high power torch and by increasing the solids concentration from 20 wt.% to high concentrations such as 55 and 70 wt.%.

2) Deposition efficiency decreases with increasing solid concentrations at low torch power because less energy is available for particle melting under low-power conditions. Conversely, at high torch power, increasing solid concentrations enhances deposition efficiency due to better penetration into the hot region of the plasma jet.

3) Using suspensions containing 70 wt.% of feedstock and varying torch power from 33 kW to 110 kW, a variety of microstructures ranging from dense to highly porous have been achieved. Low torch power and high solids concentration can produce large amounts of unmelted particles, but high torch power and high solids concentration can produce a very dense deposit (mostly composed of well-melted particles).

4) XRD analysis showed that at low torch power, the anatase content is higher than the rutile content, and the anatase percentage increases with increasing solid

concentrations. However, the anatase phase is less dominant at high torch power and would decrease with increasing solid concentrations.

Acknowledgements

The authors would like to thank the financial support of Natural Sciences and Engineering Research Council Canada (NSERC) and the Canada Research Chairs Program.

6 Chapter 6: Conclusion and future work

6.1 Conclusions

The main purpose of this research work was to investigate the use of flash boiling atomization (FBA) as a new method of suspension injection in suspension plasma spraying (SPS), to be able to inject suspension with high solids concentration into the plasma flow and create coatings. As a first step to reach the mentioned goal, an experimental injection setup for FBA technique was designed in thermal spray laboratory. In order to find an optimum design for FBA, the spray behavior of FBA for suspension was studied and important parameters have been identified. It was shown that injection temperature is the most important parameter that can influence the suspension spray structure. The spray angle for suspension spray would be increased by increasing the injection temperature and wider spray structures were achieved at higher injection temperatures. In addition, the concentration of suspension particles is another important parameter that can affect the suspension spray structure. Chapter 2 provided a detailed explanation of the experimental methodology used in this study, as well as the safety and technical considerations that were taken into account during the FBA experiments. In Chapter 3, we examined the suspension spray structure under various experimental conditions, including suspension temperature and concentration. These preliminary results were instrumental in designing the thermal spray experimental setup for FBA, aimed at coating fabrication. In addition, the FBA process in the TS diagram was explained completely and the vapor quality of generated spray was calculated at different injection temperatures, by assuming isentropic expansion for FBA. Some experiments were done to validate these thermodynamic calculations.

By considering the shadowgraphy results of FBA for suspension, an experimental injection setup was set to fabricate coatings. The generated coatings for suspension concentration of 20 wt.% were compared with conventional coatings (fabricated with mechanical injection method). No significant differences in the microstructure of coatings can be observed

between two methods. Wider coatings for FBA technique could be observed compared with conventional one. In addition, the deposition weight and coating thickness for FBA coatings are slightly higher than conventional coatings in the same suspension flow rate. Furthermore, we presented the coating microstructures obtained at different suspension concentrations, which ranged from 20 wt.% to 70 wt.%, using a low-power torch with a rating of 33 kW.

In Chapter 4, the effect of power torches and different solids concentration on the FBA coating microstructures, deposition efficiency, and coatings thickness were investigated. Generally, the solid feed rate and deposition efficiency in SPS are 2-3 times lower than other conventional thermal spray techniques. The typical deposition efficiency for SPS is 15-20 %, however this value for other techniques can reach between 55-80%. It was shown that the deposition efficiency can reach to 60% by using FBA technique, using suspension with high concentration (more than 55 wt.%) and applying high power torches (more than 70 kW). In addition, the typical thickness per pass for SPS has been reported in the literature between 1.5-2 μm/pass. However, it was observed that significant high thickness per pass (up to 14 μm/pass) can be obtained for FBA coatings by increasing the solids concentration and power torches. For suspension 70 wt.%, the coatings microstructure is changed from highly porous to very dense structure by increasing power torch from 33 kW to 110 kW. Furthermore, the XRD analysis were done to find the anatase and rutile distribution through all Tio_2 coatings. The anatase phase percentages are between 35.7% to 66.9% depend on level of power torches and feedstock concentrations.

To conclude the thesis, the FBA method has been employed to facilitate the injection of suspension with high solid concentration (up to 70 wt.%) into the plasma flow to fabricate SPS coatings. The injection of suspension with concentration more than 40 wt.% is very challenging in SPS due to low suspension followability and clogging issue. In suspension with high particle concentration, the thickness per pass for FBA coatings is approximately 10

times higher than typical thickness per pass in SPS and the deposition efficiency can be increased 3-4 times by using high power torches. This suspension injection method is novel and this study showed it is highly worthy of further investigation to understand its various aspects. Additional research is necessary to enhance the current FBA setup and establish a commercial setup for this suspension injection method.

6.2 Recommendation for future work

FBA method is a novel technique for suspension injection in SPS, the effects of many parameters have not been investigated yet. The maturation of this innovative approach will require the investigation of several additional research work including those listed below:

- In this research, titanium dioxide powder was chosen due to its sustainability, accessibility, and cost-effectiveness. On the other hand, yttria-stabilized zirconia is a powder widely used in industry for its exceptional high-temperature resistance in gas turbines and fuel cells. There are several drawbacks associated with coatings produced from aqueous zirconium suspensions compared to coatings generated with ethanol-based zirconium. For instance, water-based suspensions tend to exhibit more pores and less dense microstructures, whereas ethanol-based suspensions typically result in denser microstructures with fewer pores. Additionally, water-based suspension coatings often develop a large number of cracks, whereas ethanol-based suspension coatings tend to have fewer cracks. These limitations are primarily attributed to poor atomization and the high energy cost associated with water evaporation. However, the FBA technique holds potential for improving water-based zirconium coatings by enhancing atomization and facilitating water evaporation.
- The columnar microstructure in TBC coatings offers numerous advantages, including enhanced thermal insulation, improved erosion resistance, better crack deflection, as

well as superior adhesion and increased thermal cycling resistance. However, fabricating a columnar microstructure using aqueous zirconium suspensions can be challenging due to their high surface tension and viscosity compared to ethanol-based suspensions. The FBA technique has potential for aiding in the generation of a columnar microstructure by superheating the suspension and reducing viscosity and surface tension.

- There are some limitations to our current experimental setup, requiring further investigation and studies to improve and develop our FBA setup. For example, in our current experimental setup, few minutes taken to reach a desired temperature and have a stable spray condition. Meanwhile, the torch cannot be ignited because the spray is trying to reach stable condition in front of exit torch and substrate preheating would be impossible. A sophisticated induction heater can be used to reduce a heating time to less than few seconds. In our injection setup, we face limitations in achieving full substrate coating, requiring changes to enhance the setup and overcome this limitation. Similarly, in our current FBA setup, limitations exist in performing axial flash boiling atomization. Modifications are required to address this limitation and achieve higher particle injection into the plasma jet.

7 References

[1] V. Donadei, H. Koivuluoto, E. Sarlin, and P. Vuoristo, "Lubricated icephobic coatings prepared by flame spraying with hybrid feedstock injection," *Surf. Coatings Technol.*, vol. 403, no. July, p. 126396, 2020, doi: 10.1016/j.surfcoat.2020.126396.

[2] F. Gärtner, T. Stoltenhoff, T. Schmidt, and H. Kreye, "The cold spray process and its potential for industrial applications," *J. Therm. Spray Technol.*, vol. 15, no. 2, pp. 223–232, 2006, doi: 10.1361/105996306X108110.

[3] J. O. Berghaus, B. Marple, and C. Moreau, "Suspension plasma spraying of Nanostructured WC-12Co coatings," *Proc. Int. Therm. Spray Conf.*, vol. 15, no. December, pp. 676–681, 2006, doi: 10.1361/105996306X147072.

[4] K. Bobzin, F. Ernst, K. Richardt, T. Schlaefer, C. Verpoort, and G. Flores, "Thermal spraying of cylinder bores with the Plasma Transferred Wire Arc process," *Surf. Coatings Technol.*, vol. 202, no. 18, pp. 4438–4443, 2008, doi: 10.1016/j.surfcoat.2008.04.023.

[5] D. Tejero-Martin, M. Rezvani Rad, A. McDonald, and T. Hussain, *Beyond Traditional Coatings: A Review on Thermal-Sprayed Functional and Smart Coatings*, vol. 28, no. 4. Springer US, 2019. doi: 10.1007/s11666-019-00857-1.

[6] P. Fauchais, R. Etchart-Salas, V. Rat, J. F. Coudert, N. Caron, and K. Wittmann-Ténèze, "Parameters controlling liquid plasma spraying: Solutions, sols, or suspensions," *J. Therm. Spray Technol.*, vol. 17, no. 1, pp. 31–59, 2008, doi: 10.1007/s11666-007-9152-2.

[7] R. Vaen, H. Kaner, G. Mauer, and D. Stöver, "Suspension plasma spraying: Process characteristics and applications," *J. Therm. Spray Technol.*, vol. 19, no. 1–2, pp. 219–225, 2010, doi: 10.1007/s11666-009-9451-x.

[8] L. Łatka, "Thermal Barrier Coatings Manufactured by Suspension Plasma Spraying - A Review," *Adv. Mater. Sci.*, vol. 18, no. 3, pp. 95–117, 2018, doi: 10.1515/adms-2017-0044.

[9] O. Tingaud *et al.*, "Suspension plasma spraying of zirconia coatings : process and coating structure To cite this version : HAL Id : hal-00262292 Suspension Plasma Spraying of Zirconia Coatings : Process and Coating Structure," 2008.

[10] C. Delbos, J. Fazilleau, V. Rat, J. F. Coudert, P. Fauchais, and B. Pateyron, "Phenomena involved in suspension plasma spraying part 2: Zirconia particle treatment and coating formation," *Plasma Chem. Plasma Process.*, vol. 26, no. 4, pp. 393–414, 2006, doi: 10.1007/s11090-006-9020-8.

[11] P. Fauchais, M. Vardelle, A. Vardelle, and S. Goutier, "What Do We Know, What are the Current Limitations of Suspension Plasma Spraying?," *J. Therm. Spray Technol.*, vol. 24, no. 7, pp. 1120–1129, 2015, doi: 10.1007/s11666-015-0286-3.

[12] P. Fauchais and G. Montavon, "Latest developments in suspension and liquid precursor thermal spraying," *J. Therm. Spray Technol.*, vol. 19, no. 1–2, pp. 226–239, 2010, doi: 10.1007/s11666-009-9446-7.

[13] P. Fauchais *et al.*, "Suspension and solution plasma spraying," *J. Phys. D. Appl. Phys.*, vol. 46, no. 22, 2013, doi: 10.1088/0022-3727/46/22/224015.

[14] J. Fazilleau, C. Delbos, V. Rat, J. F. Coudert, P. Fauchais, and B. Pateyron, "Phenomena involved in suspension plasma apraying part 1: Suspension injection and behavior," *Plasma Chem. Plasma Process.*, vol. 26, no. 4, pp. 371–391, 2006, doi: 10.1007/s11090-006-9019-1.

[15] E. Meillot, R. Vert, C. Caruyer, D. Damiani, and M. Vardelle, "Manufacturing nanostructured YSZ coatings by suspension plasma spraying (SPS): Effect of injection parameters," *J. Phys. D. Appl. Phys.*, vol. 44, no. 19, 2011, doi: 10.1088/0022-3727/44/19/194008.

[16] P. Fauchais and A. Vardelle, "Solution and Suspension Plasma Spraying of Nanostructure Coatings," *Adv. Plasma Spray Appl.*, no. May, 2012, doi: 10.5772/34449.

[17] J. Mostaghimi, M. Pasandideh-Fard, and S. Chandra, "Dynamics of Splat Formation in Plasma Spray Coating Process," *Plasma Chem. Plasma Process.*, vol. 22, no. 1, pp. 59–84, 2002, doi:

10.1023/A:1012940515065.

[18] D. Li *et al.*, “Microstructure formed by suspension plasma spraying: From YSZ splat to coating,” *Ceram. Int.*, vol. 43, no. 10, pp. 7488–7496, 2017, doi: 10.1016/j.ceramint.2017.03.027.

[19] H. Kaßner, A. Stuke, M. Rödig, R. Vaßen, and D. Stöver, “Influence of porosity on thermal conductivity and sintering in suspension plasma sprayed thermal barrier coatings,” *Ceram. Eng. Sci. Proc.*, vol. 29, pp. 147–158, Jan. 2009.

[20] N. Curry, K. VanEvery, T. Snyder, and N. Markocsan, “Thermal conductivity analysis and lifetime testing of suspension plasma-sprayed thermal barrier coatings,” *Coatings*, vol. 4, no. 3, pp. 630–650, 2014, doi: 10.3390/coatings4030630.

[21] P. He, H. Sun, Y. Gui, F. Lapostolle, H. Liao, and C. Coddet, “Microstructure and properties of nanostructured YSZ coating prepared by suspension plasma spraying at low pressure,” *Surf. Coatings Technol.*, vol. 261, pp. 318–326, 2015, doi: 10.1016/j.surfcoat.2014.11.010.

[22] Y. Wang *et al.*, “A novel structured suspension plasma sprayed YSZ-PTFE composite coating with tribological performance improvement,” *Surf. Coatings Technol.*, vol. 358, no. November 2018, pp. 108–113, 2019, doi: 10.1016/j.surfcoat.2018.11.021.

[23] O. Aranke, M. Gupta, N. Markocsan, X. H. Li, and B. Kjellman, “Microstructural Evolution and Sintering of Suspension Plasma-Sprayed Columnar Thermal Barrier Coatings,” *J. Therm. Spray Technol.*, vol. 28, no. 1–2, pp. 198–211, 2019, doi: 10.1007/s11666-018-0778-z.

[24] E. Alebrahim, F. Tarasi, M. S. Rahaman, A. Dolatabadi, and C. Moreau, “Fabrication of titanium dioxide filtration membrane using suspension plasma spray process,” *Surf. Coatings Technol.*, vol. 378, no. August, p. 124927, 2019, doi: 10.1016/j.surfcoat.2019.124927.

[25] Y. Fu, Y. Liu, and H. Li, “Onion-like carbon-modified TiO2 coating by suspension plasma spray with enhanced photocatalytic performances,” *J. Nanoparticle Res.*, vol. 21, no. 8, 2019, doi: 10.1007/s11051-019-4633-z.

[26] A. Ganvir, R. F. Calinas, N. Markocsan, N. Curry, and S. Joshi, “Experimental visualization of microstructure evolution during suspension plasma spraying of thermal barrier coatings,” *J. Eur. Ceram. Soc.*, vol. 39, no. 2–3, pp. 470–481, 2019, doi: 10.1016/j.jeurceramsoc.2018.09.023.

[27] N. Curry, S. Mahade, A. Venkat, and S. Joshi, “Erosion performance of suspension plasma spray thermal barrier coatings — A comparison with state of art coatings,” *Surf. Coatings Technol.*, vol. 437, no. February, p. 128311, 2022, doi: 10.1016/j.surfcoat.2022.128311.

[28] B. Lv, R. Mücke, X. Fan, T. J. Wang, O. Guillon, and R. Vaßen, “Sintering resistance of advanced plasma-sprayed thermal barrier coatings with strain-tolerant microstructures,” *J. Eur. Ceram. Soc.*, vol. 38, no. 15, pp. 5092–5100, 2018, doi: 10.1016/j.jeurceramsoc.2018.07.013.

[29] G. Mittal and S. Paul, “Suspension and Solution Precursor Plasma and HVOF Spray: A Review,” *J. Therm. Spray Technol.*, vol. 31, no. 5, pp. 1443–1475, 2022, doi: 10.1007/s11666-022-01360-w.

[30] F. L. Toma *et al.*, “Comparative study on the photocatalytic behaviour of titanium oxide thermal sprayed coatings from powders and suspensions,” *Surf. Coatings Technol.*, vol. 203, no. 15, pp. 2150–2156, 2009, doi: 10.1016/j.surfcoat.2008.10.022.

[31] E. M. Cotler, D. Chen, and R. J. Molz, “Pressure-based liquid feed system for suspension plasma spray coatings,” *J. Therm. Spray Technol.*, vol. 20, no. 4, pp. 967–973, 2011, doi: 10.1007/s11666-011-9624-2.

[32] R. Rampon, C. Filiatre, and G. Bertrand, “Suspension plasma spraying of YPSZ coatings: Suspension atomization and injection,” *J. Therm. Spray Technol.*, vol. 17, no. 1, pp. 105–114, 2008, doi: 10.1007/s11666-007-9143-3.

[33] G. Mauer, A. Guignard, R. Vaßen, and D. Stöver, “Process diagnostics in suspension plasma spraying,” *Surf. Coatings Technol.*, vol. 205, no. 4, pp. 961–966, 2010, doi: 10.1016/j.surfcoat.2010.03.007.

[34] P. Fauchais, “Understanding plasma spraying,” *J. Phys. D. Appl. Phys.*, vol. 37, no. 9, 2004, doi: 10.1088/0022-3727/37/9/R02.

[35] H. Kassner, R. Siegert, D. Hathiramani, R. Vassen, and D. Stoever, “Application of suspension plasma spraying (SPS) for manufacture of ceramic coatings,” *J. Therm. Spray Technol.*, vol. 17, no. 1, pp. 115–123, 2008, doi: 10.1007/s11666-007-9144-2.

[36] P. Fauchais, G. Montavon, R. S. Lima, and B. R. Marple, “Engineering a new class of thermal spray nano-based microstructures from agglomerated nanostructured particles, suspensions and solutions: An invited review,” *J. Phys. D. Appl. Phys.*, vol. 44, no. 9, 2011, doi: 10.1088/0022-3727/44/9/093001.

[37] R. Siegert, “A Novel Process for the Liquid Feedstock Plasma Spray of Ceramic Coatings with Nanostructural Features,” 2005.

[38] Z. Chen, R. W. Trice, M. Besser, X. Yang, and D. Sordelet, “Air-plasma spraying colloidal solutions of nanosized ceramic powders,” *J. Mater. Sci.*, vol. 39, no. 13, pp. 4171–4178, 2004, doi: 10.1023/B:JMSC.0000033396.51316.8b.

[39] A. Joulia *et al.*, “Comparing the deposition mechanisms in suspension plasma spray (SPS) and solution precursor plasma spray (SPPS) deposition of yttria-stabilised zirconia (YSZ),” *J. Eur. Ceram. Soc.*, vol. 34, no. 15, pp. 3925–3940, 2014, doi: 10.1016/j.jeurceramsoc.2014.05.024.

[40] H. Kamoun, G. Lamanna, B. Weigand, and J. Steelant, “High-speed shadowgraphy investigations of superheated liquid jet atomisation,” *22nd Annu. Conf. Liq. ...*, no. May, 2010, [Online]. Available: http://scholar.google.com/scholar?hl=en&btnG=Search&q=intitle:High-Speed+Shadowgraphy+Investigations+of+Superheated+Liquid+Jet+Atomisation#0

[41] D. Saury, S. Harmand, and M. Siroux, “Flash evaporation from a water pool: Influence of the liquid height and of the depressurization rate,” *Int. J. Therm. Sci.*, vol. 44, no. 10, pp. 953–965, 2005, doi: 10.1016/j.ijthermalsci.2005.03.005.

[42] D. Saury, S. Harmand, and M. Siroux, “Experimental study of flash evaporation of a water film,” *Int. J. Heat Mass Transf.*, vol. 45, no. 16, pp. 3447–3457, 2002, doi: 10.1016/S0017-9310(02)00056-X.

[43] A. Günther and K. E. Wirth, “Evaporation phenomena in superheated atomization and its impact on the generated spray,” *Int. J. Heat Mass Transf.*, vol. 64, pp. 952–965, 2013, doi: 10.1016/j.ijheatmasstransfer.2013.05.034.

[44] H. Witlox and P. J. Bowen, “Flashing liquid jets and two-phase dispersion: a review prepared by Det Norske Veritas Ltd for the Health and Safety Executive,” 2002. [Online]. Available: https://api.semanticscholar.org/CorpusID:43995944

[45] M. Levy, Y. Levy, and E. Sher, “Spray structure as generated under homogeneous flash boiling nucleation regime,” *Appl. Therm. Eng.*, vol. 73, no. 1, pp. 416–423, 2014, doi: 10.1016/j.applthermaleng.2014.08.008.

[46] E. Sher and M. Levi, “Spray Formation from Homogeneous Flash-Boiling Liquid Jets,” *Europe*, no. September, 2010.

[47] J. Senda, Y. Hojyo, and H. Fujimoto, “Modelling of atomization process in flash boiling spray,” *SAE Tech. Pap.*, vol. 15, pp. 291–296, 1994, doi: 10.4271/941925.

[48] M. M. Vieira and J. R. Simões-Moreira, “Low-pressure flashing mechanisms in iso-octane liquid jets,” *J. Fluid Mech.*, vol. 572, pp. 121–144, 2007, doi: 10.1017/S0022112006003430.

[49] E. Elias and P. L. Chambré, “Flashing inception in water during rapid decompression,” *J. Heat Transfer*, vol. 115, no. 1, pp. 231–238, 1993, doi: 10.1115/1.2910654.

[50] J. H. Llenhard and M. Trela, “of Hot Water to © m High Pressure ",” vol. 100, no. August 1978, pp. 473–479, 2016.

[51] E. Sher, T. Bar-Kohany, and A. Rashkovan, “Flash-boiling atomization,” *Prog. Energy Combust. Sci.*, vol. 34, no. 4, pp. 417–439, 2008, doi: 10.1016/j.pecs.2007.05.001.

[52] J. Barták, “A study of the rapid depressurization of hot water and the dynamics of vapour bubble generation in superheated water,” *Int. J. Multiph. Flow*, vol. 16, no. 5, pp. 789–798, 1990, doi: 10.1016/0301-9322(90)90004-3.

[53] M. Alamgir and J. H. Lienhard, “Correlation of pressure undershoot during hot-water depressurization,” *J. Heat Transfer*, vol. 103, no. 1, pp. 52–55, 1981, doi: 10.1115/1.3244429.

[54] D. Kawano, Y. Goto, M. Odaka, and J. Senda, “Modeling Atomization and Vaporization Processes of Flash-Boiling Spray,” in *SAE 2004 World Congress & Exhibition*, SAE International, Mar. 2004. doi: https://doi.org/10.4271/2004-01-0534.

[55] R. D. Reitz, “A photographic study of flash-boiling atomization,” *Aerosol Sci. Technol.*, vol. 12, no. 3,

pp. 561–569, 1990, doi: 10.1080/02786829008959370.

[56] K. E. Wirth and M. Rossmeissl, “Critical mass-flow in orifice-nozzles at the disintegration of superheated liquids,” *Proc. ASME Fluids Eng. Div. Summer Meet. 2006, FEDSM2006*, vol. 1 SYPMOSIA, pp. 1381–1388, 2006, doi: 10.1115/fedsm2006-98043.

[57] R. D. Oza, “On the Mechanism of Flashing Injection of Initially Subcooled Fuels,” *J. Fluids Eng.*, vol. 106, no. 1, pp. 105–109, 1984, doi: 10.1115/1.3242383.

[58] B. Cai, X. Tuo, Z. Song, Y. Zheng, H. Gu, and H. Wang, “Modeling of spray flash evaporation based on droplet analysis,” *Appl. Therm. Eng.*, vol. 130, pp. 1044–1051, 2018, doi: 10.1016/j.applthermaleng.2017.11.083.

[59] G. A. Johnson, “Further © 1977,” *Annu. Rev. Anthropol.*, vol. 6, pp. 479–508, 1977.

[60] C. E. Brennen, *Cavitation and bubble dynamics*. 2013. doi: 10.1017/CBO9781107338760.

[61] P. Saha and C. W, “B ~ ~ - & ? % - - ~ 9 5 10’ ti85 018288,” p. 90, 1993.

[62] H. Vu and G. Aguilar, “High-Speed Internal Nozzle Flow Visualization of Flashing Jets Department of Mechanical Engineering University of California-Riverside Riverside , CA USA,” *Proc. ICLASS 2009*, no. July, 2009.

[63] A. Günther and K. Wirth, “Evaporation phenomena in the atomization of superheated liquids and their impact on the spray characteristics Institute of Particle Technology , Friedrich-Alexander-University Erlangen-Nuremberg , Germany,” pp. 1–7, 2012.

[64] B. Park and S. Lee, “An experimental investigation of the flash boiling atomization mechanism,” *At. Sprays*, vol. 4, no. July, pp. 1–23, 2020.

[65] T. Bar-Kohany and M. Levy, “State of the art review of flash-boiling atomization,” *At. Sprays*, vol. 26, no. 12, pp. 1259–1305, 2016, doi: 10.1615/AtomizSpr.2016015626.

[66] G. Lamanna, H. Kamoun, B. Weigand, and J. Steelant, “Towards a unified treatment of fully flashing sprays,” *Int. J. Multiph. Flow*, vol. 58, pp. 168–184, 2014, doi: 10.1016/j.ijmultiphaseflow.2013.08.010.

[67] Y. Kltamura, T. Takahashl, and H. Morlmltsu, “Critical Superheat for Flashing of Superheated Liquid Jets,” *Ind. Eng. Chem. Fundam.*, vol. 25, no. 2, pp. 206–211, 1986, doi: 10.1021/i100022a005.

[68] R. Brown and J. L. York, “Sprays formed by flashing liquid jets,” *AIChE J.*, vol. 8, no. 2, pp. 149–153, 1962, doi: 10.1002/aic.690080204.

[69] V. Cleary, P. Bowen, and H. Witlox, “Flashing liquid jets and two-phase droplet dispersion. I. Experiments for derivation of droplet atomisation correlations,” *J. Hazard. Mater.*, vol. 142, no. 3, pp. 786–796, 2007, doi: 10.1016/j.jhazmat.2006.06.125.

[70] M. L. Corn *et al.*, “Characterization of a superheated fuel jet in a crossflow,” *J. Eng. Gas Turbines Power*, vol. 133, no. 1, pp. 1–7, 2011, doi: 10.1115/1.4001978.

[71] Y. Zeng and C. F. F. Lee, “An atomization model for flash boiling sprays,” *Combust. Sci. Technol.*, vol. 169, no. 1, pp. 45–67, 2001, doi: 10.1080/00102200108907839.

[72] S. Shen, M. Jia, T. Wang, Q. Lü, and K. Sun, “Measurement of the droplets sizes of a flash boiling spray using an improved extended glare point velocimetry and sizing,” *Exp. Fluids*, vol. 57, no. 4, pp. 1–16, 2016, doi: 10.1007/s00348-016-2147-3.

[73] D. Yildiz, P. Rambaud, J. Beeck, and J.-M. Buchlin, “Evolution of the spray characteristics in superheated liquid jet atomization in function of initial flow conditions,” *10th Int. Conf. Liq. At. Spray Syst. ICLASS 2006*, vol. 1, 2006.

[74] J. T. Allen, “Laser-based measurements in two-phase flashing propane jets. Part two: Droplet size distribution,” *J. Loss Prev. Process Ind.*, vol. 11, no. 5, pp. 299–306, 1998, doi: 10.1016/S0950-4230(98)00016-3.

[75] R. K. Calay and A. E. Holdo, “Modelling the dispersion of flashing jets using CFD,” *J. Hazard. Mater.*, vol. 154, no. 1–3, pp. 1198–1209, 2008, doi: 10.1016/j.jhazmat.2007.11.053.

[76] G. Polanco, A. E. Holdø, and G. Munday, “General review of flashing jet studies,” *J. Hazard. Mater.*, vol. 173, no. 1–3, pp. 2–18, 2010, doi: 10.1016/j.jhazmat.2009.08.138.

[77] B. Zuo, A. M. Gomes, and C. J. Rutland, “Modelling superheated fuel sprays and vaproization,” *Int. J.*

Engine Res., vol. 1, no. 4, pp. 321–336, 2000, doi: 10.1243/1468087001545218.

[78] S. van Stralen and R. Cole, *Boiling Phenomena: Physicochemical and Engineering Fundamentals and Applications*, no. vol.~1. in Boiling Phenomena: Physicochemical and Engineering Fundamentals and Applications. Hemisphere Publishing Corporation, 1979. [Online]. Available: https://books.google.ca/books?id=6AFRAAAAMAAJ

[79] J. Yan, S. Gao, W. Liu, T. Chen, T. H. Lee, and C. F. Lee, "Experimental study of flash boiling spray with isooctane, hexane, ethanol and their binary mixtures," *Fuel*, vol. 292, no. February, p. 120415, 2021, doi: 10.1016/j.fuel.2021.120415.

[80] T. Yiamsawas, O. Mahian, A. S. Dalkilic, S. Kaewnai, and S. Wongwises, "Experimental studies on the viscosity of TiO2 and Al2O3 nanoparticles suspended in a mixture of ethylene glycol and water for high temperature applications," *Appl. Energy*, vol. 111, pp. 40–45, 2013, doi: 10.1016/j.apenergy.2013.04.068.

[81] J. Creech, V. Divino, W. Patterson, P. J. Zalesky, and C. E. Brennen, "Injection of highly supersaturated oxygen solutions without nucleation," *J. Biomech. Eng.*, vol. 124, no. 6, pp. 676–683, 2002, doi: 10.1115/1.1519558.

[82] D. Waldbillig and O. Kesler, "The effect of solids and dispersant loadings on the suspension viscosities and deposition rates of suspension plasma sprayed YSZ coatings," *Surf. Coatings Technol.*, vol. 203, no. 15, pp. 2098–2101, 2009, doi: 10.1016/j.surfcoat.2008.11.027.

[83] D. Yildiz, R. Theunissen, J. P. A. J. van Beeck, and M. L. Riethmuller, "Understanding of dynamics of a two-phase flashing jet using multi-intensity-layer PIV and PDA," *11th Int. Symp. Appl. Laser Tech. to Fluid Mech.*, no. January, pp. 1–10, 2002, [Online]. Available: http://ltces.dem.ist.utl.pt/lxlaser/lxlaser2002/papers/paper_3_6.pdf

[84] Z. Zhifu, W. Weitao, C. Bin, W. Guoxiang, and G. Liejin, "An experimental study on the spray and thermal characteristics of R134a two-phase flashing spray," *Int. J. Heat Mass Transf.*, vol. 55, no. 15–16, pp. 4460–4468, 2012, doi: 10.1016/j.ijheatmasstransfer.2012.04.021.

[85] C. W. Nagai, N., Sato, K., & Lee, "Atomization characteristics of superheated liquid jets," *Int. Conf. Liq. At. Spray Syst.*, vol. 3, pp. 1–11, 1985.

[86] M. Aghasibeig, F. Tarasi, R. S. Lima, A. Dolatabadi, and C. Moreau, "A Review on Suspension Thermal Spray Patented Technology Evolution," *J. Therm. Spray Technol.*, vol. 28, no. 7, pp. 1579–1605, 2019, doi: 10.1007/s11666-019-00904-x.

[87] E. Aubignat *et al.*, "Optimization of the injection with a twin-fluid atomizer for suspension plasma spray process using three non-intrusive diagnostic tools," *J. Vis.*, vol. 19, no. 1, pp. 21–36, 2016, doi: 10.1007/s12650-015-0281-2.

[88] O. Marchand, L. Girardot, M. P. Planche, P. Bertrand, Y. Bailly, and G. Bertrand, "An insight into suspension plasma spray: Injection of the suspension and its interaction with the plasma flow," *J. Therm. Spray Technol.*, vol. 20, no. 6, pp. 1310–1320, 2011, doi: 10.1007/s11666-011-9682-5.

[89] E. Cañas, E. Rosado, C. Alcázar, M. J. Orts, R. Moreno, and E. Sánchez, "Challenging zircon coatings by suspension plasma spraying," *J. Eur. Ceram. Soc.*, vol. 42, no. 10, pp. 4369–4376, 2022, doi: 10.1016/j.jeurceramsoc.2022.03.049.

[90] X. Li, S. Yang, T. Li, D. L. S. Hung, and M. Xu, "Investigations on near-field atomization of flash boiling sprays for gasoline direct injection related applications," *Fuel*, vol. 257, no. May, p. 116097, 2019, doi: 10.1016/j.fuel.2019.116097.

[91] J. Ivey, "Particle Formation from Evaporating Microdroplets for Inhaled Drug Delivery," *J. Chem. Inf. Model.*, vol. 53, no. 9, pp. 1689–1699, 2013.

[92] Y. Feng, W. Qi, M. H. Baghaei, Y. Zhang, and D. Zhao, "Investigation on a Novel Type of Tubular Flame Burner with Multi-stage Partially-Premixing Features for Liquid-Fueled Gas Turbine," *Combust. Sci. Technol.*, vol. 193, no. 1, pp. 110–125, 2021, doi: 10.1080/00102202.2019.1651298.

[93] J. Château and H. Lhuissier, "Breakup of a particulate suspension jet," *Phys. Rev. Fluids*, vol. 4, no. 1, pp. 1–8, 2019, doi: 10.1103/PhysRevFluids.4.012001.

[94] N. Hosseinabadi and H. A. Dehghanian, "Suspension Plasma Spray," *Suspens. Plasma Spray Coat. Adv. Ceram.*, pp. 27–33, 2022, doi: 10.1201/9781003285014-2.

[95] S. Garmeh, “Transportation of high concentration suspension using visco-plastic lubrication School of Graduate Studies,” 2019.

[96] C. Lee, H. Choi, C. Lee, and H. Kim, “Photocatalytic properties of nano-structured TiO2 plasma sprayed coating,” *Surf. Coatings Technol.*, vol. 173, no. 2–3, pp. 192–200, 2003, doi: 10.1016/S0257-8972(03)00509-7.

[97] A. Fujishima and X. Zhang, “Titanium dioxide photocatalysis: present situation and future approaches,” *Comptes Rendus Chim.*, vol. 9, no. 5–6, pp. 750–760, 2006, doi: 10.1016/j.crci.2005.02.055.

[98] N. Seelam, S. K. Gugulothu, R. V. Reddy, and B. Burra, “Influence of hexanol/hydrogen additives with diesel fuel from CRDI diesel engine with exhaust gas recirculation technique: A special focus on performance, combustion, gaseous and emission species,” *J. Clean. Prod.*, vol. 340, no. January, p. 130854, 2022, doi: 10.1016/j.jclepro.2022.130854.

[99] D. Gvozdyakov and A. Zenkov, “Improvement of atomization characteristics of coal-water slurries,” *Energy*, vol. 230, p. 120900, 2021, doi: 10.1016/j.energy.2021.120900.

[100] T. Badawy, H. Xu, and Y. Li, “Macroscopic spray characteristics of iso-octane, ethanol, gasoline and methanol from a multi-hole injector under flash boiling conditions,” *Fuel*, vol. 307, no. February 2021, p. 121820, 2022, doi: 10.1016/j.fuel.2021.121820.

[101] G. Guo, H. Deng, C. Zhu, and Z. Ji, “Spatially dependent salinity effect in actively vacuumed spray flash desalination,” *Desalination*, vol. 537, no. January, p. 115868, 2022, doi: 10.1016/j.desal.2022.115868.

[102] B. J. Myatt *et al.*, “Unlocking further understanding of the atomization mechanism of a pressurized metered dose inhaler,” *Aerosol Sci. Technol.*, vol. 56, no. 11, pp. 1022–1032, 2022, doi: 10.1080/02786826.2022.2116305.

[103] R. Karami, A. Kankkunen, N. Ashgriz, and H. Tran, “Effects of flashing on spray characteristics of splashplate nozzles,” *Tappi J.*, vol. 12, no. 5, pp. 21–27, 2013, doi: 10.32964/tj12.5.21.

[104] A. Günther and K.-E. Wirth, “Superheated Atomization,” in *Process-Spray: Functional Particles Produced in Spray Processes*, U. Fritsching, Ed., Cham: Springer International Publishing, 2016, pp. 609–645. doi: 10.1007/978-3-319-32370-1_16.

[105] P. Fauchais *et al.*, “Suspension and solution plasma spraying of finely structured layers: Potential application to SOFCs,” *J. Phys. D. Appl. Phys.*, vol. 40, no. 8, pp. 2394–2406, 2007, doi: 10.1088/0022-3727/40/8/S19.

[106] S. Amrollahy, B. Fadhel, B. Ettouil, A. C. Liberati, C. Moreau, and A. Dolatabadi, “Flash Boiling Atomization of High-Concentration Suspensions in Suspension Plasma Spraying,” *J. Therm. Spray Technol.*, 2023, doi: 10.1007/s11666-023-01679-y.

[107] A. Bily, “Development of Titanium Diboride Wettable Cathodes for Aluminium Electrolysis by Suspension Plasma Spray,” no. May, 2023.

[108] K. VanEvery, M. J. M. Krane, and R. W. Trice, “Parametric study of suspension plasma spray processing parameters on coating microstructures manufactured from nanoscale yttria-stabilized zirconia,” *Surf. Coatings Technol.*, vol. 206, no. 8–9, pp. 2464–2473, 2012, doi: 10.1016/j.surfcoat.2011.10.051.

[109] H. B. Xiong, C. Y. Zhang, K. Zhang, and X. M. Shao, “Effects of atomization injection on nanoparticle processing in suspension plasma spray,” *Nanomaterials*, vol. 6, no. 5, 2016, doi: 10.3390/nano6050094.

[110] M. Vicent *et al.*, “Effect of the initial particle size distribution on the properties of suspension plasma sprayed Al2O3-TiO2 coatings,” *Surf. Coatings Technol.*, vol. 268, pp. 209–215, 2015, doi: 10.1016/j.surfcoat.2014.12.010.

[111] H. Jamali, R. Mozafarinia, R. Shoja Razavi, and R. Ahmadi-Pidani, “Comparison of thermal shock resistances of plasma-sprayed nanostructured and conventional yttria stabilized zirconia thermal barrier coatings,” *Ceram. Int.*, vol. 38, no. 8, pp. 6705–6712, 2012, doi: 10.1016/j.ceramint.2012.05.060.

[112] B. Bernard, L. Bianchi, A. Malié, A. Joulia, and B. Rémy, “Columnar suspension plasma sprayed coating microstructural control for thermal barrier coating application,” *J. Eur. Ceram. Soc.*, vol. 36, no. 4, pp. 1081–1089, 2016, doi: 10.1016/j.jeurceramsoc.2015.11.018.

[113] V. Carnicer, M. J. Orts, R. Moreno, and E. Sánchez, “Influence of solids concentration on the

microstructure of suspension plasma sprayed Y-TZP/Al2O3/SiC composite coatings," *Surf. Coatings Technol.*, vol. 371, no. December 2018, pp. 143–150, 2019, doi: 10.1016/j.surfcoat.2019.01.078.

[114] N. Curry, K. VanEvery, T. Snyder, J. Susnjar, and S. Bjorklund, "Performance testing of suspension plasma sprayed thermal barrier coatings produced with varied suspension parameters," *Coatings*, vol. 5, no. 3, pp. 338–356, 2015, doi: 10.3390/coatings5030338.

[115] J. A. Gan and C. C. Berndt, "Nanocomposite coatings: Thermal spray procebing, microstructure and performance," *Int. Mater. Rev.*, vol. 60, no. 4, pp. 195–244, 2015, doi: 10.1179/1743280414Y.0000000048.

[116] H. Khatibnezhad, F. Ben Ettouil, and C. Moreau, "Photoactive Ce-doped TiO2 and CeO2-TiO2 composite coatings deposited by suspension/solution plasma spray," *Mater. Res. Bull.*, vol. 166, no. January, 2023, doi: 10.1016/j.materresbull.2023.112346.

[117] Y. Liu, J. Wu, H. Lu, J. Wang, Y. Qu, and L. Jing, "Enhanced photocatalytic activities of commercial P25 TiO2 by trapping holes and transferring electrons for CO2 conversion and 2,4-dichlorophenol degradation," *Mater. Res. Bull.*, vol. 92, pp. 23–28, 2017, doi: 10.1016/j.materresbull.2017.04.004.